UiT The Arctic University of Norway

The Faculty of Health Science, Department of Medical Biology

Optimization of biomarkers for morphological analysis of healthy and preeclamptic term human placental tissue sections using advanced fluorescence microscopy methods

Maddhusja Nalliah

Master's thesis in Biomedicine (MBI-3911), July 2021

Supervisor: Mona Nystad (PhD)

Women's Health and Perinatology Research Group, Department of Clinical Medicine

Co-supervisor: Luis Villegas (MSc)

Optical Nanoscopy Research Group, Department of Physics and Technology

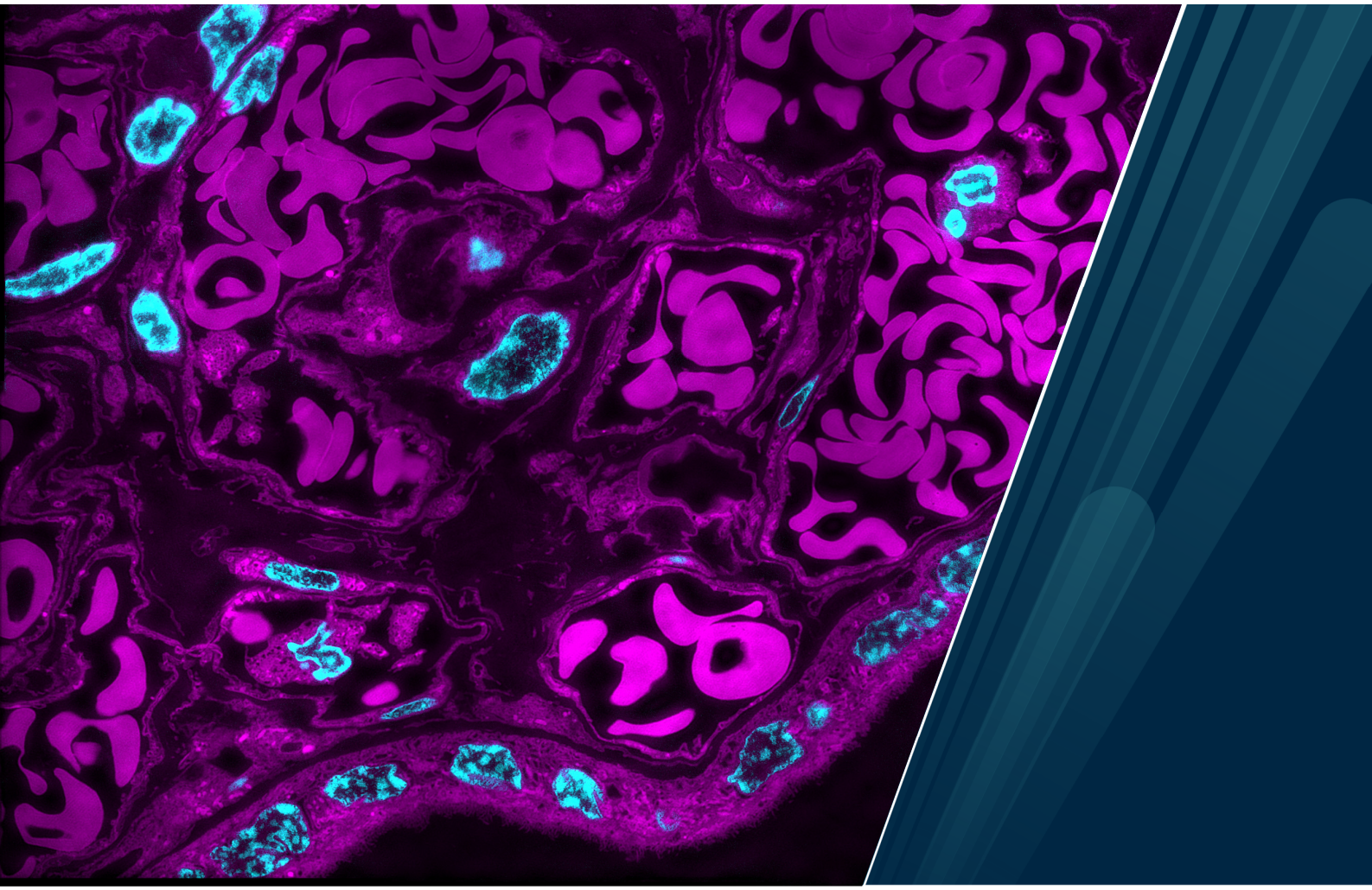

Acknowledgment

This master project was conducted at the Women's Health and Perinatology Research Group at the Department of Clinical Medicine, and the Optical Nanoscopy Research Group at the Department of Physics and Technology, at The Arctic University of Norway (UiT).

I am forever grateful to my supervisors; the main supervisor Mona Nystad and co-supervisor Luis Villegas for making this master project and creating a wonderful learning environment for me. Their exemplary guidance, meticulous assistance, and constant encouragement have inspired and motivated me to fulfill the thesis. I am very grateful for all the scientific discussions and ideas we have shared. I consider myself fortunate to have had the opportunity to be mentored by them. I am very thankful for Mona for improving the technique of scientific writing and for always believing in me and my ideas. Thank you for the weekly informal coffee meetings where you have shared your ideas, given me good feedback, and references to read which have enhanced my work. My sincere gratitude goes to Luis who has been a major impact on improving my laboratory skills including advanced optical microscopy. Thank you for sitting several hours at the microscopy lab to generate extraordinary images, and especially for always answering all the questions I have and giving me good feedback and tips on how to improve my knowledge.

A huge and special thanks to numerous people from the Optical Nanoscopy Research Group for their contributions and help to this project; Prof. Balpreet Singh Ahluwalia for permitting me to use their facilities; Deanna Wolfson for training me to use the DV microscope and always be available for answering any questioned I had. Thank you, Dr. Ganesh Acharya for providing me with normal and preeclamptic full-term human placenta samples for this study. My heartfelt thanks go to numerous laboratory specialists at UiT, Mona Pedersen, Randi Olsen, Augusta Sundbø and Ana Paola Lombardi for teaching me tissue sectioning, providing me with samples and materials for this project, including allowing me to use their laboratory during this study. Thank you for all the advice and help I have received. Kenneth Bowitz Larsen, thank you for making it possible to take the outstanding whole-slide scanner images and helping me understand the software during the thesis.

At last, my deepest gratitude goes to my mother, sister and brother for always supporting and motivating me to never give up.

Abstract

Preeclampsia (PE) is a pregnancy-related disorder affecting 5-8% of women worldwide (4% in Norway). It is believed that placental ischemia is the initial event in the development of PE and is characterized by placental insufficiency and clinical symptoms such as hypertension and proteinuria. In this project, we aimed to study suitable biomarkers for morphological analysis of human term placenta from normal pregnancies and women with PE using advanced fluorescence microscopes.

To reach this objective, we optimized the labeling steps for advanced fluorescence optical microscopy imaging of formalin-fixed paraffin-embedded (FFPE) and cryo-preserved tissue sections of the human placenta. Furthermore, morphological and subcellular differences between healthy and preeclamptic placentas were investigated. For this, various fluorescence microscopy techniques were explored, including whole-slide scanner, high-resolution deconvolution microscopy (DV) and super-resolution structured illumination microscopy (SIM), along with diverse image processing tools and analysis of the microscopy images. In this thesis, diverse strategies were examined for the labeling of placental biomarkers including immunofluorescence staining of laeverin, cytokeratin-7 (CK-7) and placental alkaline phosphatase (PLAP), as well as direct labeling of F-actin, membranes and nuclei via phalloidin-Atto 647 N, CellMask Orange (CMO) and DAPI, respectively.

The microscopy investigation revealed actin spots abundantly localized in subtypes of the chorionic villi in both healthy and PE placentas, such as terminal villi (p-value 0.55), mature intermediate villi (p-value 0.50), immature intermediate villi (p-value 0.54) and stem villi (p-value 0.47), thus no observable differences. However, we found significant differences (p-value 0.015) of syncytial knots in PE compared to healthy tissue. A disorganized brushborder at the apical surface seems to be observed in the PE chorionic villi. Moreover, we found PLAP expression in the syncytial microvesicles in healthy placentas. The immunofluorescence study using laeverin and CK-7 antibodies seem to show co-localization in the syncytial plasma membrane in healthy placentas, though the labeled PE tissues showed laeverin expression in the syncytial plasma membrane and cytoplasm, including overexpression of laeverin in the fetal capillaries.

In conclusion, the biomarkers explored in this study may have the potential to play an important role in understanding and predict PE in the future.

Table of contents

List of figures

List of tables

Abbreviations

Ab	Antibody
AF-488	Alexa Fluor 488
AF-647	Alexa Fluor 647
AT_1	Type-1 angiotensin II receptor
BP	Blood pressure
BSA	Bovine serum albumin
CK-7	Cytokeratin-7
CMO	CellMask Orange
DAPI	4',6-diamidino-2-phenylidole, dihydrochloride
DNA	Deoxyribonucleic acid
DV	DeltaVision Elite High-resolution Microscope / Deconvolution microscopy
ECM	Extracellular matrix
FA	Formaldehyde
FC	Fetal capillary
FFPE	Formalin-fixed paraffin-embedded
FOV	Field of view
fRBC	Fetal red blood cells
GDM	Gestational diabetes mellitus
hD	Human decidua
hBP	Human basal plate
hCP	Human chorionic plate
hCTB	Human cytotrophoblast cells
hCV	Human chorionic villi (chorion frondosum)
HE	Hematoxylin and eosin
HELLP	Hemolysis, elevated liver enzymes and low platelet
hEVT	Human extravillous trophoblast cells
hSTB	Human syncytiotrophoblast
hTB	Human trophoblast cells
hTED	Human trophectoderm
hUC	Human umbilical cord
hUCA	Human umbilical cord arteries
hUCV	Human umbilical cord veins

ICM	Inner cell mass
IgG	Immunoglobulin G
IHC	Immunohistochemistry
IIV	Immature intermediate villi
IUGR	Intrauterine growth restriction
MIV	Mature intermediate villi
MLT	Multiple labeling technique
MSV	Mesenchymal villi
OMX	DeltaVision OMX V4 Blaze Microscope
PBS	Phosphate-buffered saline
PE	Preeclampsia
PHEM	PIPES-HEPES-EGTA-Magnesium sulfate
PIGF	Placental growth factor
PLAP	Placental alkaline phosphatase
PSF	Point spread function
PTL	Preterm labor
ROI	Region of interest
SBB	Sudan black B
sFlt-1	Soluble fms-like tyrosine kinase receptor-1
SIM	Structured illumination microscopy
SK	Syncytial knots
STBEV	Syncytiotrophoblast extracellular vesicles
STBM	Syncytiotrophoblast microvesicles
SV	Stem villi
TBS	Tris buffered saline
TBST	Tris buffered saline with Tween 20
TV	Terminal villi

Introduction

The placenta is a highly specialized organ only present during pregnancy. The organ is vital for the normal growth and development of the fetus and maternal health (1). When the placenta fails to develop normally, several complications such as preeclampsia (PE) may rise. Preeclampsia is a pregnancy-specific disorder affecting 5-8% of women during pregnancy worldwide (4% in Norway) (2, 3). The only cure for the disorder is to fully remove the organ. The etiology of preeclampsia is still unknown. However, it is believed that placenta ischemia produces soluble toxic factors that are released into the maternal circulation causing placental dysfunction. Because placenta ischemia might be the root cause of PE, it is necessary to investigate the differences between normal healthy placentas and preeclamptic placentas, thus various placental-specific biomarkers are used to investigate morphological changes in the placenta (4, 5). For this reason, placental biomarker studies may potentially play a key role in understanding the disorder and for prediction at an early stage.

The morphology studies of placental pathology are one of the cornerstones of diagnosis of abnormal pregnancies and one of the research focuses of the Women's Health and Perinatology Research Group at the Department of Clinical Medicine at The Arctic University of Norway (UiT). Their main emphasis is on translational and clinical research in women's health and perinatology which includes fetal-maternal physiology and genetics, placenta, reproductive biology and immunology, evidence-based pregnancy care and epidemiology, urogynaecology and chronic pelvic pain (6).

The Master thesis was performed at the Women's Health and Perinatology Research Group, Department of Clinical Medicine (UiT) in collaboration with the Optical Nanoscopy Research Group, Department of Physics and Technology (UiT). The aim of the collaboration was to shed light on the pathophysiological mechanisms of preeclampsia with the use of advanced fluorescence microscopy methods.

Due to the interest in this field in addition to limited studies associated with advanced optical fluorescence microscopy methods, this master project was created. Thus, the primary aims for the master project were to optimize the sample preparation-steps of formalin-fixed paraffin-embedded and cryo-preserved human placental tissue sections for fluorescence high-resolution and super-resolution imaging using advanced microscopy methods. These included a whole-slide scanner (Olympus VS120), high-resolution deconvolution microscope (DV) and super-

resolution structured illumination microscope (SIM). The secondary aim of the thesis was to investigate relevant and suitable fluorescence placental biomarkers for ultrastructural and subcellular investigation of placentas. Additionally, we wanted to compare placentas from women that have had preeclampsia with placentas from women with healthy pregnancies and to identify morphological changes between them.

Furthermore, the findings from the study using different placental-specific biomarkers and direct fluorescent dyes might contribute to a better understanding of the preeclampsia. Additionally, our ultimate goal for future research is to develop a type of pregnancy test, which can be taken early in pregnancy to detect and monitor women at risk of developing preeclampsia to mitigate potential threats to women and their fetuses. This study was the first step in the direction to reach that goal; the goal of developing a prediction assay for PE.

The preliminary study for immunofluorescence investigation started with optimization of the methods for FFPE- and cryo-sections of human full-term placenta tissues from healthy and preeclamptic pregnancies. The optimization stage – 75% research time (**Figure 1**) included optimizing the sample preparation, concentration and incubation times for biomarkers and direct fluorescent dyes and investigating different labeling techniques suitable for FFPE- and cryo-sections for the advanced optical imaging method. Both, DV and OMX microscopes were used for the optimization stage. After acquiring the optimal methodology, the morphology investigation began – 25% research time. The morphology study included investigating structural and subcellular differences of the immunofluorescence labeled and direct fluorescent-labeled healthy and PE placentas using various microscopes (Olympus VS120, DV, OMX).

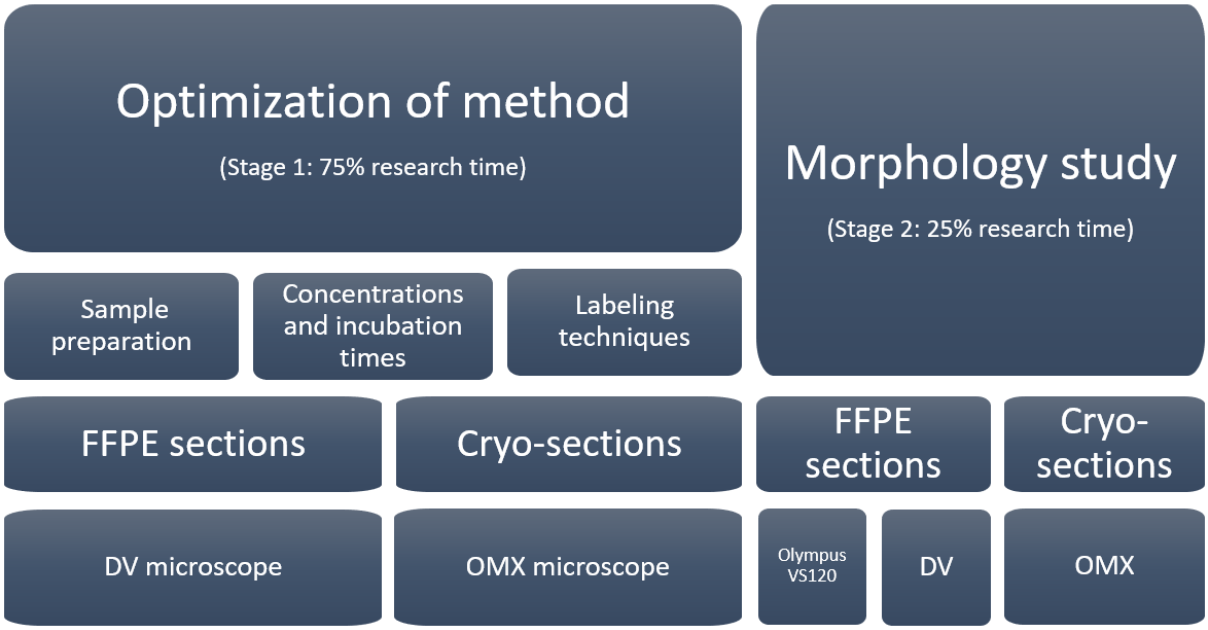

Figure 1 The master project setup. *Flowchart represents an overview of the project setup for the experimental plan. Stage 1 was the optimization of the methods used for the study, and stage 2 was the morphology study in the thesis.*

The Master thesis starts with the theoretical framework, followed the methodology used in this study. The third and fourth sections consist of experimental results and discussion, respectively. The final sections include the conclusion and the future perspectives for the project.

1 Theoretical background

The following section outlines the theoretical background of this study. All the information is given to recapitulate the current state of knowledge.

1.1 Human placenta

The human placenta is a highly specialized organ present only during pregnancy and plays a central role in the health of the mother and the fetus. The organ is essential for normal fetal growth and development, ensuring nutrition and oxygen exchange in addition to transporting carbon dioxide and metabolic waste away from the fetus (1). Placental pathology may lead to abnormal fetal development.

1.1.1 Early placental development

Embryonic development, also known as embryogenesis, begins with fertilization which initiates the pregnancy. Human fertilization occurs when a male haploid gamete (sperm cell) fuses with the female haploid gamete (ovum) forming a diploid zygote (7, 8). The fusion of two gametes activates the zygote to frequently divide while migrating down the Fallopian tube (**Figure 2**) (9). During 3-4 days after fertilization, a transition from 4- or 8-cell to a compacted morula occurs. On day 5, the morula matures into an early blastocyst, consisting of cells forming an outer layer of human trophectoderm (hTED), a fluid-filled cavity and an inner cell mass (ICM). The human trophectoderm gives rise to human trophoblast cells (hTB). The ICM is the origin of the human embryo and human umbilical cord (hUC) including placental mesenchyme (1, 10). Day 6-7, the blastocyst hatches leaving the protective zona pellucida and thus allowing trophoblast migration and invasion into the maternal uterine epithelium wall which initiates the formation of the human placenta (10). The formation of the placenta starts when hTB differentiates into the human syncytiotrophoblast (hSTB) invading the myometrium.

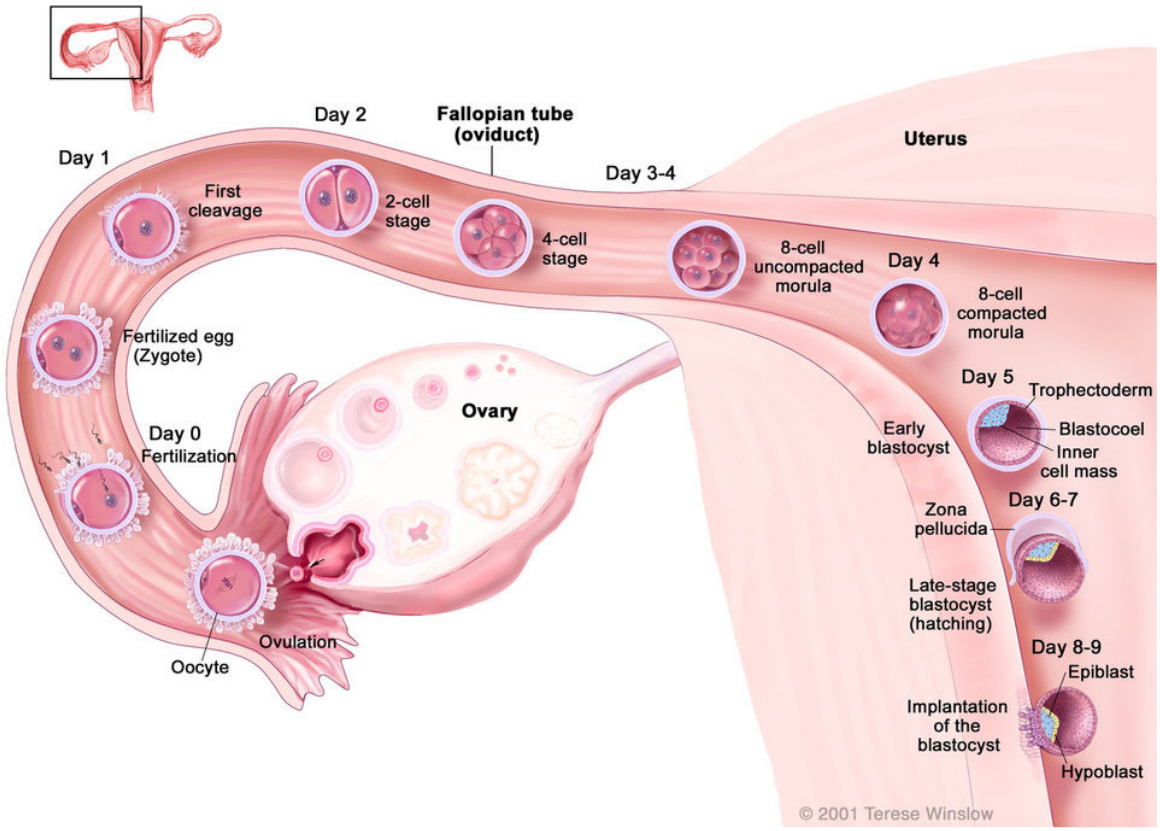

Figure 2 Fertilization of a human egg in the Fallopian tube and implantation of a blastocyst. *Fertilization of the egg with a sperm cell occurs on Day 0. The fertilized egg proliferates and divides while migrating through the Fallopian tube in the uterus (Day 1-4). On day 5, the preimplantation stage begins, where the morula gives rise to an early blastocyst consisting of human trophectoderm (hTED), blastocoel (blastocyst cavity) and inner cell mass (ICM). On day 6-7 the blastocyst hatches and day 8-9, the blastocyst implants in the uterine wall (maternal decidua). Formation of the human placenta has begun when the human trophoblast cells (hTB) differentiate into human syncytiotrophoblast invading the myometrium. From: Winslow, T., 2001 (11).*

1.1.2 Trophoblasts – the major constituents of the placenta

The structure of the human placenta is complex. The uterine wall (epithelial wall) is located in the uterus and transforms into human decidua (hD) (**Figure 3A**) (10). The human trophoblast cells (hTB) undergo extensive proliferation and differentiates into various types of cells forming the human chorionic villi (hCV) (1). The human cytotrophoblasts (hCTB) are stem cells forming the inner layer of the human chorionic villi (hCV) with the basement membrane (**Figure 3B**). Further, the hCTB cells divide and differentiate into multinucleated syncytiotrophoblast (hSTB), also called syncytium, localized at the outer layer of hCV (10). The hSTB are in direct contact with the maternal blood and are the site of maternal-fetal gas and nutrients exchange. The remaining hCTB that are in contact with the hD, which differentiates into human extravillous trophoblast cells (hEVT) (10). The hEVT migrates into

the hD and initiates uterine artery remodeling and enables maternal blood to flow into the intervillous space of the placenta (1, 12, 13). The hEVT anchor the placenta. The villous tree is furthermore developed by the remaining hSTB located in between the lacunae which are called trabeculae (13, 14).

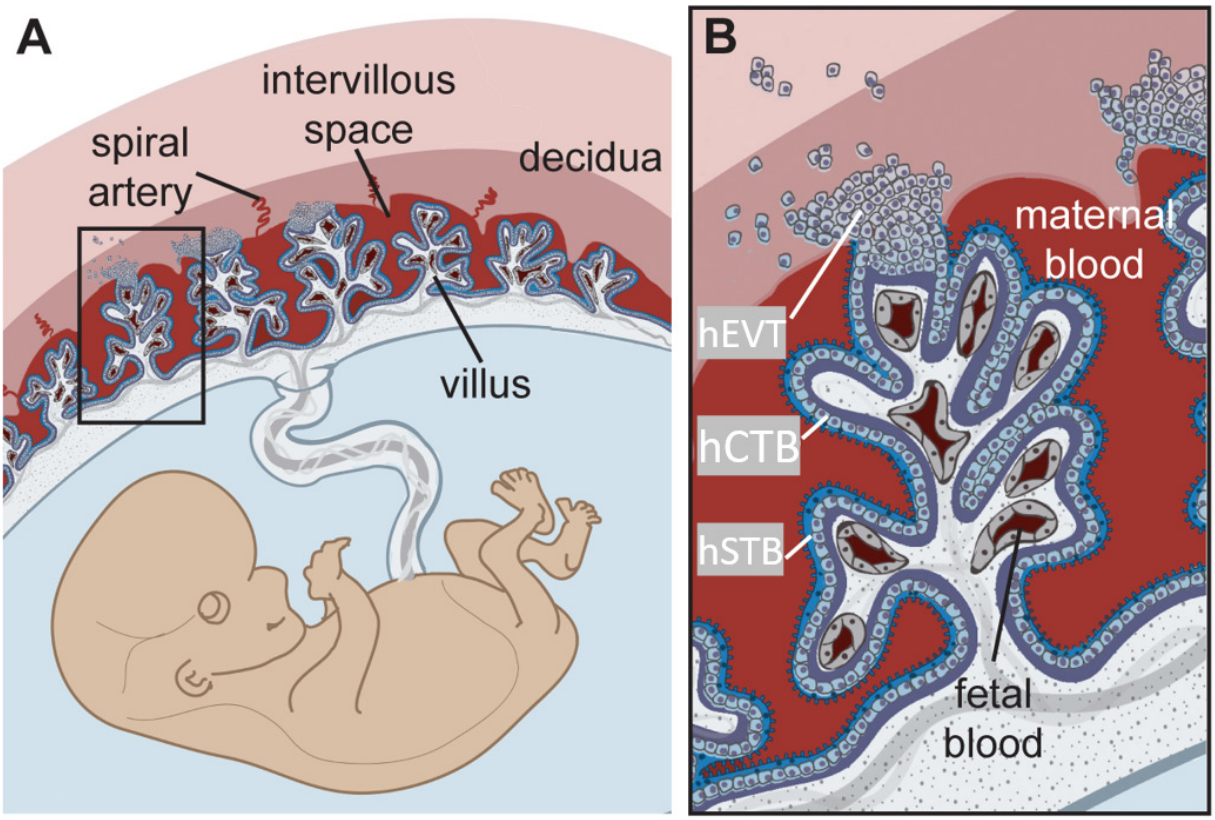

Figure 3 Structure of human term placenta. *(A) Structure of a placenta and fetus in a human uterus. The fetus is connected to the placenta through the umbilical cord. The uterine epithelial wall transforms into human decidua (hD). Human trophoblast cells (hTB) proliferate and differentiate into forming human chorionic villi (hCV) which are in direct contact with the maternal blood. (B) Enlargement of boxed region from (A). An overview of the villous tree in the placenta which is covered by a basement membrane (purple) and human cytotrophoblast cells (hCTB) that are overlined by the human syncytiotrophoblast (hSTB/syncytium). HSTB forms a barrier between the fetus and the mother where gas and nutrients exchange. The fetal blood vessels (fetal capillaries) are located inside the villous. Some cytotrophoblast cells differentiate into human extravillous trophoblast cells (hEVT) which are in direct contact with the hD and anchor the placenta in the uterus. The figure is retrieved and modified from: Zeldovich et al., 2011 (12).*

1.1.3 From trophoblast differentiation to fully developed human placenta at term

A fully developed human placenta at term is 500-600 gram, 2-3 centimeter thick and 15-20 centimeter in diameter (15, 16). The human placenta is composed of both maternal tissues derived from the endometrium and the fetal tissues derived from hTB (1). The fetal region of the human placenta, called the human chorionic plate (hCP), consists of fetal blood vessels branching from the human umbilical cord arteries (hUCA) and the human umbilical cord veins (hUCV) (**Figure 4**) (1). The human basal plate (hBP) is located at the maternal part of the placenta. This region consists of the maternal spiral artery, maternal vein and human decidua (hD). Numerous branched human chorionic villi (hCV) are submerged in maternal blood (1, 12).

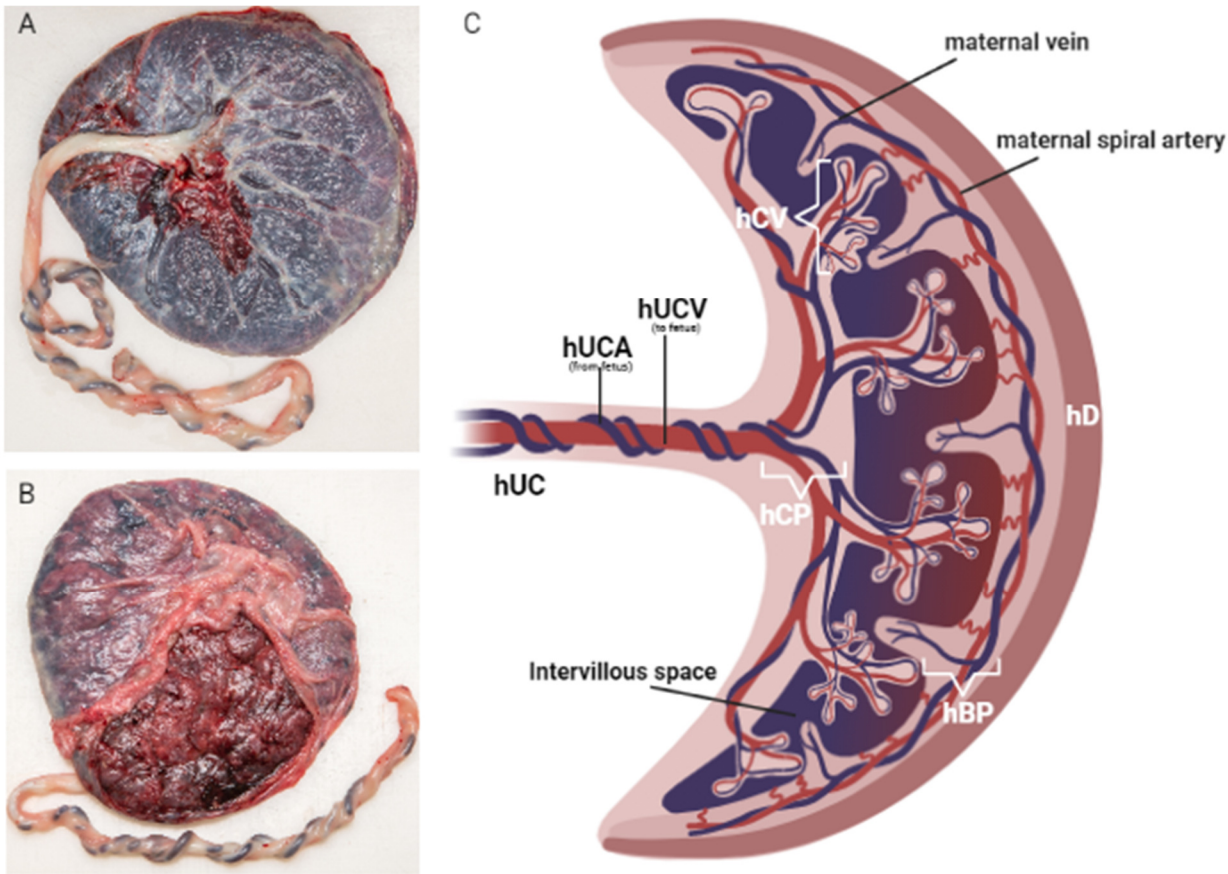

Figure 4 Normal human placenta at term. *(A-B) Macroscopic image of a healthy placenta delivered from a pregnant woman at term. (A) Fetal side of the placenta showing human umbilical cord (hUC) at the human chorionic plate (hCP). (B) The maternal side of the placenta showing human decidua (hD) partly removed. (C) Schematic illustration of normal placenta showing the human chorionic plate (hCP) located at the fetal side of the human placenta, where the fetal blood vessels branching from the human umbilical cord arteries (hUCA) and human umbilical cord vein (hUCV), located within the human umbilical cord (hUC). The intervillous space is filled with maternal blood and the human chorionic villi (hCV) that are submerged in the maternal blood. The human basal plate (hBP) and human decidua (hD) are located at the maternal region of the placenta. Schematic image made with BioRender.com. Macroscopic photos (17), Photo: Bjørn-Kåre Iversen, UiT-The Arctic University of Tromsø, Norway.*

1.1.4 Chorionic villi - microscope identification of subtypes

The human chorionic villi are a complex structure categorized into different subtypes (**Figure 5A**). The hCV are composed of mesenchymal villi (MSV) which are present during the early stages of pregnancy and gradually transformed into immature intermediate villi (IIV) (18). Mature intermediate villi (MIV) are longer and lack fetal vessels in the stroma compared to the immature intermediated villi (18, 19). MIV develops furthermore into terminal villi (TV) that are connected to the stem villi (SV) by intermediate structures (18). Large amounts of TV are commonly visualized in term placentas. However, it can be difficult to differentiate the different subtypes of villi in a histological investigation due to different shapes, sizes and structures. One of the factors that may affect the observation is the sectioning angle of the tissue sample, resulting in a microscope observation of different forms of the same subtype of the villi (**Figure 5B**).

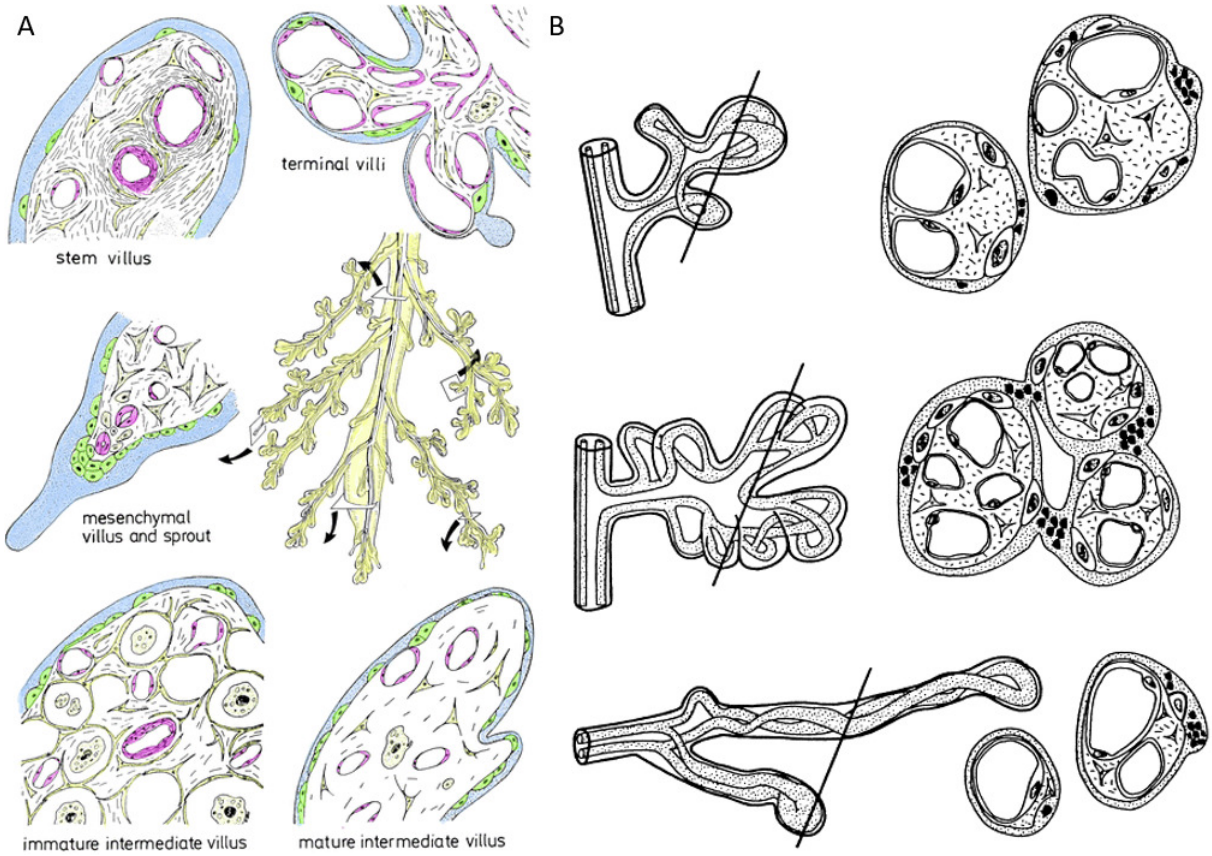

Figure 5 Schematic representation of placental chorionic villi. *(A) The chorionic villi (yellow) in the middle show where the different subtypes of villi are located. The arrows display the different subtypes of chorionic villi. The chorionic villi are a complex structure in different subtypes: stem villi (SV), terminal villi (TV), mesenchymal villous (MSV), immature intermediate villi (IIV) and mature intermediate villi (MIV). The figure is retrieved from Baergen RN., 2010 (20). (B) Tissue sectioning at different angles results in observing different shapes, sizes, and structures of chorionic villi with the microscope. The black line indicates where the section is made and the representative images are shown at the right. The figure is retrieved and modified from: Kingdom, J., 2000 (21).*

1.1.5 The role of chorionic villi placental function

The human placenta plays a key role in feto-maternal transport, metabolism, protection against foreign and dangerous pathogens and endocrine secretion (1, 22). Terminal villi exchange nutrients and gases over the syncytial trophoblast membrane (23, 24). It transports oxygen, water, carbohydrate, amino acids, lipid, vitamins, minerals and other essential nutrients to the fetus (1, 16). Removal of carbon dioxide, water, urea and other waste products from the fetus to the mother occurs over the syncytial plasma membrane to the maternal blood (23). The placenta maintains the protection of the fetus from certain xenobiotic molecules, infections, and maternal diseases (1). Additionally, the placenta releases hormones that circulate in the maternal blood and affect the pregnancy, metabolism, fetus growth, parturition and other functions (1, 16, 25).

1.2 Abnormal pregnancy and pregnancy-related disorders

Health problems may occur during pregnancy affecting either the mother, the fetus or both. The most common pregnancy-related disorders that occur before, during or after pregnancy include preeclampsia (PE), intrauterine growth restriction (IUGR), preterm labor (PTL) and gestational diabetes mellitus (GDM) (26-28).

1.2.1 Preeclampsia

Preeclampsia (PE) is a pregnancy-related hypertensive disorder affecting 5-8% of women worldwide (2, 4). The disease generally occurs in women during their pregnancy after 20 weeks of gestation and frequently near term (29). Diagnosis of preeclampsia is based on hypertension (defined as BP ≥140 mmHg systolic and/or BP ≥90 mmHg diastolic) and proteinuria after 20 weeks of gestation (4). In absence of proteinuria, preeclampsia is defined as the onset of hypertension with thrombocytopenia, renal insufficiency, impaired liver function, pulmonary edema and cerebral or visual symptoms evidence of systemic disease (4).

Preeclampsia may be classified into two groups: early preeclampsia (<34 weeks) with a higher risk of maternal and fetal complication and late preeclampsia (≥34 weeks) (4). Early-onset preeclampsia is characterized as a fetal disorder referred to as a reduction in placental volume, intrauterine growth restriction, abnormal uterine and umbilical artery Doppler, low birth weight, multi-organ dysfunction, perinatal death and adverse maternal and neonatal outcomes (29). Late-onset preeclampsia is often related to the maternal condition with a characterization

of a normal placenta, large placental volume, normal fetal growth, normal uterine and umbilical artery Doppler and normal birth weight (30). However, early-onset is more severe in comparison to late-onset preeclampsia.

1.2.2 Pathophysiology of preeclampsia

The root cause of preeclampsia is unknown. However, the disorder results from ischemia of the placenta which initiates releases of various soluble factors (earlier called toxins) into the maternal circulation that interrupts the pregnancy immunomodulation and thus induces the clinical manifestation of the disease (5, 31). Various agents such as genetic factors, abnormal trophoblasts, oxidative stress and increased anti-angiotensin II receptor type 1 (AT_1) autoantibodies may contribute to reduced migration and invasion of the spiral arteries resulting in placental dysfunction (**Figure 6**) (4). Thus, the condition of preeclampsia occurs when adaptive responses release inflammatory cytokines, AT_1 antibodies, angiogenesis, antiangiogenic factors and syncytiotrophoblast-derived particles into the circulatory system of the mother (4, 32). All these different factors induce the activation of leukocytes, intravascular inflammation, endothelial cell dysfunction and excessive thrombosis. The stimulation of this process in various target organs is the reasoning behind the multiorgan pathogenicity of preeclampsia (4).

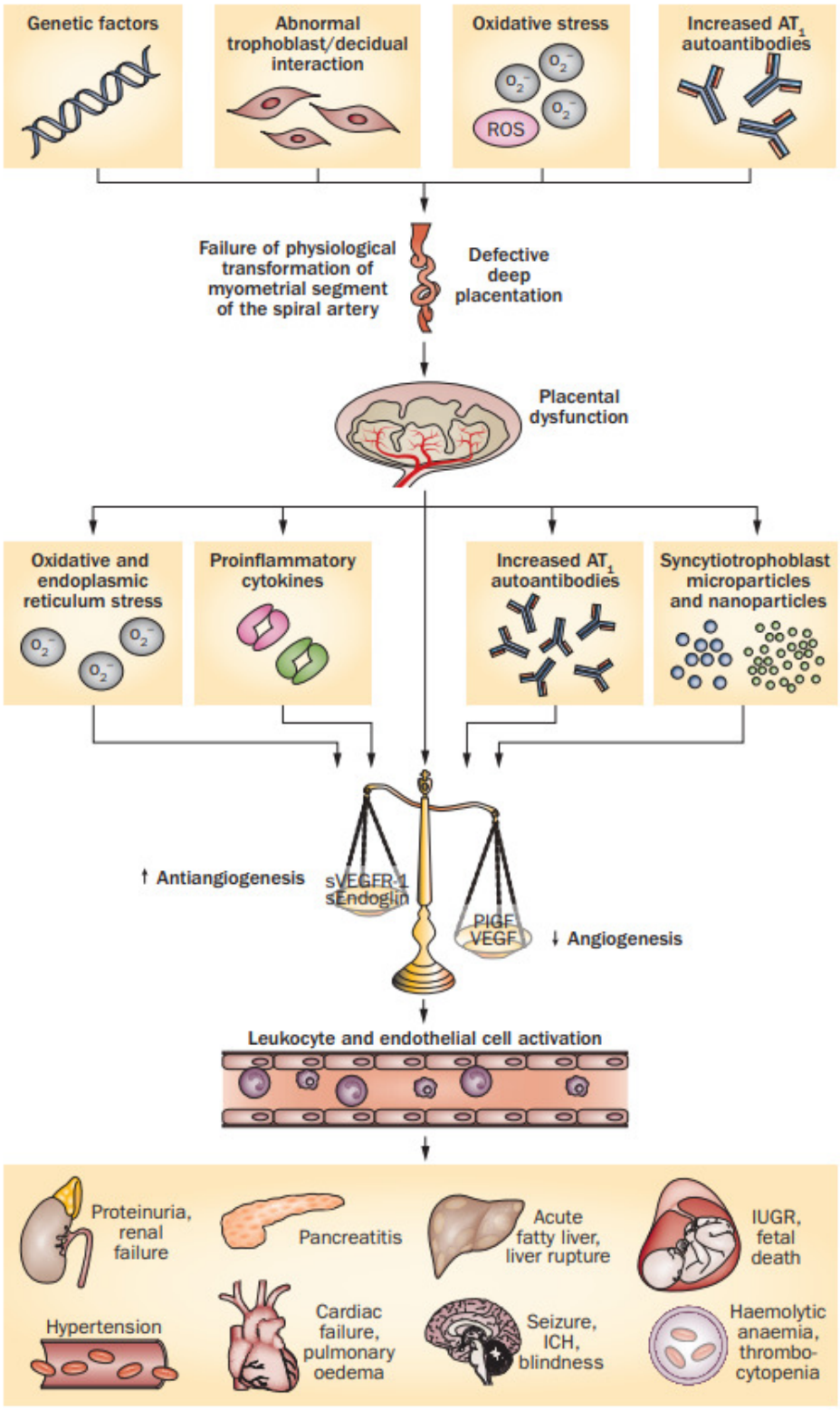

Figure 6 Pathophysiology of preeclampsia. *Different factors including genetic factors, abnormal trophoblast/decidual interaction, oxidative stress, and increased AT_1 autoantibodies increases the failure of physiological transformation of the myometrial segment of the spiral arteries (deep placentation) which leads to placental dysfunction. The effect of these factors results in preeclampsia which occurs when adaptive responses release inflammatory cytokines, anti-AT_1 antibodies, angiogenesis, antiangiogenic factors, and syncytiotrophoblast-derived micro-and nanoparticles into the maternal circulatory system. Further, these factors initiate leukocytes, intravascular inflammation, endothelial cell dysfunction, and excessive thrombosis may be the cause of the multiorgan pathogenicity of preeclampsia. From: Chaiworapongsa et al., 2014 (4).*

1.2.3 Treatment of Preeclampsia

To date, there is no specific treatment for preeclampsia. Thus, the only cure is to remove the placenta to manage the symptoms (33). Numerous interventions have been tested for the prevention of preeclampsia, including low-salt diets, diuretics, fish oil, calcium supplement, antioxidants, aspirin and heparin (4, 33, 34). To date, aspirin is the only substance that has been shown to have a prophylactic effect for the prevention of PE (33).

1.2.4 Eclampsia – extreme complication of the preeclampsia

Eclampsia is an extreme complication of preeclampsia that causes damage to maternal arteries and other blood vessels which might restrict the blood flow, leading to swelling in blood vessels in the brain, resulting in seizures and maternal death (35-37). The complications followed by eclampsia include stroke, hemolysis, elevated liver enzymes, and low platelets (HELLP) syndrome, and disseminated intravascular coagulation (38).

1.3 Biomarkers

The World Health Organization (WHO) defines biomarkers as "*any substance, structure, or process that can be measured in the body or its product and influence or predict the incidence of outcome or disease*" (39, 40). Biomarkers, also known as biological markers, are key tools in clinical and biomedical research. These types of indicators provide vital information about biological mechanisms, pathogenic processes, pharmacologic processes, or therapeutic intervention depending on the type of application used for the research purpose.

1.3.1 Placental biomarkers

There are several types of biomarkers used to investigate the biological and clinical mechanisms of placental and fetal development, including protein-based biomarkers, DNA-based biomarkers, RNA-based biomarkers, or biomarkers for predicting fetal outcomes (41). Placental biomarkers are used to understand the placental function linking to placental physiology, maternal-fetal physiology, including placental abnormality (42). Various angiogenic and anti-angiogenic biomarkers are used to investigate PE, where a study led to the discovery of over-expression of soluble fms-like tyrosine kinase receptor-1 (sFlt-1) and decreased levels of placental growth factor (PIGF) circulating in PE patients (43). Today, the sFlt-1/PIGF ratio is used as a predictor for early PE (44). For this study, different chorionic villi-specific biomarkers were used such as laeverin (aminopeptidase-Q), cytokeratin-7 (CK-

7), and placental alkaline phosphatase (PLAP). These biomarkers were chosen for this study due to their specificity of expression in the placental cells within the chorionic villi.

1.3.1.1 Laeverin

Laeverin is an aminopeptidase-Q specific to the placenta expressed in the plasma membrane of human trophoblasts and was first identified by Fujiwara *et al*., in 2004 (45). The protein is expressed on the cell surface of the human embryo-derived extravillous trophoblasts (45, 46). According to a study by Nystad *et al*., the laeverin was expressed in syncytiotrophoblast, including cytotrophoblasts cells and extravillous trophoblast cells in the human placenta (47). The expression of laeverin protein in the preeclamptic placenta was shown to be significantly higher and might be expressed in cytoplasm and microvesicles in cytotrophoblast compared to normal placentas (47, 48).

1.3.1.2 Cytokeratin-7

Cytokeratin-7 (CK-7) is a low molecular weight cytoskeletal intermediate filament protein of cytokeratins. Studies have shown that the expression of the CK-7 is expressed in the cytoplasm of the human trophoblast (49, 50). Thus, the CK-7 is commonly used as a cytoplasmic marker for identifying the human placental trophoblast cells (47, 50).

1.3.1.3 Placental Alkaline Phosphatase

Placental alkaline phosphatase (PLAP) is a syncytiotrophoblast marker used in immunoassays and has been proved that PLAP is a particularly useful marker for detecting syncytiotrophoblast extracellular vesicles (STBEV) (microvesicles) derived from syncytiotrophoblast (51). Several studies have shown an increase in the number of circulating STBEV in early-onset PE compared to a normal pregnancy (52, 53).

1.4 Mechanism of fluorescence

Fluorescence microscopy requires that the objects of interest have fluorescence capacity. Fluorescence is a spontaneous emission of light that occurs within nanoseconds after the absorption of light that is typical of a shorter wavelength. The difference between the excitation and emission wavelengths, known as the Stokes shifts, is the critical property that makes fluorescence a powerful tool for microscopy (54-56). Fluorophore molecules absorb energy at a specific wavelength and re-emit at a different wavelength. Within the fluorophore molecules, some electrons will absorb the photon energy and transition from the ground state to an excited state (57). When transitioning back to the ground state, the electrons will emit photons at higher wavelengths and, consequently, lower energy (58). By using the appropriate filter set, it is possible to completely filter out the excitation light and collect the emitted fluorescence, allowing the visualization of the fluorescent signal. This approach provides superior contrast to conventional labeling techniques in which objects are stained with agents that absorb light, such as hematoxylin and eosin (HE) staining, where the amount of light absorbed becomes only infinitesimally different from the background (54).

1.4.1 Direct fluorescent dyes

Direct fluorescent dyes are reactive dyes (i.e., not raised in animals) conjugated to fluorophores. The direct fluorescent dyes are widely used for targeting specific proteins, compartments, molecules and structures within a tissue of interest (59). They allow the detection of structures of interest on a fluorescence microscope without performing histochemical or immunohistochemical methods (60). For this study, the Phalloidin-Atto 647 N marker was used to target F-actin and CellMask Orange was used for membrane staining. Additionally, DAPI is a common marker for deoxyribonucleic acid (DNA) staining and was used for detecting placental nuclei.

1.4.2 Immunofluorescence technique

Immunofluorescence microscopy is a powerful technique extensively used in biomedical research labs worldwide to analyze and visualize molecules (antigens) of interest. This technique provides both high contrast and high specificity of the labeled structures, enabling the study of biological mechanisms in both healthy and diseased models (61-63). The principle of this technique is to use fluorescently-conjugated antibodies that recognize and detect antigens of interest by a fluorescence microscope (64). In this study, immunofluorescence

labeling was used as a tool to investigate the occurrence of different biomarkers targeting molecular structures within the placenta tissue, such as the laeverin, CK-7 and PLAP.

1.4.2.1 Antibody and antigen

An antibody (Ab) is a protein compartment produced as a defense mechanism within the host in response to the exposure of a foreign substance called an antigen (65). An antigen is a substance that activates the immune system to produce antibodies against it (65). An antigen consists of molecules such as proteins, polypeptides, polysaccharides, lipids, or nucleic acids. The structure of an antibody is classically Y-shaped and consists of two heavy chains and two light chains within a binding site on the short arms (66). The binding site of the antibody is highly specific to a particular combination of molecular conformation and component molecular groups such as a specific region in an amino acid sequence. The antibody binds to the epitope (specific region) located on the surface of the antigen. Antibodies can be either monoclonal or polyclonal. Monoclonal antibodies recognize only one epitope, whereas, polyclonal antibodies are formed by repeated immunization of the animal that binds to the antigen of interest (67).

1.4.2.2 The direct and indirect technique

Direct immunofluorescent labeling uses only a single antibody conjugated to a fluorophore which binds directly to the antigen (68). Whereas the indirect immunofluorescent assay uses unconjugated primary antibodies binding to fluorophore-conjugated secondary antibodies to detect the antigen of interest. In the latter method, it is also important that primary and secondary antibodies are originated from different species, to avoid cross-reactivity in the sample of the secondary antibodies with endogenous immunoglobulin G (IgG) (69). **Figure 7** illustrates the mechanism behind the production of primary and secondary antibodies. First, an antigen is inoculated into a rabbit, which produces primary antibodies that are raised against that specific antigen, thus enabling the specific binding to the epitope of the antigen. Second, an inoculated donkey with rabbit IgG will produce a secondary antibody that will enable the binding to the primary antibody raised against the specific rabbit IgG (66).

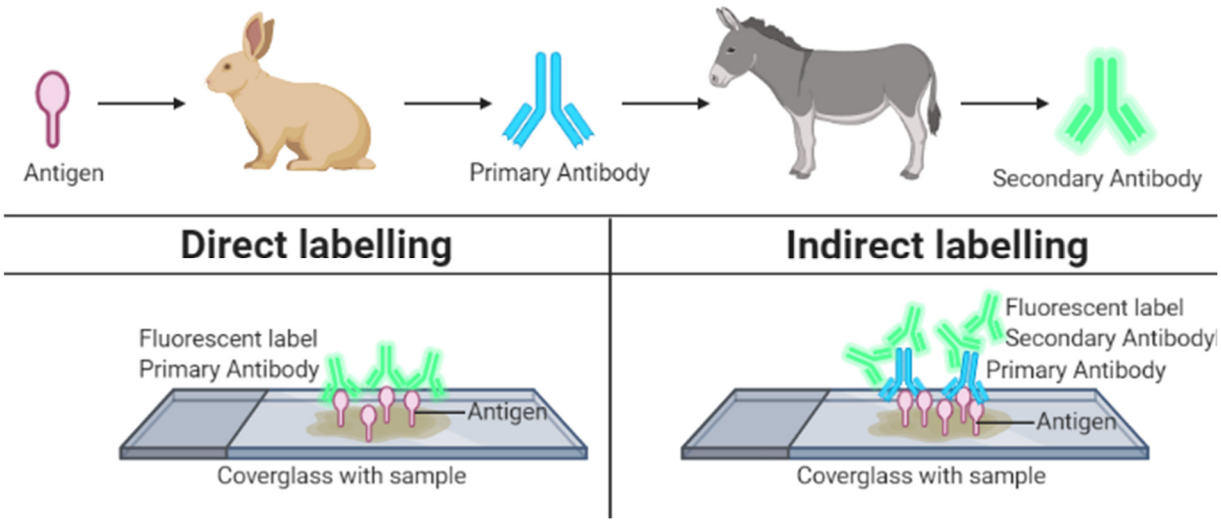

Figure 7 Direct and indirect labeling technique used in immunofluorescence assay. *The top panel illustrates the mechanism behind the production of primary and secondary antibodies. An antigen is inoculated into a rabbit who then produces primary antibodies against that antigen. An inoculated donkey with rabbit IgG produces secondary antibodies against that rabbit IgG, enabling the binding to the primary antibodies. The bottom panel shows the working principle of both direct and indirect immunofluorescent labeling. In the direct labeling method, a fluorescently-tagged primary antibody binds directly to a specific antigen, whereas the indirect labeling technique uses two antibodies: a primary antibody bound to a fluorescently-tagged secondary antibody. Schematic image made with BioRender.com.*

1.4.3 Autofluorescence background

Generally, successful observation of fluorescence dyes in formalin-fixed paraffin-embedded (FFPE) tissue sections is significantly hampered due to natural autofluorescence occurring in the tissue. This prevents clear visualization of the labeled tissue section. Autofluorescence appears when a biological structure emits fluorescence at a natural level without being manipulated by fluorescent dyes (70). Studies have shown that the cause of autofluorescence might be due to the presence of native cell components such as red blood cells, collagen, elastin, flavins, porphyrins, chlorophyll, lipofuscin, including cyclic ring compounds (NADPH and riboflavin), aromatic acids, and cellular organelles (mitochondria and lysosomes) (71-77). Additionally, autofluorescence may also occur from fixatives such as neutral buffered formalin, a commonly used fixative in tissue preservation that forms covalent bonds between amino groups (78). Consequently, fluorescent products are formed resulting in an intense fluorescent background (79). Most of the induced autofluorescence in tissue has an emission between $450\,nm$ and $650\,nm$ which overlaps the emission wavelength of fluorophores. Thus, autofluorescence might affect the interpretation of the fluorescence signal coming from the samples.

1.5 Advanced fluorescence optical microscopy

1.5.1 Deconvolution microscopy

Deconvolution microscopy (DV) is a diffraction-limited computational technique permitting a stack of images to be processed by inexpensive computers in a short time depending on the acquisition size and the deconvolution algorithm (56, 80). This technique aims to remove the optical blur and reduce statistical noise by using information about the images from the microscope to estimate the original object. The cause of blurring and noise in the microscope is largely due to the limited aperture of the microscope objective lens. The out-of-focus blur and photon noise that degrades the image of the object is removed by the optical sectioning (56, 81). By moving the focal plane of the objective along the optical axis, it is possible to determine the point spread function (PSF) of the microscope (56). If the PSF is known, then deconvolution can be performed to remove the blur from the acquired data, thus improving the contrast and resolution of the microscope image. DV images are susceptible to reconstruction artifacts derived from non-symmetric PSF. Therefore, careful oil matching is required before the acquisition of the raw image stack.

1.5.2 Structured illumination microscopy

Structured illumination microscopy (SIM) is a super-resolution technique using laser-based widefield configuration (82). SIM permits for observation of fluorescence-labeled samples at a lateral and axial resolution below the diffraction limit, reaching at most $100\ nm$ and $300\ nm$, respectively (83). In SIM, diffracted laser beams at zero-order and/or first order are used to illuminate the sample. After passing the microscope objective, the beams interfere at the sample plane with each other creating a high spatial frequency stripe-like pattern (82). The overlapping between the stripe illumination and the high spatial frequency of the sample creates low spatial frequency patterns called Moire fringes that are now within the resolution capabilities of the objective lens (82, 84). The information of the small structures in the sample can be computationally retrieved from the Moiré fringes. To capture isotropic information in all regions and spatial directions, the illumination pattern needs to be shifted in five lateral phase steps and rotated in three angles for every focal plane (82). A stack size of at least eight planes is required to reconstruct an optical section with super-resolution in all three axes (x, y, z). Due to sensitivity to out-of-focus light, artifacts might be generated by imaging with SIM (84).

1.5.3 Limitations of fluorescence microscopy

Despite the advantages of the microscopy methods mentioned above compared to commercial brightfield microscopy, fluorescence microscopy has some disadvantages. Photobleaching is one of the limitations that might occur using all kinds of fluorescence microscopes. Photobleaching is the permanent loss of fluorescence of the dyes due to an irreversible chemical reaction that changes the absorption and emission capabilities, becoming non-fluorescent (85, 86). Advanced microscopy methods such as DV and SIM require photo-stable dyes for optimal image reconstruction. Thus, in these methods photobleaching hampers the quality of the reconstructed image. Furthermore, the broad emission spectra of autofluorescence pose a challenge in computationally-based microscopy techniques such as DV and SIM. Additionally, in the case of live-cell imaging, a process called phototoxicity will also limit the imaging acquisition. In live processes, prolonged exposure of cells to light leads to chemical reactions that alter the biochemistry of the samples (86-88).

2 Materials and methods

In this project, full-term human placenta from healthy pregnancies and women with preeclampsia were used to investigate suitable placental biomarkers for ultrastructural and subcellular detection of the protein-specific signal associated with preeclampsia. FFPE and cryopreservation techniques were used to prepare and preserve the tissue specimens (**Figure 8**). Placental samples were collected, preserved, sectioned, immunofluorescence-labeled, and investigated using advanced fluorescence optical microscopes. **Table S1** in Supplementary provides a detailed list of all the equipment, reagents and solutions used for the study. The labeling experiments with the different combinations of markers are presented in **Table S2** in Supplementary.

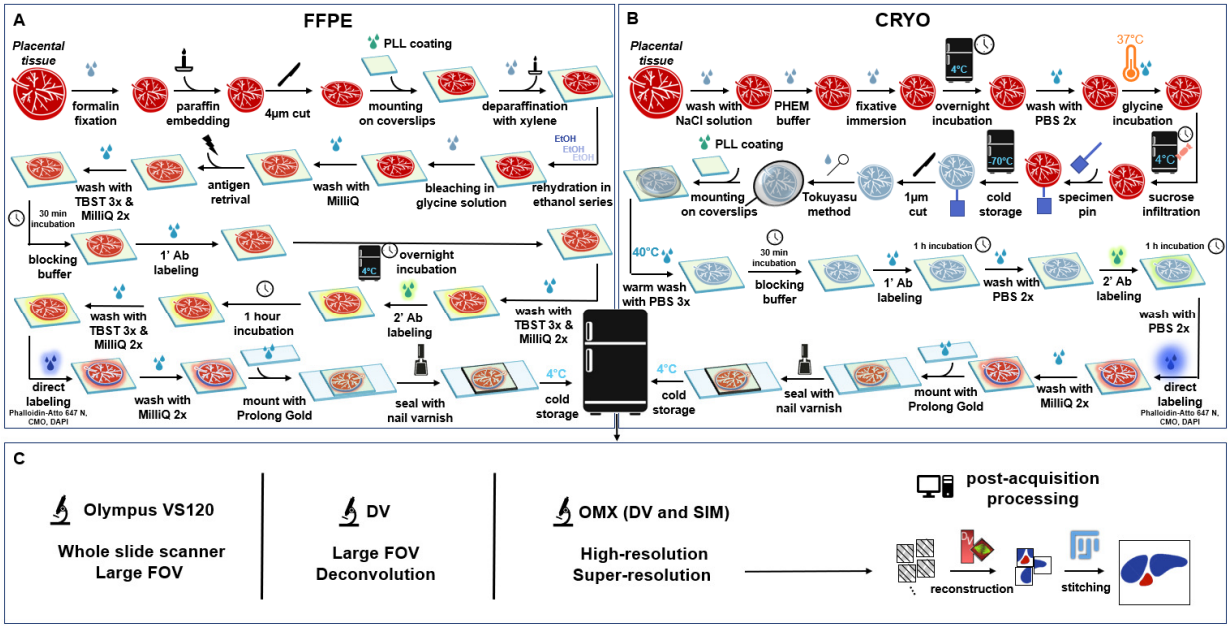

Figure 8 Schematic overview of sample preparation protocols for advanced fluorescence microscopy of placental tissue.*(A) FFPE tissue sections sample preparation procedure. (B) Cryopreserved tissue section preparation procedure. (C) Different advanced fluorescence microscopy methods were performed to generate images, including the Olympus VS120 whole-slide scanner, the DV microscope, and the OMX microscope. From: Villegas-Hernández et al., 2020 with permission from Villegas-Hernández.*

2.1 Clinical evaluation of full-term placentas

Clinical evaluation of the normal and preeclamptic full-term placentas were performed by clinicians at the University Hospital of Northern Norway (UNN) (89) following the Norwegian guidelines for diagnosis at the Department of Obstetrics and Gynaecology.

2.2 Collection of human placental tissue samples

Full-term placentas from normal and preeclamptic patients were collected as referred to in **Table 1**. For optimization, normal (n=2) and PE (n=2) placenta samples and for morphological investigation, normal (n=6) and PE (n=6) samples were collected immediately after delivery (within 30 minutes). The study was approved by the Regional Committee for Medical and Health Research Ethics-North Norway (REK Nord ref.# 2010/2058-4). The written consent was obtained from the participants. All the samples were anonymized.

Table 1 Overview of full-term placentas from Caucasian patients used for this study.

Human term placenta	For optimization		For investigation	
FFPE sections	Normal (n=1)	PE (n=1)	Normal (n=5)	PE (n=5)
Cryo-sections	Normal (n=1)	PE (n=1)	Normal (n=1)	PE (n=1)

2.3 Tissue preparation of FFPE sections

2.3.1 Formalin fixation

The collected placenta tissues were processed following standard histological procedures. The tissue processing was performed by the bioengineer at the pathology department. Tissue fixation is crucial for obtaining the high-quality morphology needed for targeting and identifying structures of interest in histopathological diagnosis and analysis. Tissue fixation entails a series of complex chemical modifications of macromolecules in tissues to preserve their structure and chemical composition as close to their natural state (90, 91). It prevents autolysis, mitigates putrefaction and preserves the morphology while maintaining antigenicity (63). The human placental tissues were quickly submerged in formalin fixative after the biopsy to prevent autolytic degradation by proteolytic enzymes and contamination within the tissue (91). The formalin fixative is commonly used in pathology examination because of its degree of accuracy and adaptability (91). Longer fixation of the tissue may harden the further processing of paraffin infiltration, which may hamper the quality of sectioning. Thus, this procedure was vital for acquiring adequate tissue sections.

2.3.2 Dehydration, paraffin embedding and sectioning

After fixation, the tissue specimens were further processed for dehydration with graded ethanol and Xylene to remove the water. Thereafter, the tissue was infiltrated with an infiltration agent (molten paraffin wax) to remove Xylene from the dehydration step before embedding in paraffin which permits the tissue to be cut into thin sections. This process solidified and formed a hard matrix which was then cut into semi-thin sections of 4-5µm thickness using a microtome (HM 355S Automatic Microtome, Thermo Fisher Scientific, Waltham, Massachusetts, USA). With co-assistance and training from a histo-technologist, adequate paraffin blocks of FFPE were sectioned into 4 µm thickness and mounted on a microscope glass slide.

2.3.3 Deparaffinization and rehydration

The tissue sections were incubated at 60ºC overnight before performing deparaffinization and rehydration. Incubation overnight was performed to obtain good adhesion of the sample to the slide including melting the substantial amount of paraffin. Overnight incubated tissue sections were then deparaffinized in Xylene (3 x 10 minutes) and rehydrated in graded alcohol:100% ethanol (2 x 10 minutes), 96% ethanol (2 x 10 min), 70% Ethanol (10 minutes). Xylene is a flammable toxic organic solvent that is commonly used to solubilize paraffin for deparaffinization of the tissue sections. The series of degraded alcohol concentration solutions

removed Xylene and reintroduces the water molecule into the tissue. The deparaffinized and rehydrated tissue sections were washed with 150mM glycine bleaching solution (30 minutes) to neutralize free aldehydes in the tissue and enhance the binding capabilities of the antibodies and dyes to the sample. Lastly, the FFPE sections were washed with MilliQ-water (5 minutes) to remove the bleaching solution.

2.3.4 Antigen retrieval

Following deparaffinization and rehydration, antigen retrieval was performed using citrate buffer (pH 5.98) which enabled the antibodies to access the target proteins within the tissue and separate the crosslinks that were formed during fixation (63). This technique was highly beneficial to restore epitope-antibody reactivity. The citrate buffer solution was pre-warmed to around 95°C (10 minutes), and the samples were placed in a glass-beaker filled with hot buffer. The glass-beaker containing tissue sections were microwaved (2 x 5 minutes) at 50% power (filled up with hot buffer in between if the level got low). Thereafter, the sections were cooled down in the buffer solution (20 minutes) at room temperature.

2.3.5 Immunofluorescence labeling

After antigen retrieval, immunofluorescent labeling was employed. The FFPE sections were washed with MilliQ-water (3 x 2 minutes) and washing buffer (TBST; 1X TBS and 0.05% Tween 20) (2 minutes) before incubating in a blocking buffer (1% BSA in TBST) (30 minutes) at room temperature. Blocking buffer prevents the unspecific binding of antibodies in the tissue sections. Primary and secondary antibodies were prepared by diluting in blocking buffer according to the optimized concentrations shown in **Table 3** (**Table S2** in Supplementary). The slides were then placed in a wet chamber to avoid drying of the sample during incubation and started with applying primary antibody on the slide and incubated overnight at 4°C.

After overnight incubation, the FFPE slides were washed with washing buffer/TBST (3 x 5 minutes) and PBS (2 x 5 minutes) before secondary incubation (1 hour) at room temperature. All steps from labeling with secondary antibodies were performed under aluminum foil to prevent photobleaching. Thereafter, proceed with washing buffer/TBST (3 x 5 minutes) and PBS (2 x 5 minutes) washing step. Direct fluorescent labeling was used in combination with immunofluorescence labeling to visualize structural features on the tissue according to **Figure 9**.

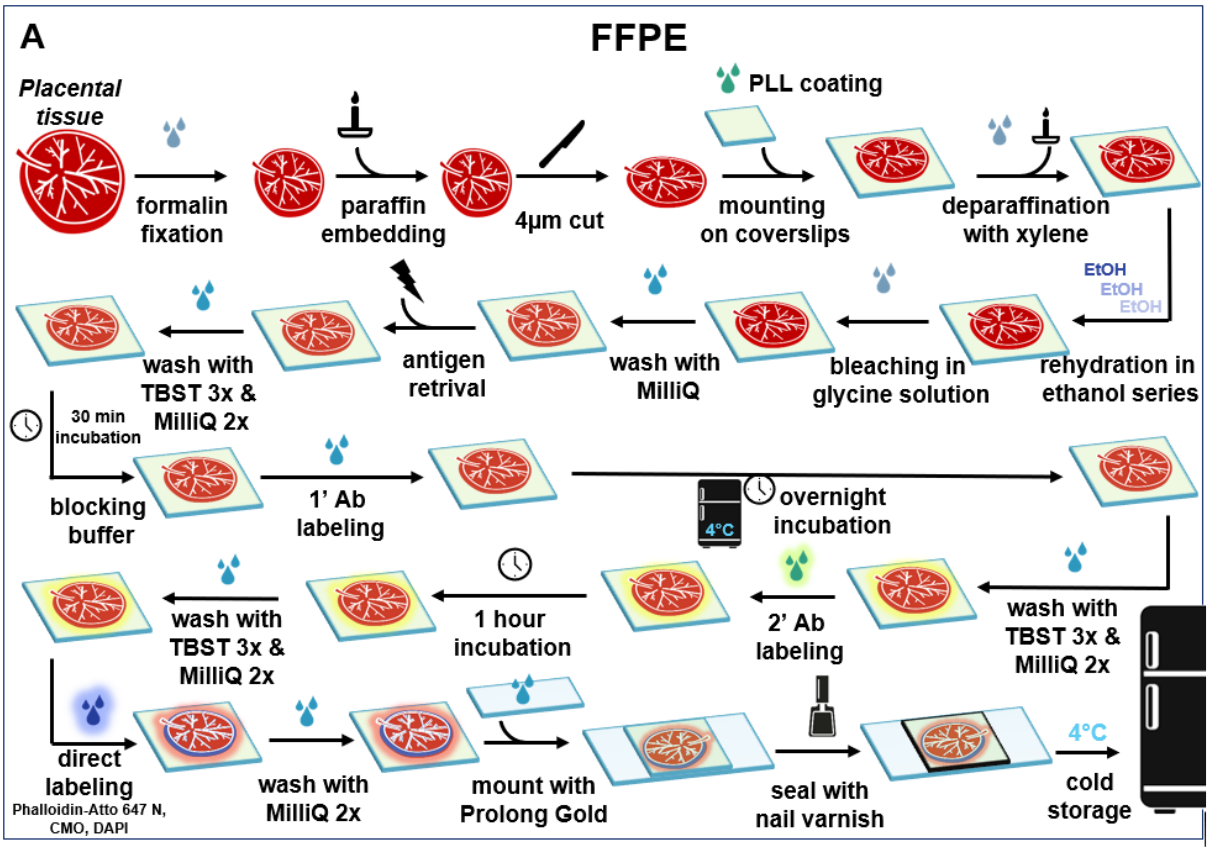

Figure 9 Sample preparation for FFPE sections using indirect labeling technique. *Enlarged and modified image from Figure 8.*

2.3.6 Direct fluorescence labeling

Figure 10 represents the preparation of fluorescence labeling for FFPE sections. For fluorescence labeling, antigen retrieval was not included as fluorescence dyes can bind to the target structure directly. The following steps were performed under aluminum foil to prevent photobleaching of the fluorescence dyes. After deparaffinization and rehydration, the FFPE samples were directly incubated with phalloidin-Atto 647 N for F-actin staining (15 minutes), then washed with PBS (2 x 5 minutes) before labeling with CellMask Orange (CMO) for membrane staining (15 minutes). The slides were again washed with PBS (2 x 5 minutes) and then incubated in DAPI for nuclei staining (15 minutes). The labeled slides were finally washed with MilliQ water (2 x 5 minutes) to remove any dyes left on the slide. The FFPE samples were thereafter mounted and sealed according to **section 2.3.8**.

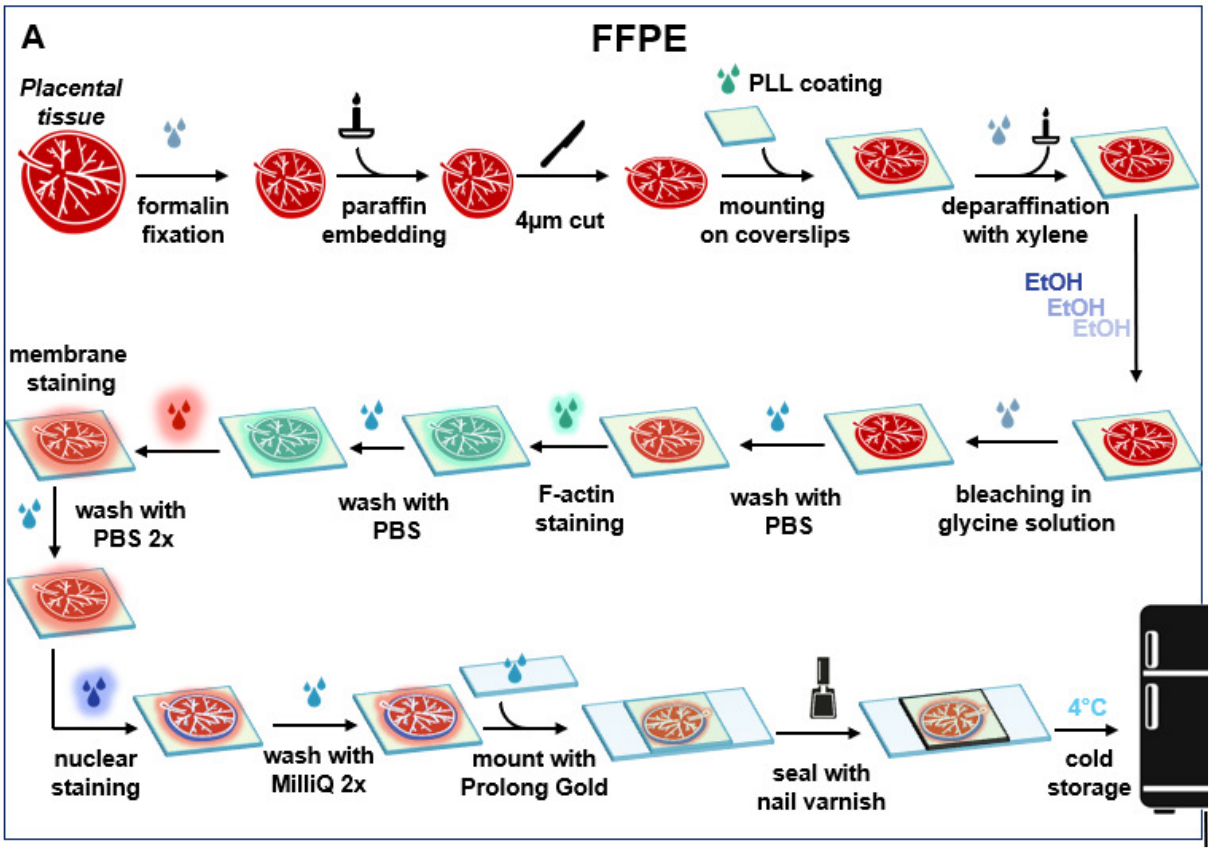

Figure 10 Sample preparation for FFPE sections using direct labeling technique. *Enlarged and modified image from Figure 8.*

2.3.7 Multiple immunofluorescence labeling

In addition to direct and indirect labeling techniques, multiple labeling technique (MLT) was also performed and optimized for FFPE- and cryo-sections. This technique is widely used to identify co-localization, different cell populations, or to obtain multiple antigen localization within the tissue or sample. However, some criteria were required in multiple labeling using the indirect method. It involved using primary antibodies and secondary antibody conjugates raised in different species of animals to successfully get the result without cross-reaction complications. The other criteria were to use secondary antibodies conjugated to different fluorochromes (92). For this study, the first labeling technique (mixed technique) implied mixing two primary antibodies and labeling the tissue section before incubation overnight (**Figure 11**). Thereafter, the tissues were labeled with mixed secondary antibodies and incubated for 1 hour. The second technique (sandwich technique) indicated labeling with one biomarker before labeling with the second biomarker according to **Figure 11**. The labeled FFPE sections were thereafter mounted and sealed according to **section 2.3.8**.

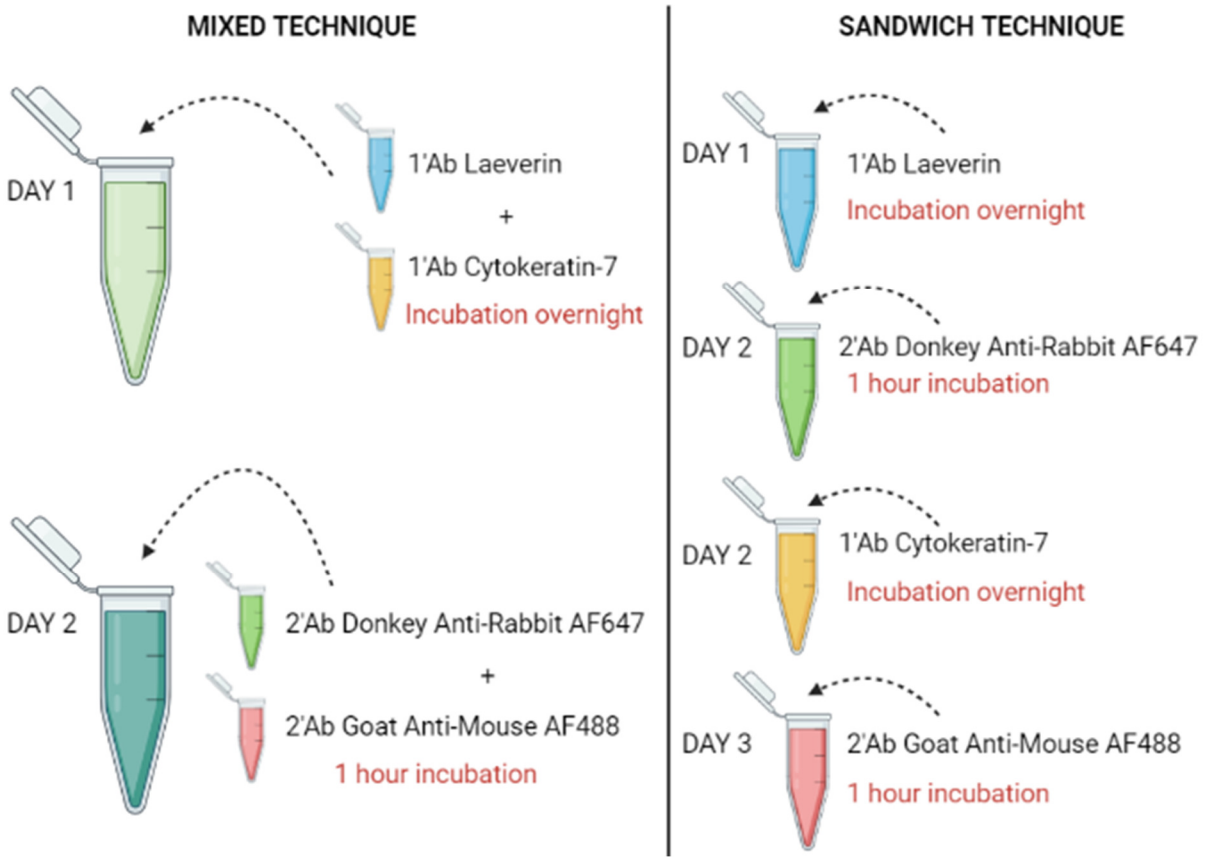

Figure 11 Schematic representation of two types of multiple labeling techniques*. The first technique is called the mixed technique: mixing two biomarkers in one solution and labeled them together. The second technique is called the sandwich technique: labeling with one biomarker before labeling with the second biomarker. Schematic image made with BioRender.com.*

2.3.8 Mounting and sealing

The excess liquid of the FFPE glass slides with the labeled tissue sections was aspirated and mounted with Prolong Gold to prevent photobleaching and to closely match the refractive index of the objective lens. The mounted slides were then covered with #1.5 Poly-L-Lysine coated coverslips and sealed with dental glue Picodent twinsil 22 (1:1 mixture of solution A and B). Then, stored at 4 °C protected from the light until further use.

2.4 Tissue preparation of cryosections

The cryo-sections were prepared using the Tokuyasu method. The Tokuyasu method is a simple protocol that includes simple chemical fixation, snap-freezing in presence of sucrose, cutting into 100-400 nm cryo-sections, then labeling and storage at 4ºC until further use (93, 94).

2.4.1 Fixation of cryosections

The collected tissues (REK Nord ref.# 2010/2058-4) were macro-dissected approximately 3 cm beside the umbilical cord on the fetal side and 3 cm from the peripheral side at the maternal side to obtain the maternal and fetal side of the placenta tissue (48, 95). The placental samples were rinsed with 9 mg/mL sodium chloride to remove the remaining maternal blood and frozen at high pressure (EMPACT 2 HPF; Leica Microsystems, Vienne, Austria) to prevent crystallization of ice (more details Nystad *et al*., 2014 (48)). Tissue samples were infiltrated in 5 mL of 1 x PIPES-HEPES-EGTA-Magnesium sulfate (PHEM) buffer (see **Table S1** for chemicals used to make the 1x PHEM buffer**).** PHEM is a non-toxic buffer (pH 6.96) used for preserving the cell structure as it gives better ultrastructural preservation by stopping the enzymes from digesting the tissue (96). Placental samples were further dissected into 1 mm^3 and immersed in 5 mL 8% paraformaldehyde (PFA) in PHEM buffer and incubated at 4ºC overnight (94).

2.4.2 Storage in liquid Nitrogen

The overnight fixed tissue samples were washed in 5 mL 1M PBS (2 x 5 minutes) following immersion in 12% gelatine at 37 ºC in a Tube Rotator B7925 (Agar Scientific Ltd.) for 1 hour. The 12% gelatine immersed tissue samples were incubated in 0.12% glycine and infiltrated in 1 mL 2.3 M sucrose overnight at 4ºC on a tube rotator to avoid crystallization during the freezing process. The samples were assembled into specimen pins and stored in liquid Nitrogen. Before transferring the tissue sample to the pin, a small drop of 2.3 M sucrose was applied to each specimen pin to enhance attachment of the specimen and placed in cryogenic vials before storage in a liquid nitrogen tank.

2.4.3 Cryo-sectioning

To obtain high-quality cryo-sections, an experienced engineer cut the snap-frozen samples into 100-400 nm thick slices using a cryo-ultramicrotome (EMUC6 ultramicrotome, Leica Microsystems, Vienna, Austria). The sectioned samples were collected with a wire loop and transferred on #1.5 Poly-L-Lysine coated coverslips. Sucrose infiltration was performed to prevent crystallization into ice by disrupting the water molecule interaction. This was

performed by applying 2% methylcellulose and 2.3 M sucrose on the tissue specimen placed on the coverslips to prevent structure collapse, shrinking, and minimize cell deformation. The sections were then placed on a parafilm-covered clean petri dish for storage at 4°C until further use.

2.4.4 Immunofluorescence labeling

Figure 12 represents the protocol for immunofluorescence labeling on cryo-sections. The cryo-sections were prepared on a parafilm-covered metal plate. To make sure the methylcellulose-sucrose mixture was dissolved, the coverslips were warm washed with PBS (3 x 20 min) on a heating plate at 40°C. The immunofluorescence labeling protocol was performed at room temperature and started with incubating the tissue in blocking buffer (30 minutes), washed in PBS (2 x 5 minutes), incubated in primary antibody (1 hour) and then washing with PBS (2 x 5 minutes). All steps from labeling secondary antibodies were performed under aluminum foil to prevent photobleaching. The tissue sections were incubated in secondary antibody (1 hour) at room temperature and washed with PBS (2 x 5 minutes). The sections were then labeled with CMO and DAPI via direct fluorescent techniques to visualize the membranes and nuclei, respectively. Thereafter, the labeled cryo-sections were washed with MilliQ-water (2 x 5 minutes) and prepared for mounting and sealing according to **section 2.4.6**.

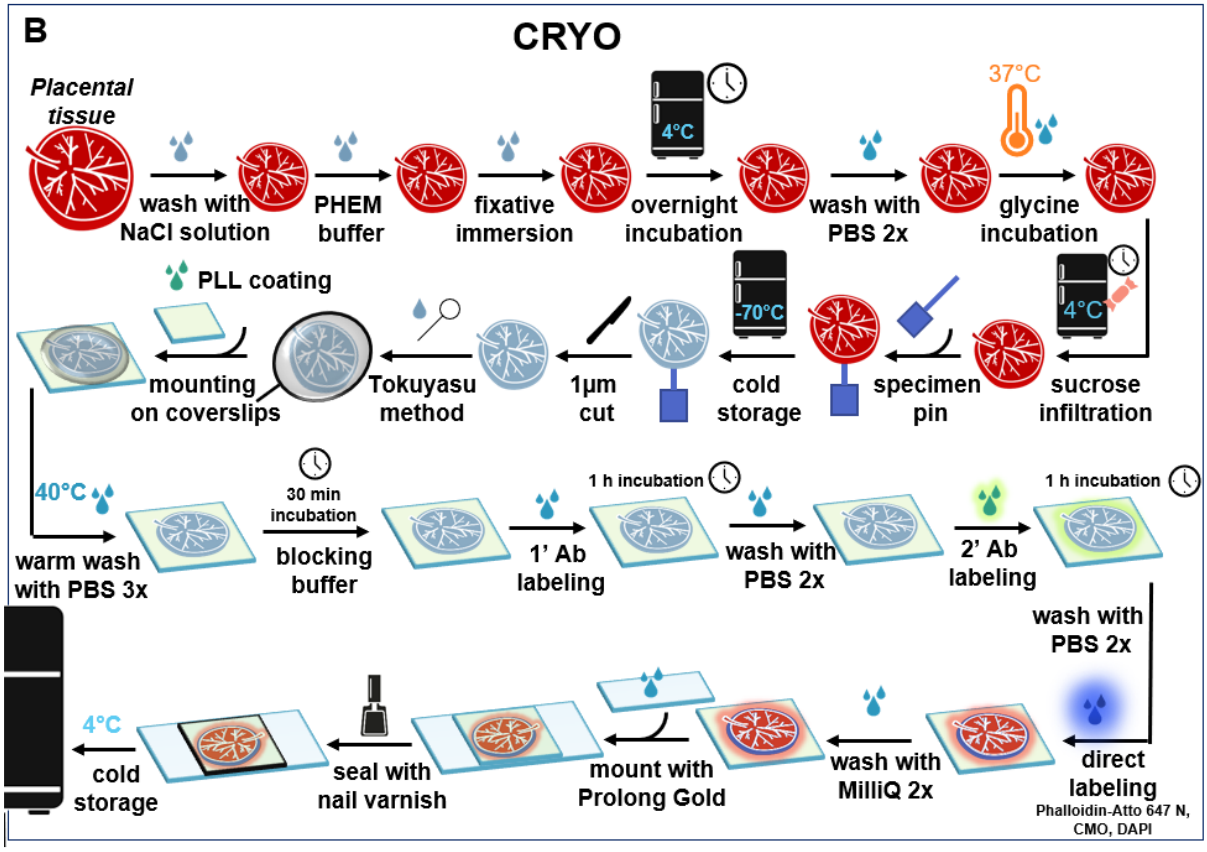

Figure 12 Sample preparation for cryo-sections using indirect labeling technique. *Enlarged and modified image from Figure 8.*

2.4.5 Direct fluorescence labeling

Figure 13 represents the protocol for fluorescence labeling on cryo-sections. The labeling process for the cryo-sections was similar to the FFPE fluorescent labeling technique. The same reagents and dyes were used including the dye concentration presented in **Table 3**. Direct fluorescence labeling started with incubation in phalloidin-Atto 647 N (10 minutes), then washed with PBS (2 x 5 minutes) before labeling with CMO (10 minutes). The cryo-sections were washed again with PBS (2 x 5 minutes) and incubated in DAPI (10 minutes). The labeled sections were then washed with MilliQ-water (2 x 5 minutes) and prepared for mounting and sealing according to **section 2.4.6**.

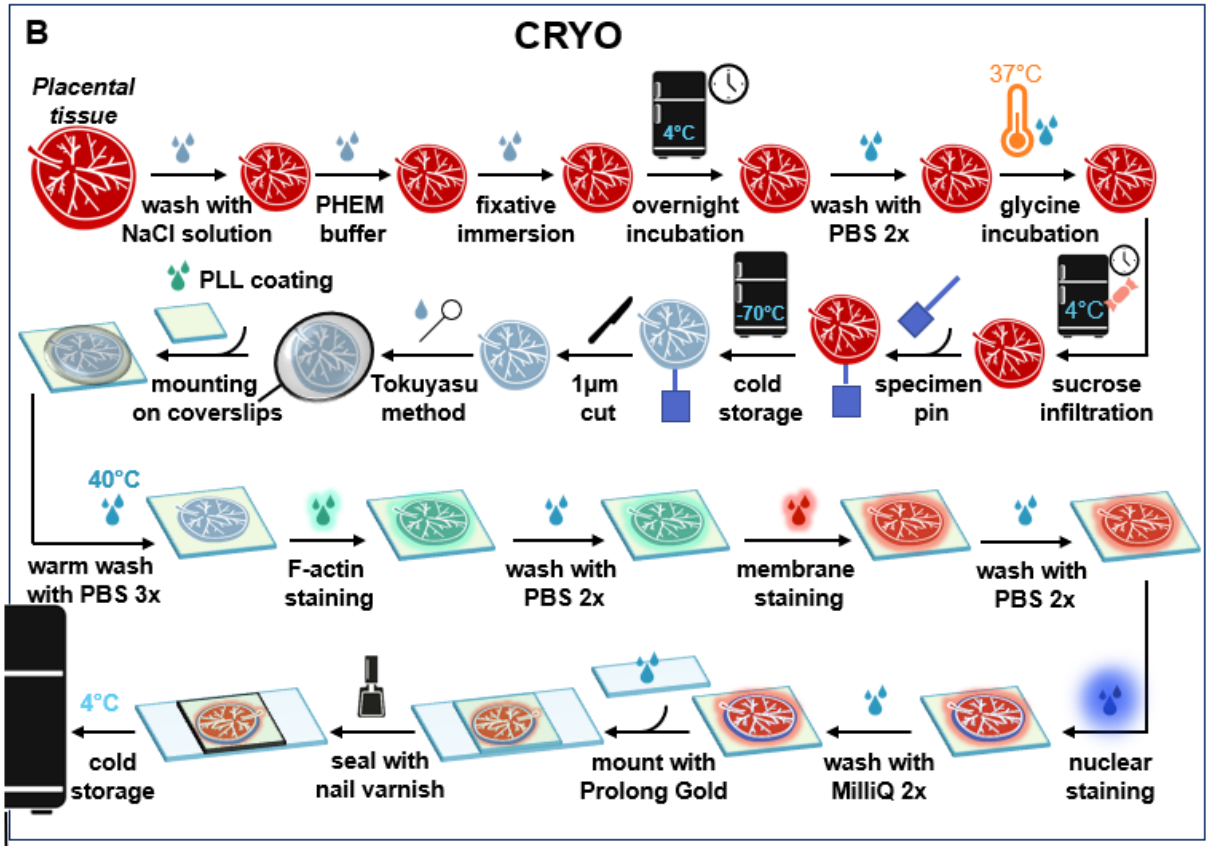

Figure 13 Sample preparation for cryo-sections using direct labeling technique. *Enlarged and modified image from Figure 8.*

2.4.6 Mounting and sealing

The excess liquid from the cryo-sections were aspirated before mounting with Prolong Gold Antifade Mountant in the center of the microscopy glass slide and placed the sample facing the mounting medium. The excess mounting medium was removed by tapping gently on top of the slides and aspirated the excess on the edges of the coverslip. The visible air bubbles were also removed by tapping gently with a plastic tweezer. The slides with the sample on were then sealed with dental glue Picodent twinsil 22 (1:1 mixture of solution A and B) and stored at 4°C protected from the light until further use.

2.5 Microscopy

For this study, 3 advanced fluorescence microscopes were used. The Olympus VS120 whole-slide scanner Microscope (Olympus Life science, Massachusetts, USA), the DeltaVision Elite High-resolution Microscope (GE Healthcare, Chicago, USA), referred to as DV microscope, and the DeltaVision OMX V4 Blaze (GE Healthcare, Chicago, USA), referred to as the OMX microscope. The Olympus and DV microscopes were used to acquire a large field of view (FOV) fluorescent images, whereas the DV and the OMX microscopes were used to generate high-resolution (deconvolution) and super-resolution (SIM) images, respectively.

2.5.1 Whole-slide scanner

Olympus VS120 is a whole-slide scanning microscope that allows multicolor imaging of fluorescently-labeled samples in manual and automated mode (97). For a large field of view (FOV), a 20X/NA 0.75 objective lens (Olympus, Tokyo, Japan) was used. The image acquisition was performed by a specialized technician at the Advanced Microscopy Core Facility, UiT. Further, whole-slide scanning images were reconstructed and processed using Olympus Soft Imaging Solution GmbH software.

2.5.2 DV and OMX

The labeled slides were gently cleaned with 70 % ethanol to make sure the coverslip was dust-free and cleaned before microscopy. The labeled and non-labeled samples were imaged on the DV microscope with four channels (**Table 2**). Started with a 20X/NA 0.75 objective lens to generate a large FOV. Then, progressively increased the magnification to 60X/NA 1.42 oil-immersion objective lens to identify regions of interest (ROI). Used the same coordinates of the ROI on the OMX microscope with 60X/NA 1.42 oil-immersion objective lens, three sCMOS cameras, including four channels to obtain high-resolution and super-resolution microscopy images.

Table 2 Overview of excitation wavelength and emission filter for the four channels in the OMX microscope.

Channels	Excitation wavelength [nm]	Emission filter [nm]
Channel 1	642	683/40
Channel 2	568	609/37
Channel 3	488	528/48
Channel 4	405	436/31

To ensure that the refractive index of the immersion oil matched that of the coverslip, a PSF optimization was required. PSF optimization was carried out by orthogonal visualization of single emitters on diverse z-stacks acquired with immersion oils of different refractive indices (**S4** in Supplementary). The PSF of single emitters was monitored in the orthogonal view of the constructed images until symmetrical shapes were obtained. This was essential as a mismatch can lead to artifacts in the reconstructed images. Following, the generated images were reconstructed and processed using SoftWoRx and Fiji, respectively.

2.6 Autofluorescence controls

A test to visualize the autofluorescence was performed by following all the steps except labeling on a normal FFPE- and cryo-sections. The unlabeled normal healthy placenta sections were mounted and sealed according to **section 2.3.8** and **section 2.4.6**, respectively. The FFPE- and cryo-sections were then imaged using the DV microscope with a 20X/NA 0.75 objective lens. Autofluorescence control was performed to evaluate and control the fluorescence dyes and their excitation ratio.

2.7 Quantitative analysis

The quantification analysis was performed on placental features independently localized using large FOV images generated from Olympus VS120 microscope and DV microscope. A grid was placed above the large FOV image. Then, the placental features were counted on each box using naked eyes (**Figure 14**).

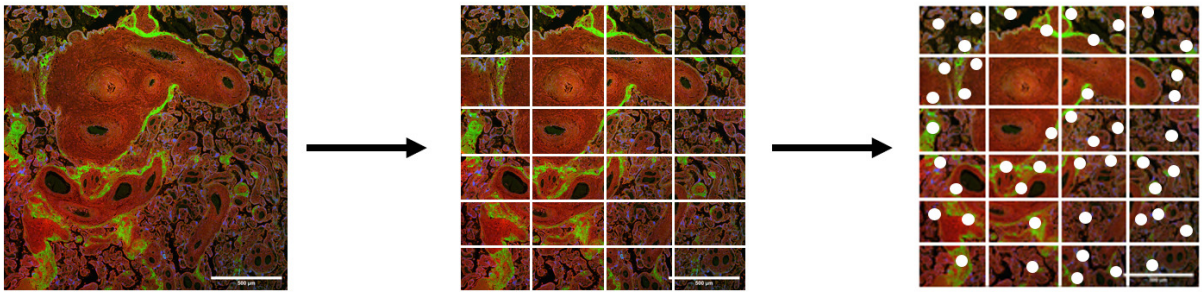

Figure 14 Methodology for quantitative analysis. *The quantitative measurements of placental features were characterized by using a large field of view (FOV) image. A grid was placed above the large FOV image. The placental features were identified by counting the presence of the features in each box with naked eyes.*

3 Results

The results were obtained from two stages of research (**Figure 15**). Stage 1 included optimization of the methods for FFPE- and cryo-sections which was 75% of the research time. The placenta samples of FFPE sections (normal n=1 and PE n=1) and cryo-sections (normal n=1 and PE n=1) were used for the optimization stage. DV microscope and OMX microscope were used to generate large FOV, high-resolution (DV) and super-resolution (SIM), respectively, for quality and optimization control of the labeled sections. Stage 2 took 25% of the research time. This part included morphology study of FFPE sections from normal (n=5) and PE (n=5) using the Olympus VS120 microscope and the DV microscope to generate large FOV and high-resolution images, respectively. Large FOV was also used for quantitative analysis. The cryo-sections of normal (n=1) and PE (n=1) were used to investigate subcellular- and ultrastructure in high-resolution (DV) and super-resolution (SIM) images generated by the OMX microscope. The morphological investigation was performed using different biomarkers to analyze the morphological and quantitative differences comparing placentas from healthy pregnancies and pregnancies of preeclamptic women.

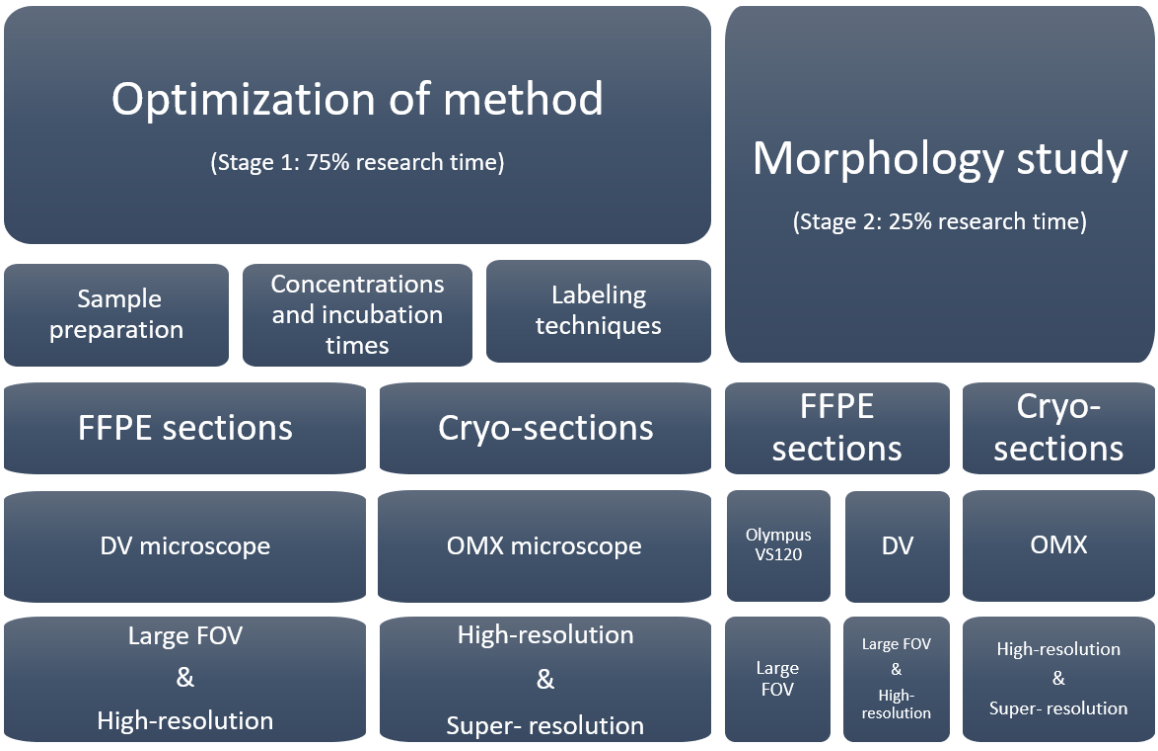

Figure 15 Experimental plan of the master project*. Flowchart representing two stages of the master project. Stage 1 included optimization of the methods on FFPE- and cryo-sections and occupied 75% of the research time. Large FOV and high-resolution images were generated using DV microscope and OMX microscope for super-resolution images. Stage 2 of the study was the morphology investigation of labeled FFPE sections and cryo-sections using Olympus VS120 and DV microscope for generating large FOV and high-resolution (DV) images, respectively. Whereas OMX microscope was used for generating super-resolution (SIM) images. Stage 2 of the thesis took 25% of the research time.*

3.1 Autofluorescence characterization

Autofluorescence was observed in the human placental FFPE sections (**Figure 16**) and cryo-sections (**Figure 17**) in all the fluorescent channels of the microscope, with maximum signal strength (50% excitation intensity and $50ms$ acquisition time). More details of excitation wavelength and emission filters for the different channels are presented in **Table 2**. Natural autofluorescence responses from maternal and fetal red blood cells were observed in all channels in the FFPE section but not in the cryo-section.

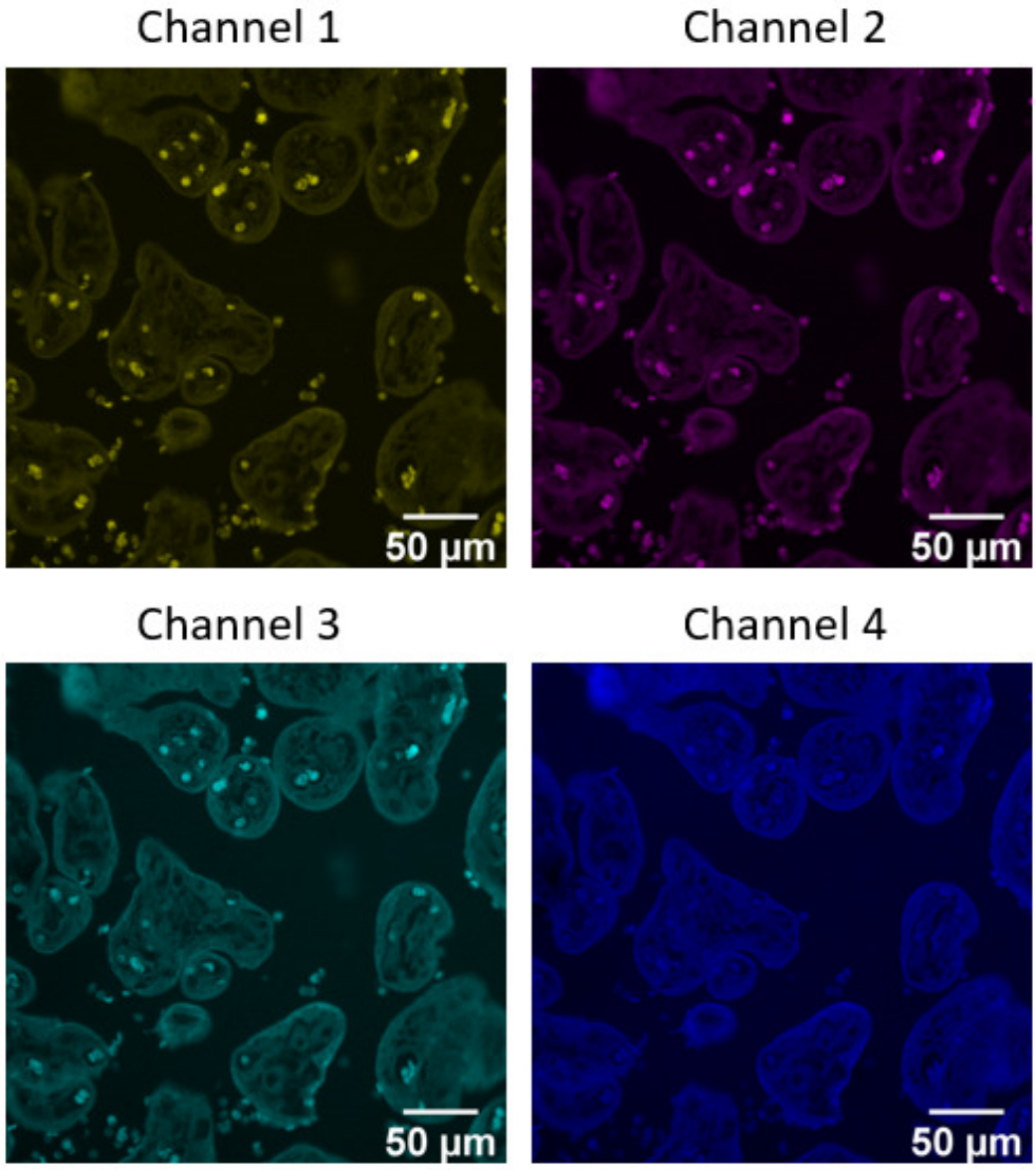

Figure 16 Autofluorescence control of unlabelled FFPE placenta section. *A normal placenta section of 4 µm thickness was used for observation of the autofluorescence response in the four channels. The channels were set to 50% excitation intensity and 50ms acquisition time. Channel 1(yellow) with excitation wavelength 642 nm and the emission filter 683/40nm. Channel 2 (magenta) with excitation wavelength 568nm and emission filter 609/37nm. Channel 3 (cyan) with excitation wavelength 488nm and emission filter 528/48mn. Channel 4 (blue) with excitation wavelength 405 nm and emission filter 436/31 nm. Natural autofluorescence was observed from fetal and maternal red blood cells in all channels.*

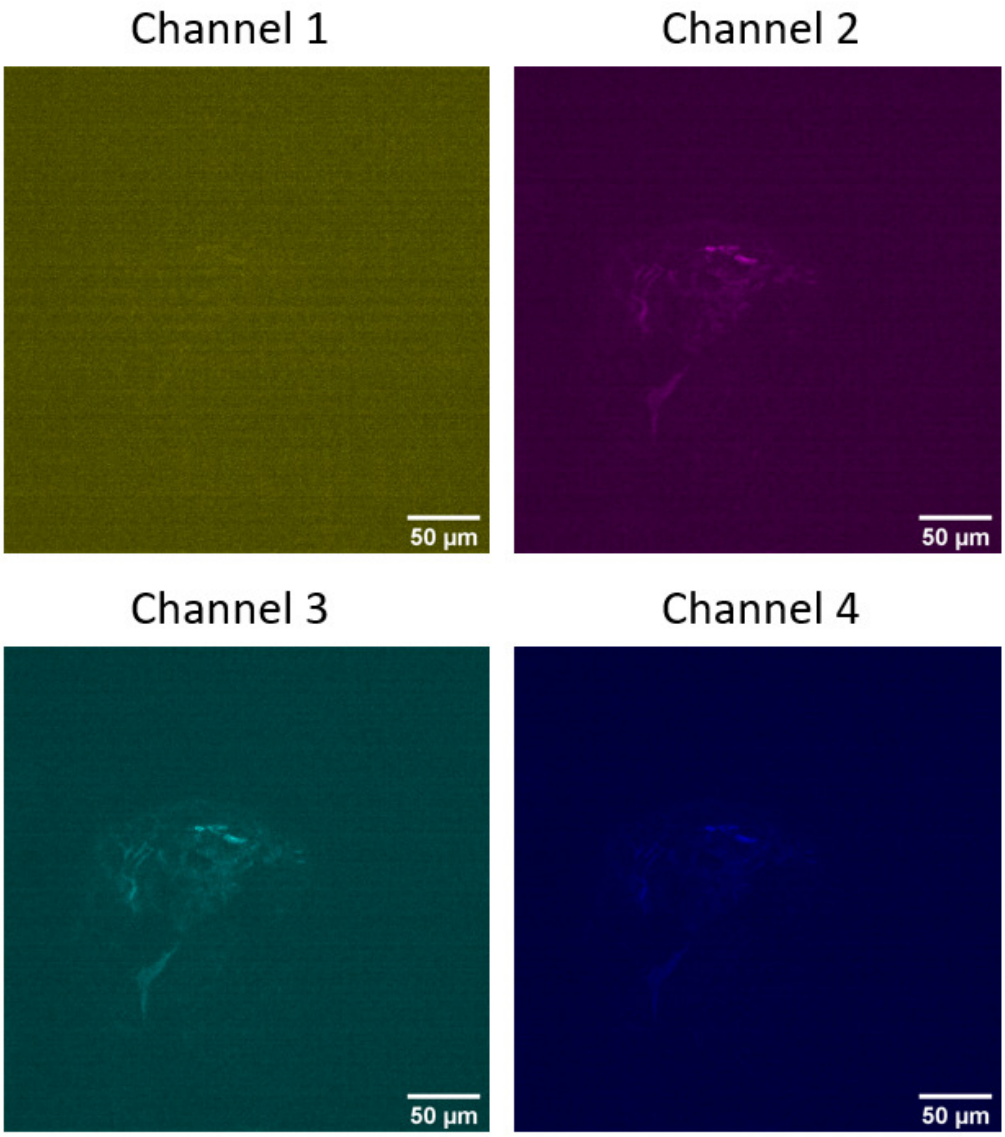

Figure 17 Autofluorescence control of unlabelled cryo- placenta section. *A normal placenta section of 400 nm thickness was used for observation of the autofluorescence response in the four channels. The channels were set to 50% excitation intensity and 50ms acquisition time. Channel 1(yellow) with excitation wavelength 642 nm and the emission filter 683/40nm. Channel 2 (magenta) with excitation wavelength 568nm and emission filter 609/37nm. Channel 3 (cyan) with excitation wavelength 488nm and emission filter 528/48mn. Channel 4 (blue) with excitation wavelength 405 nm and emission filter 436/31 nm.*

3.2 Optimization of concentration and incubation times of markers for FFPE and cryo-sections

Optimization of biomarkers and incubation times of each marker on FFPE- and cryo-sections was required to obtain adequate quality for high-resolution and super-resolution microscopy. It was a lengthy process that took 75% of the research time for this study. Optimized concentrations and incubation times are presented in **Table 3**. The optimized concentrations of the different markers were the same for FFPE- and cryo-sections, whereas the optimized incubation times were different. The optimization of the placental biomarkers included laeverin, CK-7 and PLAP, as well as fluorescent markers non-specific to placentae such as phalloidin-Atto 647N, CMO and DAPI.

Table 3. List of optimized concentrations and incubation times of markers used in this study for FFPE sections and cryo-sections.

		Markers	Target	Concentrations		Incubation times	
						FFPE[9] sections	Cryo-sections
Indirect labeling	Placental biomarkers	Laeverin	hTB[5] plasma membrane	1:100	Diluted in BB[7]	Overnight	1 hour
		CK-7[1]	hTB[5] cytoplasm	1:100		Overnight	1 hour
		PLAP[2]	hSTB[6] microvesicles	1:50		Overnight	1 hour
Direct labeling	Fluorescent dyes	Phalloidin-Atto 647 N	F-actin	1:100	Diluted in PBS[8]	15 minutes	10 minutes
		CMO[3]	Membrane	1:2000		15 minutes	10 minutes
		DAPI[4]	Nuclei	1:1000		15 minutes	10 minutes

[1]CK-7: Cytokeratin-7
[2]PLAP: Placental alkaline phosphatase
[3]CMO: CellMask Orange
[4]DAPI: 4′,6-diamidino-2-phenylindole
[5]hTB: human trophoblast cells
[6]hSTB: human syncytiotrophoblast
[7]BB: Blocking buffer
[8]PBS: Phosphate-buffered Saline
[9]FFPE: Formalin-fixed paraffin-embedded

An example of the optimization process for PLAP is shown in **Figure 18**, where cryo-sections were labeled with PLAP (yellow), CMO (magenta), and DAPI (cyan) (see reference #1 in **Table S2** in Supplementary). Cryo-tissue sections were labeled with different concentrations of PLAP antibody (namely 1:50, 1:100, 1:500, and 1:1000). The strongest signals were observed from PLAP 1:50 concentration, compared with the other dilution (1:100 concentration), thus used for comparisons of healthy and PE tissue sections.

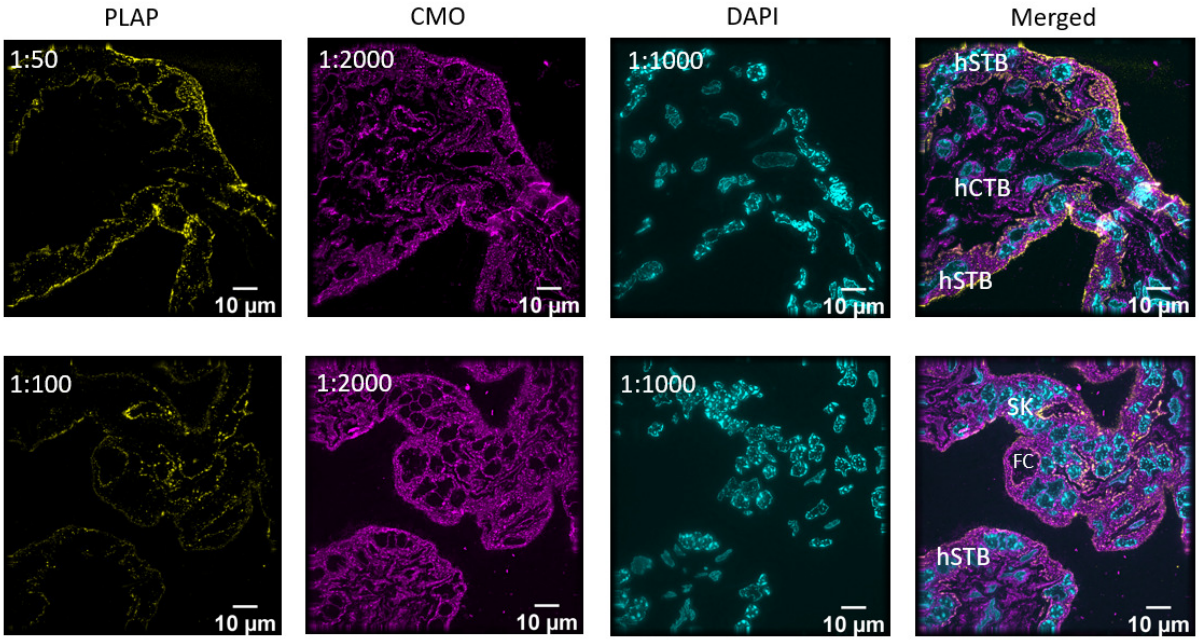

Figure 18 Concentration optimization for PLAP in cryo-sections of healthy placentas. *Syncytial microvesicles stained with PLAP (yellow), membrane stained with CMO (magenta), nuclei staining with DAPI (cyan). One cryo-section of 4 µm thickness was labeled with 1:50 concentration, and the second cryo-section was labeled with 1:100 concentration. The strongest signals were detected from 1:50 concentration compared with the 1:100 concentration. FC: fetal capillary, hCTB: human cytotrophoblast cells, hSTB: human syncytiotrophoblast. CMO: CellMask Orange, DAPI: 4',6-diamidino-2-phenylindole, PLAP: placental alkaline phosphatase.*

3.3 Optimization of multiple labeling technique

In addition to improvement and optimization of biomarker concentrations and incubation times, optimization of the multiple labeling technique (MLT) was also part of this study. MTL was investigated to obtain high-quality and optimal labeling using two different biomarkers in the same placental tissue sample. Normal placenta FFPE tissue sections of 4 µm thickness were labeled using the mixed technique and the sandwich technique of MLT (see **Figure 11** and reference #2 in **Table S2** for details). High-resolution images were generated using a DV microscope with a 60X/NA 1.42 oil-immersion objective lens. The experiment showed similar results for both techniques using laeverin and CK-7 as biomarkers focusing on the syncytiotrophoblast membrane of the chorionic villi (**Figure 19**). The sandwich technique included 3 days of preparation, whereas the mixed technique was only 2 days of preparation. Thus, the mixed technique was deduced to be more efficient for MLT.

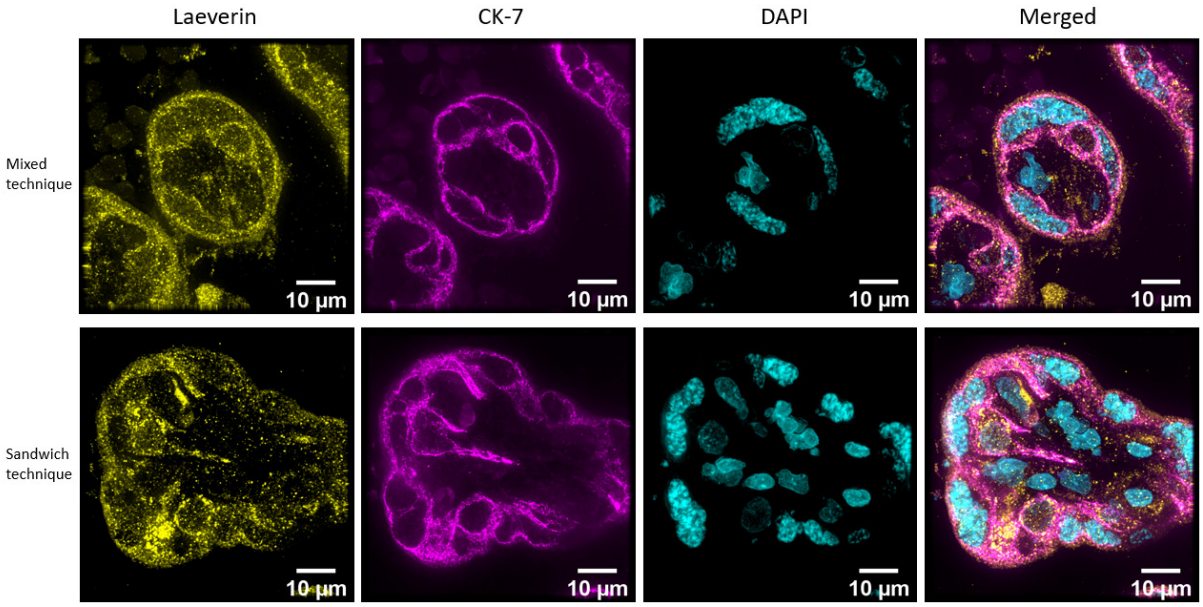

Figure 19 Two different multiple labeling techniques were performed on 4µm thick FFPE normal healthy placenta sections. *Mixed technique: a high-resolution deconvolved image of syncytiotrophoblast located at the terminal villi in normal healthy human placenta tissue with 60X magnification using mixed labeling technique. Sandwich technique: high-resolution deconvolution image of syncytiotrophoblast in normal healthy human placenta tissue of the same magnification using the sandwich labeling technique. Laeverin (yellow), CK-7 (magenta), and nuclei (cyan). DAPI: 4',6-diamidino-2-phenylindole, MLT: multiple labeling technique, CK-7: cytokeratin-7.*

3.4 Large FOV imaging of chorionic villi

The FFPE placenta tissue sections of 4 µm thickness from normal (n=5) and PE (n=5) placentas were immunofluorescence-labeled with CK-7 (green) for human trophoblast cytoplasm staining, CMO (red) for membrane staining and DAPI (blue) for nuclei staining (see reference #3 in **Table S2**). A large FOV was generated using a DV microscope with a 20X/NA 0.75 objective lens (**Figure 20**). Various parts of chorionic villi such as stem villi (SV) and terminal villi (TV) were observed in both healthy (**Figure 20A**) and preeclamptic (**Figure 20B**) placentas. In addition, syncytial knots (SK) (arrowhead) were identified in the large FOV images.

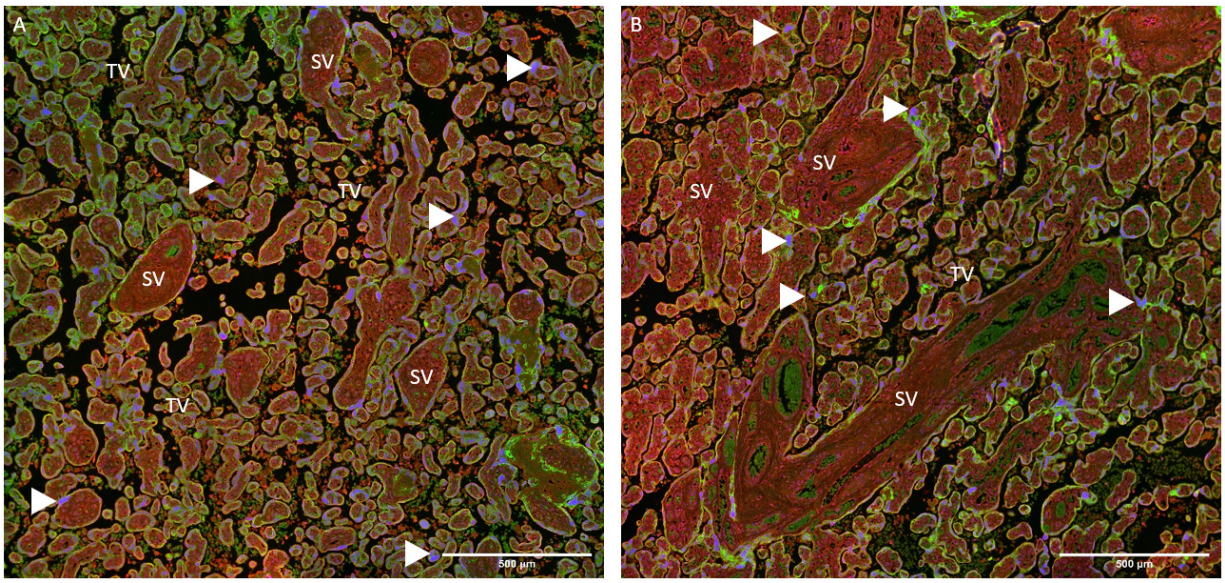

Figure 20 Large FOV of normal and PE human chorionic villi. *(A) A large FOV image of a normal placenta with a 20X/NA 0.75 objective lens. (B) A large FOV of a preeclamptic placenta with a 20X/NA 0.75 objective lens. Human trophoblast cytoplasm was stained with CK-7 (green), membrane stained with CMO (red), and nuclei counterstained with DAPI (blue). CK-7: cytokeratin-7, DAPI: 4',6-diamidino-2-phenylindole, FOV: field of view, SV: stem villi, TV: terminal villi, arrowhead: syncytial knots.*

3.4.1 Actin filament spots found in chorionic villi

The FFPE placenta tissue sections of 4 µm thickness from normal (n=5) and PE (n=5) placentas were direct fluorescence-labeled with phalloidin-Atto 647 N (magenta), CMO and DAPI (blue) for actin, membrane and nuclei staining, respectively, according to reference #4 in **Table S2** in Supplementary. The large FOV images generated by Olympus VS120 with 20X/NA 0.75 objective lens not only provided an overview of the chorionic villi (hCV) but also revealed actin filament localization in the preeclamptic placenta tissue section (**Figure 21**). For better visualization of the morphology, the CMO channel was turned off in **Figure 21.** F-actin filaments were observed at the basement membrane of the chorionic villi and in the terminal web regions of the placenta villi in both normal (**Figure 21A,B**) and PE placentas (**Figure 21C,D**). Additionally, several actin filament spots were observed randomly and independently localized at the hCV in both normal (**Figure 21A**) and PE sections (**Figure 21C**).

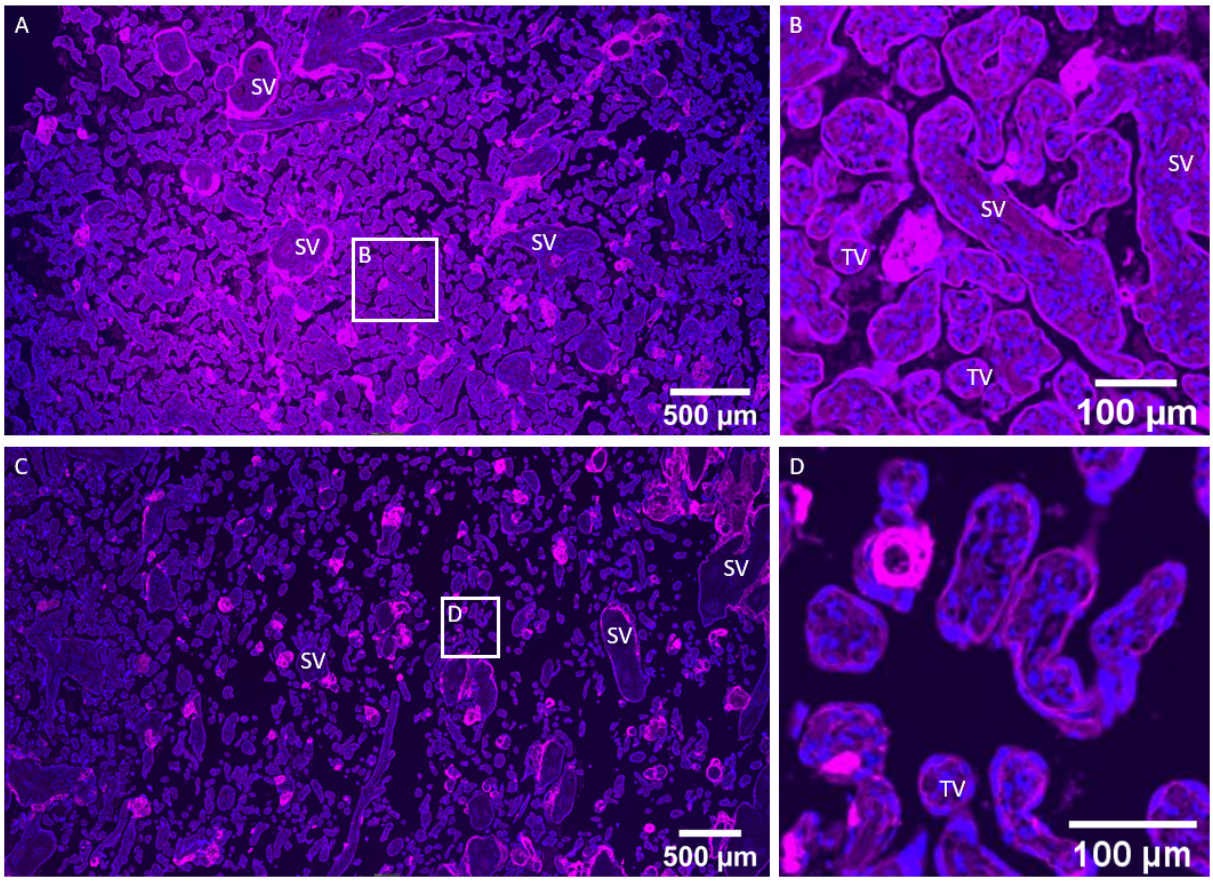

Figure 21 F-actin filament present in 4 µm thick normal and PE chorionic villi*. F-Actin labeled with phalloidin-Atto 647 N (magenta), and nuclei counterstained with DAPI (blue). (A-D) Olympus VS120 images with 20X/NA 0.75 objective lens. (A) Normal FFPE section. Actin spots are located randomly and independently of each other in the chorionic villi. (B) A magnified region from (A). F-actin is located in the basement membrane of hCV and actin spots are also identified. (C) Preeclamptic FFPE section. Actin spots are located randomly and independently of each other in the chorionic villi. (D) A magnified region from (C). F-actin is located in the basement membrane of hCV and actin spots are also identified. DAPI: 4',6-diamidino-2-phenylindole, FOV: field of view, SV: stem villi, TV: terminal villi, hCV: human chorionic villi, hSTB: human syncytiotrophoblast.*

3.4.2 No significant differences of actin spots in normal and PE placentas

Quantitative analysis was performed to identify the number of actin spots present in normal and PE placenta tissues. The analysis was performed according to **Figure 14**. The quantitative measurement was performed to understand the specific localization of actin spots expression. **Table 4** represents the quantitative analysis of actin spots localized randomly and independently in normal and PE chorionic tissues. The actin spots were identified in different subtypes within the chorionic villi in both normal (n=5) and PE (n=5) placenta tissue sections. The *p*-value was estimated using Student's t-test. The mean *p*-value was higher than 0.05 for the actin spots localization in the different subtypes in the chorionic villi. This indicates no significant difference between normal and PE placentas.

Table 4 Quantitative analysis of actin spot localization in normal and PE tissue.

Actin spots localization	Mean value		
	Normal (n=5)	PE[5] (n=5)	*P* value
TV[1]	146	178	0.55
MIV[2]	46	21	0.50
IIV[3]	12	27	0.54
SV[4]	44	76	0.47

[1]TV: Terminal villi
[2]MIV: Mature intermediate villi
[3]IIV: Immature intermediate villi
[4]SV: Stem villi
[5]PE: Preeclamptic placenta

3.4.3 An increased amount of syncytial knots in PE

A quantitative study of syncytial knots presence in PE and normal chorionic villi was identified by naked eyes according to **Figure 14**. The FFPE samples of normal (n=5) and PE (n=5) placenta were labeled using CK7 (green), CMO (red), and DAPI (blue) according to reference #3 in **Table S2** in Supplementary. Large FOV images of immunofluorescent-labeled normal (n=5) placenta sections and PE (n=5) placenta sections were used to quantify the syncytial knots. **Table 5** represents the number of syncytial knots quantified. In normal placentas were 427 syncytial knots identified, whereas 689 syncytial knots were present in PE placentas. The mean *p*-value of 0.015 was estimated using Student's t-test. The *p*-value is lower than 0.05 which indicates that there are significant differences between PE and normal placentas.

Table 5 Overview of the number of syncytial knots observed in normal and preeclamptic term placentas.

	Mean value		
	Normal (n=5)	PE[2] (n=5)	*P* value
SK[1]	427	689	0.015

[1]SK: Syncytial knots
[2]PE: Preeclamptic placenta

3.5 Different contrast from FFPE- and Cryo-section

Healthy full-term placenta of FFPE sections of 4 µm thickness and cryo-section of 400 nm thickness were labeled using phalloidin-Atto 647N (yellow), CK-7 (magenta) and DAPI (cyan) (see reference #5 in **Table S2**). Microscopy images of the tissue sections were generated using the DV microscope with a 60X/NA 1.42 oil-immersion objective lens to obtain high-resolution images. The representative images of the FFPE section and cryo-section are presented in **Figure 22**. The high-resolution images allowed for observation of placental compartments such as terminal villi (TV), human syncytiotrophoblast (hSTB) and fetal capillaries (FC) in both sections. The FFPE section showed background signals and artifacts including decreased contrast (**Figure 22A**), whereas enhancement of contrast and signal detection was observed in the cryo-sections (**Figure 22B**). Additionally, finer structural details were observed in the cryo-section image compared to the FFPE images.

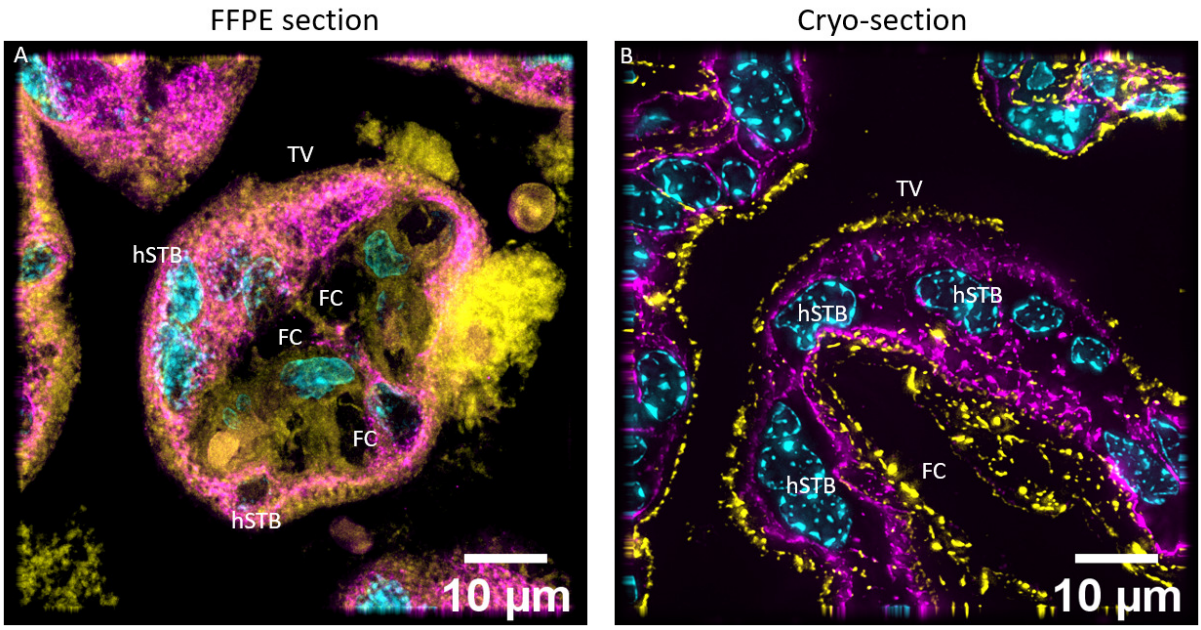

Figure 22 High-resolution deconvolved image of normal placental chorionic terminal villi. *F-actin stained with phalloidin-Atto 647 N (yellow), CK-7 (magenta), and nuclei labeled with DAPI (cyan). High-resolution image generated by DV microscope with 60X/NA 1.42 oil-immersion objective lens. TV, hSTB, and FC were identified in both sections. (A) High-resolution image of FFPE section. (B) High-resolution image of cryo-section. Contrast and signal enhancement in cryo-section compared to FFPE-section. DAPI: 4',6-diamidino-2-phenylindole, CK-7: cytokeratin-7, FC: fetal capillaries., hSTB: human syncytiotrophoblast, TV: terminal villi.*

3.6 High-resolution vs super-resolution of chorionic villi

PE human placenta cryo-section of 100 nm thickness was labeled using CMO (magenta) and DAPI (cyan) (see reference #6 in **Table S2).** High-resolution (DV) and super-resolution (SIM) images were generated using an OMX microscope with a 60X/NA 1.42 oil-immersion objective lens (**Figure 23**). Microscopy images of DV (**Figure 23A**) and SIM (**Figure 23B**) allowed for visualization of chorionic villi morphology in PE placenta tissues. The DAPI channel was turned off due to better visualization of the membrane structures. The images show membrane staining in magenta.

DV and SIM images show similar results in terms of signal detection and contrast of the placental tissues. Placental features were identified in both images such as hSTB, syncytial plasma membrane and fetal capillaries (FC) located inside the chorionic villi. The high-resolution images were generated by deconvolution. The DV images show great contrast and signal detection. Super-resolution images were generated by SIM reconstruction. The SIM images show enhancement in contrast and resolution, allowing the identification of subcellular structures such as the syncytial microvilli brushborder located at the apical surface of the syncytial plasma membrane (**Figure 23D)**. In comparison, these features are not discernible on the DV images (**Figure 23C**).

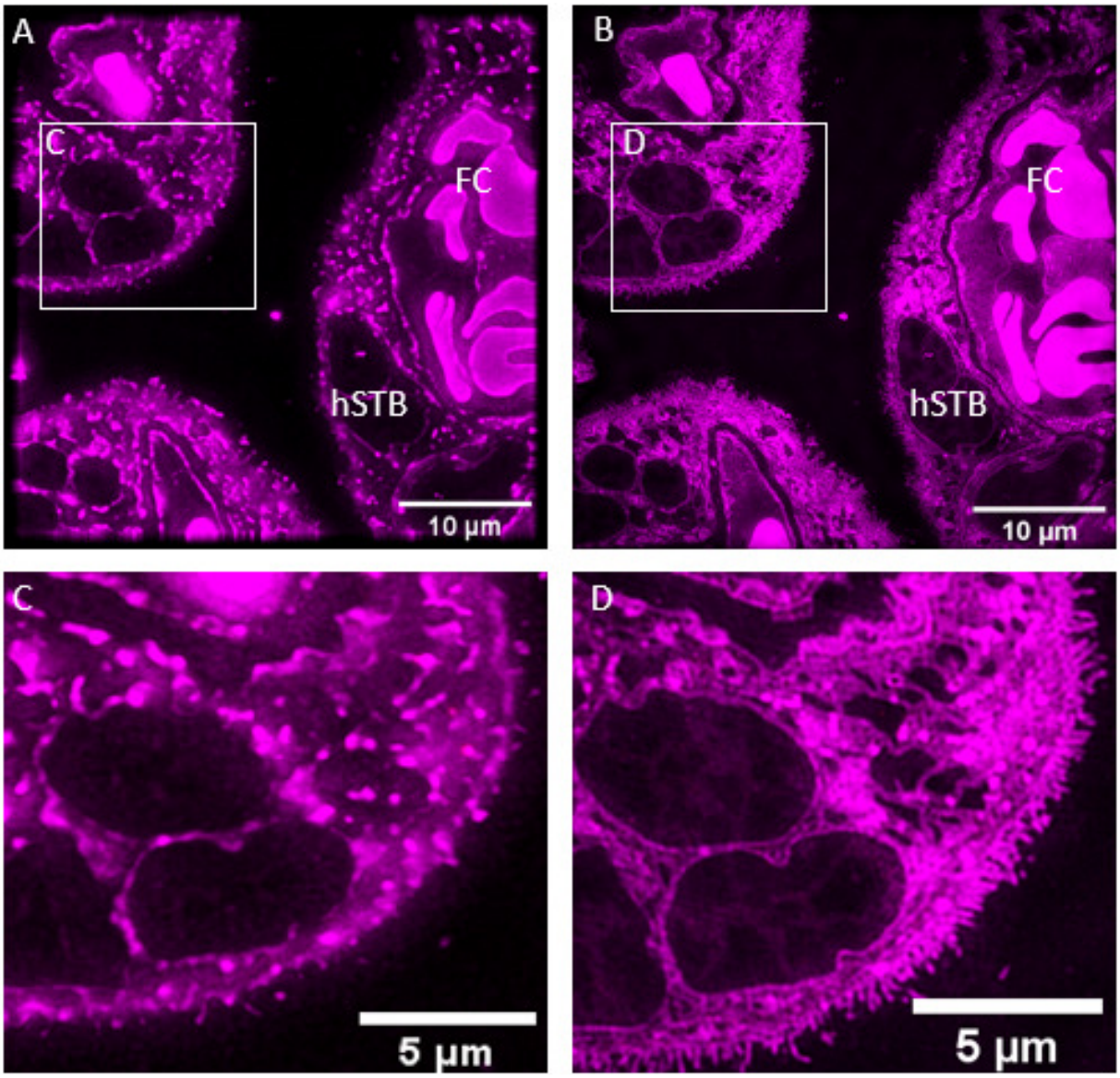

Figure 23 Comparison of high-resolution and super-resolution of hSTB in PE placenta tissue. *DV images and SIM images generated by OMX microscope with 60X/NA 1.42 oil-immersion objective lens. Membrane staining in magenta. (A) DV images of hCV in PE placenta. (B) SIM image of hCV in PE placenta. (C) Magnified DV image of the boxed region in (A). High-resolution and contrast enhancement is obtained, hence structures not easily distinguishable (D) Magnified SIM image of the boxed region in (B). SIM image allows for higher resolution and structural observation of placental membrane which allows for visualization of chorionic microvilli. FC: fetal capillary, hSTB: human syncytiotrophoblast cells, hCV: human chorionic villi.*

3.7 Microvilli identified by super-resolution imaging

Normal and PE placenta cryo-sections of 100 nm thickness were direct fluorescent-labeled with CMO and DAPI according to reference #6 in **Table S2** in Supplementary. The reconstructed SIM images were generated using an OMX microscope with a 60X/NA 1.42 oil-immersion objective lens. Super-resolution images were generated and the representative image show membrane staining in magenta (**Figure 24**). The contrast enhancement provided by SIM allows for a clearer observation of placental morphology. The membranes and nuclear structures are well observed in the representative image. The structures of membranes are easily distinguishable and allow for fine details in the magnified images (**Figure 24C-D**).

The SIM images show human chorionic villous in normal (**Figure 24A**) and PE (**Figure 24B**) placentas. Fetal capillaries (FC) and human syncytiotrophoblast (hSTB) are identified. SIM images allow the visualization of ultrastructural details of the placental morphology. The magnified images from **Figure 24A** and **Figure 24B** show normal syncytial plasma membrane and PE syncytial plasma membrane, respectively. The magnified images allow for observing chorionic microvilli (arrow) located at the brushborder of the hSTB in normal (**Figure 24C**) and PE placentas (**Figure 24D**). The microvilli are located at the apical surface of the syncytium which physiologically is in direct contact with the maternal blood. The arrows point to the area of the PE microvilli at the apical surface seems to look disorganized compared to the normal microvilli.

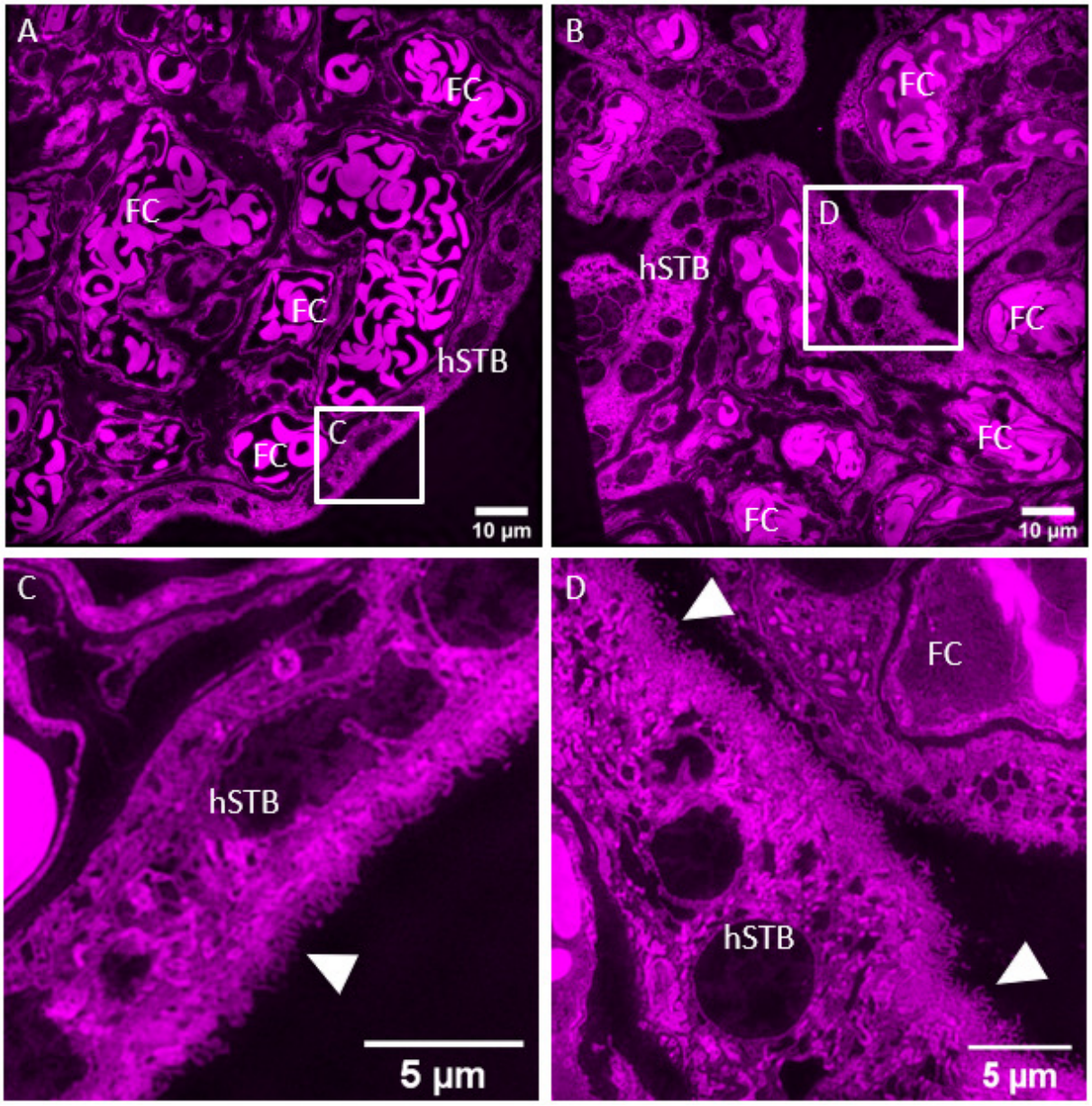

Figure 24 Super-resolution of chorionic villi in normal and PE placenta. *CMO was used for membrane staining (magenta). (A) 100 nm thick cryo-section of the normal placenta. (B) 100 nm thick cryo-section of PE placenta. (C) Enlarged image from (A) showing normal plasma membrane of hSTB and syncytial microvilli located at the surface of the plasma membrane. The arrow represents the localization of microvilli at the apical surface of normal villi. (D) Enlarged image from (B) showing PE plasma membrane of hSTB and syncytial microvilli located at the surface of the plasma membrane. The arrow represents the localization of microvilli at the apical surface of PE villi, where it seems to be disorganized compared to the healthy microvilli. CMO: CellMask Orange, FC: fetal capillary, hSTB: human syncytiotrophoblast.*

3.8 PLAP expression observed in microvesicles at the microvilli brushborder

Reconstructed SIM image of normal cryo-section of 400 nm thickness was immunofluorescence labeled with CMO (magenta), PLAP (yellow) and DAPI (cyan) according to reference #1 in **Table S2** in Supplementary**.** The representative image was generated using the OMX microscope with a 60X/NA 1.42 oil-immersion objective lens to perform SIM reconstruction. The representative images identify mature intermediate villous (MIV) and terminal villous (TV) within a normal placental tissue (**Figure 25**). In addition, placental cells were also identified, such as human and syncytiotrophoblast (hSTB), which are located in MIV and TV. The super-resolution image allowed for observing PLAP expression in normal chorionic villi. Increased signal detection from PLAP (yellow) was observed at the apical surface of the syncytial plasma membrane border of MIV and TV. The SIM image of 400 nm thick cryo-section did not allow for structural detailed observation as observed in the previous SIM images of 100 nm thick cryo-sections (**Figure 23** and **Figure 24**).

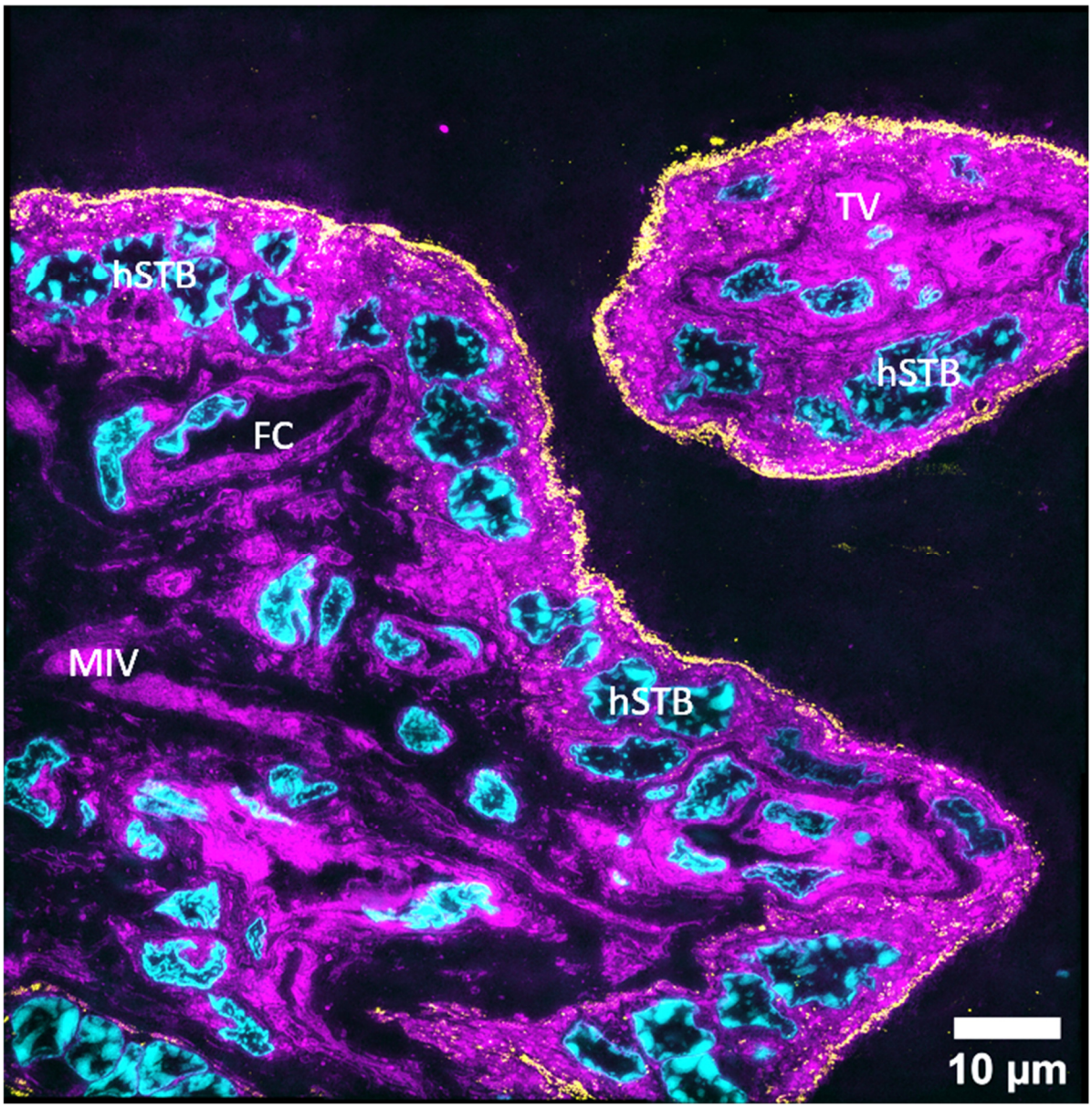

Figure 25 PLAP expression located at the apical syncytial trophoblast membrane of healthy chorionic villi. *Cryo-section of normal placenta labeled with CellMask Orange for membrane staining (magenta), PLAP for syncytial microvesicles (yellow), and DAPI for nuclei staining (cyan). Imaged using SIM with 60X/NA 1.42 oil-immersion objective lens. PLAP expression is observed in the syncytial microvesicles localized at the brushborder of hSTB. Additionally, placental compartments are identified as human syncytiotrophoblast (hSTB), fetal capillaries (FC) located inside the mature intermediate villous (MIV), and terminal villous (TV).*

3.9 Laeverin expression at the apical side of the syncytiotrophoblast membrane

Multiple labeling technique (the mixed technique) was performed using laeverin (green) and CK-7 (red) biomarkers on 4 µm thick FFPE normal (n=5) and PE (n=5) sections. The sections were counterstained with DAPI (blue) for nuclei staining (see reference #2 in **Table S2**). The whole slide was scanned making images with large FOV (Olympus VS120 with 20X/NA 0.75 objective lens). Low-resolution with large FOV was obtained for the FFPE sections for the morphology study.

The microscope images appear to show laeverin (green) expression, CK-7 (red) expression and nuclei (blue) (**Figure 26**). Laeverin expression appears to be observed in the apical syncytiotrophoblast plasma membrane and CK-7 expression in syncytial cytoplasm in normal samples, where colocalization (yellow) of the markers appeared to be observed (**Figure 26A**). In PE samples, the laeverin expression seems to be observed in the syncytial plasma membrane and the trophoblast cytoplasm (**Figure 26B**). Additionally, the microscope observation appears to show laeverin expression in the fetal capillary walls in both normal and PE chorionic villi.

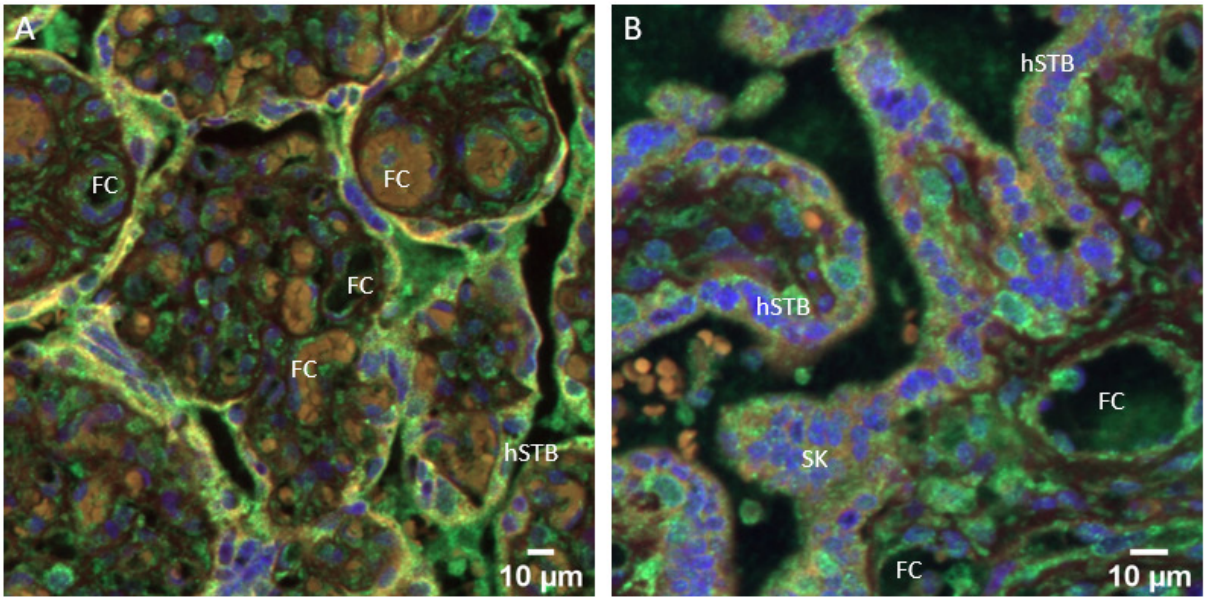

Figure 26 Laeverin expression in normal and PE hSTB plasma membrane. *Human chorionic villi present in normal and PE 4µm thick FFPE placenta tissue section. Laeverin expression in the syncytiotrophoblast plasma membrane and cytoplasm in green, cytokeratin-7 expressed in hTB cytoplasm in red, and nuclei stained with DAPI in blue. Images generated by Olympus VS120 (whole-slide scanner) with 20X/NA 0.75 objective lens. (A) Laeverin expression in normal chorionic villi. Laeverin expression appears to be observed in the syncytial plasma membrane. Co-localization of laeverin and CK-7 appeared to be observed (yellow) (B) Laeverin expression in PE chorionic villi. Laeverin expression seems to be observed in the syncytial plasma membrane and trophoblast cytoplasm. Additionally, laeverin expression appeared to be observed in normal and PE fetal capillary walls. CK-7: Cytokeratin-7, hSTB: human syncytiotrophoblast, FC: fetal capillary, DAPI: 4',6-diamidino-2-phenylindole.*

3.9.1 Laeverin expressed in fetal capillaries

Cryo-sections of 100 nm thickness from normal and PE placentas were immunofluorescent labeled with laeverin (yellow) and CMO (magenta) and DAPI (channel turned off in the image) according to reference #7 in **Table S2** in Supplementary. SIM images were generated using an OMX microscope with a 60X/NA 1.42 oil immersion objective lens. In the SIM images, contrast enhancement and signal detection from the markers are observed (**Figure 27**). Fetal capillary (FC) and fetal red blood cells (fRBC) in normal and PE chorionic tissue were identified in the representative image. The representative images show laeverin expression in the fetal capillary wall including on fRBC in the normal placenta (**Figure 27A**). In PE tissue, the laeverin is observed as overexpressed inside the fetal capillary with the presence of fRBC inside (**Figure 27B**).

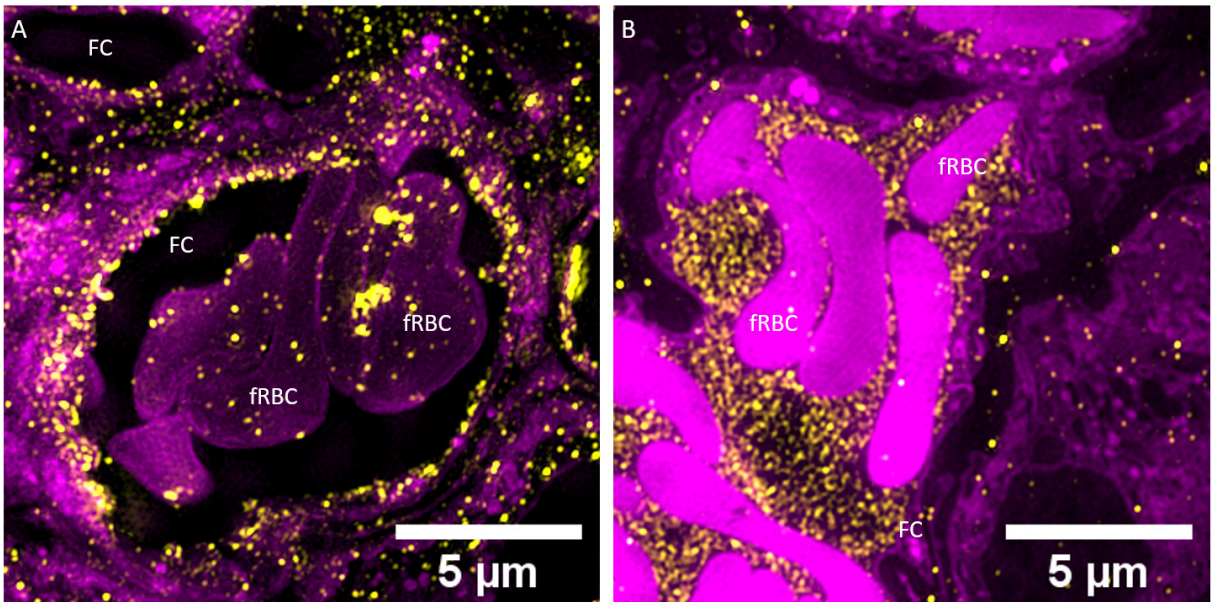

Figure 27 Laeverin expression in the fetal capillary. *Normal and PE placenta tissues cryo-sections of 100 nm thick labeled with laeverin (yellow), CMO (magenta), and DAPI (turned off) to identify laeverin expression and localization. Super-resolution image generated by OMX with 60X/NA 1.42 oil-immersion objective lens. (A) Laeverin expression in normal fetal capillary wall. (B) Overexpression of laeverin expression in PE fetal capillary. FC: fetal capillary, fRBC: fetal red blood cells, CMO: CellMask Orange, DAPI: 4',6-diamidino-2-phenylindole.*

4 Discussion

In this study, optimization of sample preparation, labeling concentrations and incubation times of biomarkers for immunofluorescence labeling was essential for advanced fluorescence microscopy methods. The morphological studies included different biomarkers for the cytoplasm of human trophoblast cells (CK-7), syncytial membranes (laeverin) and syncytial trophoblast-derived microvesicles (PLAP). These biomarkers including direct fluorescence dyes (phalloidin-Atto 647 N, CMO and DAPI) were used for the identification of placental subcellular structures and lesions which discriminates between term placentas of healthy pregnancies and placentas of women with preeclampsia.

4.1 The progression during optimization

4.1.1 Artifacts affected imaging of FFPE sections

Solid FFPE preservation was a good basis for acquiring high-quality microscope images since a vast majority of tissue samples are preserved in paraffin blocks. However, several artifacts appeared in the fluorescently stained FFPE slides. Artifacts might have arisen from improper fixation, the type of fixative used for the tissue, poor dehydration and paraffin infiltration, unsuitable reagents, poor sectioning, poor deparaffinization and rehydration, defective labeling technique and/or inadequate oil matching at the imaging site. All of these artifacts vary from sample to sample leading to imperfect imaging results. It is not possible to control artifacts that stems from the tissue processing, and paraffin-embedding since these were performed by different pathologists at different time points.

One of the poor qualities in imaging at the beginning of the project came from the laboratory technique, such as poor deparaffinization and rehydration steps (**S3** in Supplementary). Poor deparaffinization and rehydration were easily visualized as reduced signal detection, blurriness and unclear regions in the imaged FFPE sections. This artifact was improved by a longer incubation time (overnight incubation) for the FFPE tissue sections in a 60°C incubator to remove the paraffin. To be sure the paraffin is melted properly, a longer incubation time was preferred since it was easier to remove the excess paraffin in the deparaffinization and rehydration step. In addition, using clean (pure) deparaffinization and rehydration reagents instead of reusing the reagents was also preferred to avoid contamination and properly removing the paraffin excess. Sufficient removal of paraffin had a major influence on the labeling and the imaging result.

4.1.2 Limitations with direct fluorescent dyes

Commercial fluorophores are designed with maximum excitation and emission wavelength which allows the researcher to choose an ideal fluorescent dye within these excitation and emission wavelengths. However, choosing a fluorophore with poor extinction coefficients and quantum yields will lead to fluorophore appearing as dim and might lead to photobleaching (63). Photobleaching was one of the artifacts that appeared during the study. To limit the bleaching, we chose bright and photostable fluorophores to reduce the duration and intensity of the excitation, in combination with antifade mounting reagents to minimize the photobleaching (63). Another limitation with fluorescence dyes was spectral overlapping. Spectral overlap can occur when two fluorophores are within the same spectrum of excitation and emission, which leads to overlap. It was crucial to avoid spectral overlap of fluorophores when multiple fluorophores were in use in the study. This can be a consequence when imaging using a fluorescence microscope where the researcher does not know which fluorophore was emitted and cross-linking of the dyes may appear. To avoid the problem, we looked for spectral overlap in reference to the manufacturer's spectrum viewer (63).

4.1.3 The mixed technique is optimal for multiple labeling

As already mentioned in the result, optimization of multiple labeling techniques was a part of this project. Antibodies combination using multiple labeling techniques was exceedingly difficult and sensitive to optimize compared to direct fluorescence labeling. The difficulty of multiple labeling technique optimizations is cross-reactivity between different antibodies. To avoid this, the researcher must be aware of which antibodies are utilized, the animal the antibody is raised in, and which fluorophores are conjugated to the secondary antibody. Additionally, avoid using antibodies that are raised in the same species to avoid cross-reactions and thereby non-specific binding of antibodies. With this in consideration, we were able to combine laeverin and CK-7 antibodies and label both FFPE and cryo-sections using multiple labeling techniques. We were able to experiment with two different techniques, where the sandwich technique and the mixed technique showed similar results. Both the sandwich technique and the mixed technique showed sufficient contrast and signal detection using the DV microscope with a 60X/NA 1.42 oil-immersion objective lens (**Figure 19**). Thus, we choose to continue with the mixed technique due to this technique was optimal and time-efficient compared to the sandwich technique.

4.1.4 Challenges of imaging FFPE placenta sections on the OMX (SIM)

OMX is an extremely sensitive microscope, thus it was necessary to obtain a high-quality labeled sample for generating high-resolution and super-resolution images with the OMX. Sample preparation-steps for both FFPE and cryo-sections were crucial and necessary to be optimized. However, challenges did occur while imaging FFPE sections on the OMX. The main challenge was the natural autofluorescence in the placenta sections which made it difficult to distinguish the signals from the fluorescence markers used in this study. The autofluorescence signal interfered with the imaging and resulted in creating artifacts from the reconstruction in SIM in the form of haloing effect, which limited the capabilities of the instrument to properly reconstruct the image, and not allowing for clear observation of cellular structures within the tissue.

There are various methods for diminishing autofluorescence in FFPE samples, ranging from exposure to light to a variety of chemical treatments (70, 98-100). One of the methods chosen for this study was to incubate the slides in a 150 mM glycine solution after the deparaffinization step. As mentioned in the Methods section, the solution was used to neutralize free aldehydes that might lead to cross-binding of the markers in the sample. The autofluorescence control in FFPE placenta sections were characterized by preparing unlabeled sections which were imaged by DV microscope. We set all the channels to 50% excitation intensity and $50ms$ acquisition time to observe the response of autofluorescence through the four channels (**Figure 15**). Natural autofluorescence signals from fetal- and maternal red blood cells were observed in the FFPE section but not in the cryo-section (**Figure 17**).

To our knowledge, there have been published studies focusing on reducing autofluorescence background (70, 77, 98). The study by Viegas *et al*. reported that pre-treating the FFPE tissue with short duration, high-intensity UV irradiation and Sudan Black B (SBB) reduced the autofluorescent background (77). Thus, this application could be tested in placenta samples to diminish autofluorescence. Due to time limitations, we were not able to investigate this hypothesis. However, it could be implied in future studies.

Another challenge that occurred with imaging FFPE sections (and cryo-sections) generated by OMX was oil matching. This is a standard challenge occurring during OMX imaging which is still thoroughly investigated by the Optical Nanoscopy Research Group at UiT. Oil mismatch can be monitored by observing the point spread function (PSF) in the orthogonal view of the OMX software (**S4** in Supplementary). Observing asymmetrical PSF in the orthogonal view

indicated oil mismatch. This artifact could be optimized by adjusting the refractive index of the immersion oil. Changing the oil will lead to refractive index enhancement of the PSF (symmetrical shape can be observed) and thus reduction of the artifact. However, oil match for multi-color samples is challenging. Due to oil matching corresponding to one specific excitation wavelength, it leads to haloing or doubling artifacts because of suboptimal oil matching for different excitation wavelengths. Therefore, the best solution to minimize the artifacts was to match the oil with the excitation wavelength (channel) of interest.

4.1.5 Super-resolution obtained using cryo-sections instead of FFPE sections

DV microscope was used to generate high-resolution deconvolved images with a 60X/NA 1.42 oil immersion objective lens. For further investigation of the region of interest (ROI) of the tissue, the same parameters were used to generate super-resolution with OMX using SIM reconstruction. Acquiring high-resolution images was challenging and needed optimization. It also depended on the different markers and types of sections used for this study. Regardless of using the same labeling markers, the results from FFPE-section and cryo-section were significantly different. Contrast enhancement and the reduced out-of-focus signal were generated from the cryo-section (**Figure 22B**). Hence signal detection from the FFPE section showed poor contrast and signal which made it difficult to observe morphological structures (**Figure 22A**). A complementary study was performed in this master project to optimize the FFPE section imaging with OMX (not presented in the thesis). However, due to the artifact challenges mentioned above, we excluded super-resolution studies with FFPE sections, thus cryo-sections were used for super-resolution investigation of ROIs in the sample from normal and PE placentas.

The cryo-sections were prepared following the Tokuyasu method, developed by Kiyoteru Tokuyasu in the 1970s for preparing fixed cryo-sections and cryo-protected biological specimens for electron microscopy (93). The microscopy results following the Tokuyasu method for human placenta cryo-sections have been shown to work sufficiently from previous studies (94). The technique included sucrose infiltration which was performed on placenta specimens during tissue preparation to prevent tissue collapse and avoid crystallization during freezing of the biological material. Placenta tissues are a complex structure of chorionic villi submerged in the maternal blood. To maintain the structure, the sucrose immersion step was a crucial step for tissue preservation. The protocol designed by Bernhard and Virion early in the 70s has been modified since then and optimized for this thesis (101).

Furthermore, the optimization of dissolving the cryoprotectant mixture of sucrose-methylcellulose from the sample before labeling was also optimized. Previous super-resolution studies on Tokuyasu sections used cold washing of the cryo-protectant (94). However, we experienced unspecific and/or poor labeling on the cryo-sections using this approach. We found that prolonged incubation of the sample (1 hour) at 40°C was effective to remove the cryoprotectant and achieve optimal labeling of the placental cryosections. Therefore, we implemented warm wash with PBS at 40°C on a heating plate, which gave better results with reduced artifacts and background signals (**Figure 24**). In addition to performing the warm-wash method, we labeled the cryo-sections of 100 nm thickness instead of 400 nm thick cryo-sections to omit artifacts. This application (warm-wash and 100 nm thickness of cryo-sections) to our protocol enabled ultrastructural investigations. Significantly reduced background signals and artifacts including structure enhancement were observed in the SIM images obtained from normal and PE cryo-sections of 100 nm thickness.

The out-of-focus light contribution, the refractive index mismatch and the autofluorescence appearing while imaging with the FFPE section posed an enormous challenge on the reconstructive algorithm of SIM microscopy. Thus cryo-sections were preferred and suitable for SIM reconstruction which allowed for greater ultrastructural preservation. As mentioned, the cryo-section with 100 nm thickness increases the axial resolution of the microscope image. The thin section thickness provides optical sectioning beyond the axial resolution of the objective lens. Thereby, super-resolution generated using SIM on 100 nm thick cryo-sections is more preferable. Regardless of obtaining super-resolution on 100 nm thick samples, it was difficult to find regions to image. Cryo-sections with 100 nm thickness were indeed fragile because of the thin section and were more susceptible to sectioning artifacts such as folds, wrinkles and tearing, as compared to the 400 nm thick cryo-sections. Therefore, limited regions were available to image. This limitation will hence affect histopathology studies due to these studies involves examining tissues in large FOV to pinpoint abnormal observations. Consequently, imaging cryo-sections can lead to overlook or miss abnormal regions within the tissue which would not be valuable for diagnostic analysis. However, an advantage with cryo-section is that the simple sample preparation protocol is time-efficient compared to the FFPE section protocol.

To sum up, the major advantage of using FFPE tissue sections over cryo-sections was the observation of the morphological structures and preservation in a large FOV. The comparison study of acquiring large FOV of FFPE and cryo-sections indicated that FFPE sections were

preferable for histological investigations. This study also revealed that FFPE sections were not adequate for the investigation of ultrastructural changes in the tissue. Nevertheless, the frozen sections (cryo-sections) might be beneficial of examine tissues in small regions which cannot be visualized in a large FOV image.

4.2 Microscope observations of term placentas

4.2.1 Actin spots – a sign of fibrin clots?

The present morphology study of the human placenta from normal and PE pregnancies using phalloidin-Atto 647 N dye revealed an interesting observation of actin spots in the FFPE tissue sections. We found that the actin spots were abundantly localized in the chorionic villi in both normal and PE placentas (**Figure 21**). It is evident from the results and previous findings that placental actin filaments are present in the chorionic villi including the syncytium microvilli brushborder, endothelial cells, and pericytes (102). It could be argued that the actin spots may have been an artifact representing some sort of unspecific binding during tissue preparation and labeling, thus not staining actin filaments. This observation merits further study.

The limited number of publications regarding actin filaments in human placenta tissue made it difficult to understand our findings of the specific actin spots. However, it could be hypothesized that our observation of actin spots might be associated with placental fibrosis. Previous studies have documented that fibrin deposition is morphologically important in contrast to earlier discoveries that fibrin marks pathological process and placental aging, including observing fibrin deposition in the healthy and pathological placentas at all stages of pregnancies (103). Placental fibrosis is present through the pregnancy and a large amount was recognized at the term placenta (103). It is known that fibrosis is a common pathologic process that takes place in tissue inflammation or injury (104). Disease-related injuries and inflammations in organs might trigger a cascade effect of cellular responses that result in the accumulation of tissue fibrosis (104-106). This is identified in the connective tissues as overproduction of the extracellular matrix (ECM). Furthermore, studies have confirmed that fibrosis has a significant key role in the maintenance of ECM and regulation of injury and inflammation in the connective tissues (106).

The mechanism of fibrosis in the PE chorionic villi remains unclear, but studies have suggested that placental ischemia and hypoxia might be involved (107, 108). Another study confirmed that overexpression and deposition of collagen I were found in the ECM (106). A newly published study by Feng *et al*. have analyzed the fibrin deposition and expression of collagen I in the human placenta, in immortalized first-trimester placental trophoblast cells and mice models (109). They demonstrated that collagen I induce preeclampsia-like symptoms by repressing the invasion of trophoblasts.

Several studies have demonstrated that the majority of ECM in mammalian cells are collagen and involved in the maintenance of tissue structures, development and ECM-remodeling (106, 109-111). Furthermore, studies have speculated that fibrosis might be an important pathological event in the PE placenta depending on the excess of collagen I deposition (110, 112, 113). This led to the finding of overproduction of collagen 1 in form of fibrosis in PE stem villi and terminal villi compared to the normal placentas (109, 114-116). In our study, we were not able to find any significant difference (p-value > 0.05) in the number of actin spots present in PE placentas compared to healthy placentas. However, it can be assumed that our quantitative analysis was not accurate due to the low quality of the method. Thus, a thorough quantification needs to be performed to verify the observations.

Additionally, another study reported that actin filaments were released into the ECM from the cells while dying (115). Thus, it could be argued that the reason for the detection of actin filaments using an actin-specific marker (phalloidin-Atto 647 N) in different subtypes of the chorionic villi might be linked to the fact that deposition of actin in ECM is related to the fibrosis in chorionic villi. However, a thorough investigation is needed following quantitative analysis on multiple placenta samples from normal and PE with z-stack serial sectioning to be sure of specific localization of the actin spots. Additionally, a preliminary study on collagen I marker could be also performed to control the actin spots observations.

4.2.2 Quantification of syncytial knots

In 1893 the German pathologist Georg Schmorl reported the presence of multinucleated syncytial fragments trapped in the lungs of women with eclampsia who died during pregnancy (32, 117). The multinucleated syncytiotrophoblast is identified as syncytial fragments or syncytial knots and differs in size and shape (32, 118). The nuclei are present arbitrarily in the surface of hSTB and the cytoplasm in early pregnancy. However, at term regions of syncytiotrophoblast with nuclei become aged and apoptotic leading to extrude and aggregate as membrane-enclosed multinucleated structures (119). Studies have revealed that deportation of SK was found in the maternal circulation, thus trapped in the arterioles and capillaries of the maternal lungs causing severe complications (21, 32, 119, 120). Numerous studies have found an increased number of SK in term placenta that is associated with pregnancy-related disorders cases, such as IUGR and PE (119). Yet the cause of the shed and deposition of SK from the placenta is largely unknown.

In the current study, we were able to identify SK in full-term healthy placentas and preeclamptic placentas (**Figure 20**). Additionally, we found that there were significant differences (*p*-value > 0.05) in the number of syncytial knots in PE and normal. Thus the research indicates that an increased number of syncytial knots were present in full-term PE placentas compared to normal placentas (**Table 5**), which supports the previous findings (32, 121-124). To date, the function of SK and the mechanisms of the formation and transportation, including the increased number of syncytial knots in PE are still unclear. Nevertheless, a study by Tenney and Parker hypothesized that syncytial knots in PE may reflect on hSTB aging or apoptotic death due to the inactivation of transcription and replication of hSTB which may have led to several molecular apoptotic signaling pathways activation (120, 125). Moreover, another study hypothesized that SK formation is linked to decreased and inactivity of anti-apoptotic proteins (125). Thus they quantified the density of SK in chorionic villi and identified an increased amount in PE which might be a result of hypoxia, hyperoxia or oxidative stress (125). Additionally, it can be assumed that the significant increase in the formation of SK in the PE placenta might indicate the changes in hormonal factors, leading to cause changes in blood flow (126).

Although, it can be argued that in this study the quantitative measurement was not accurate due to the measurement being done by using naked eyes. In addition, only a single large FOV image of each sample (normal (n=5) and PE (n=5)) was used to estimate the number of SK. Hence limits the quantitative analysis of SK within the tissues to only measuring one region of the whole tissue section. However, the optimization and enhancement of quantitative measurements need to be addressed in future work. Another limitation is the number of placentas used for this study. The limited amount of available placenta tissue might decrease the quality and quantity analysis for this study. Thus, it would be preferable to enhance the study by including more placentas from the PE and normal pregnancies to obtain more precise information. Lastly, the observation of SK in the large FOV images could simply be artifacts caused by tangential sectioning (**Figure 5B**). Therefore, it would be wise and beneficial to acquire z-stack serial sectioning and perform labeling on the z-stack serial sections to ensure the abnormal structures. Z-stack serial sectioning allows for a z-section visualization of the tissue, thus enhance the observation and pinpoint the abnormal features and lesions in the placenta tissue.

4.2.3 Disorganized brushborder in PE?

The preliminary study of normal and PE cryo-sections fluorescent-labeled with CMO and DAPI showed features of syncytiotrophoblast microvilli at the apical surface (**Figure 24**), thus we were able to pinpoint the localization of microvilli in normal and PE chorionic villi due to super-resolution of the chorionic villi acquired from the SIM reconstruction. The PE syncytial microvilli seem to look disorganized compared to healthy tissue, however difficult to predict our observation. A review article by Redman *et al*. have reported the microscopy finding of microvilli clothing the apical surface in the normal term, whereas PE syncytium microvilli were observed to be distorted and shed as placental debris (127). The microscope observation from the study did not look similar to our observation. It could be argued that tangential sectioning differences of the healthy and PE samples may have given a false-positive or false-negative observation of the microvilli.

Another argument for not observing the same observation as Redman *et al.* could be the different preparation methods applied. In this study, the frozen tissues were rinsed with sodium chloride to remove the maternal blood and then fixed in PHEM buffer to preserve the structures. This method may have led to removing all the shed materials at the apical surface of the chorionic villi, thus could be the reason for not observe the same distorted microvilli and placental debris shedding as Redman's ultrastructural electron microscope observations. An application for future study could involve using another tissue preparation (fixation) method that excludes the removal of maternal blood and placental debris.

Although, it is known that placental debris is shed from microvilli and out in the maternal circulation (127). The placental debris ranges from multinucleated deported syncytiotrophoblast (20-100 μm) to sub-cellular fragments (10-60 nm) and have different biological functions, cargo and modes of production that may contribute to normal placentation (127). Hence, oxidative and inflammatory stress occurring in PE might activate hSTB to produce more and larger microvesicles that have pro-inflammatory, anti-angiogenic, and procoagulant activity (127). Thus could be hypothesized the reason for observing microvilli disorganized in PE tissue compared to normal tissue.

Nonetheless, Redman *et al.* were able to generate ultrastructure of the normal and PE syncytial surface using an electron microscope. We can confirm from this investigation that we were also able to generate super-resolution images using an OMX microscope, thus observe structural details of the microvilli in both normal and PE chorionic villi. Hence the distorted microvilli

and placental debris observations were limited which may have resulted from the biological implication as mentioned earlier and not from the instrument. Using SIM was beneficial for this study due to the reconstruction improved the resolving of structures beyond the diffraction-limited resolution of a conventional optical light microscope, such as confocal microscopy and deconvolution microscopy. Additionally, this method allowed for 2X spatial resolution compared to the conventional fluorescence microscopes (84, 128). Although electron microscope is capable of greater resolution studying at a molecular and atomic level, SIM is easier, faster and more conventionally available to use as to the sample preparation is similar as for the optical fluorescence microscopes (94, 129). Whereas EM sample procedures are long and complicated.

Nevertheless, in-depth investigation is needed with more placenta samples and optimization of the preparation method. Additionally, for future studies it would be favorable to explore PLAP and phalloidin-Atto-647 N markers together to observe the microvilli disorganization in PE tissue due to the PLAP marker is STBM specific and phalloidin-Atto 647N to stain the actin filaments composed in the microvilli. This might give a better understanding of the disorganized brushborder of syncytial microvesicles and placental debris in spatial resolution. Due to time limitations in this project, we were not able to investigate with this approach, but could address to the future preliminary studies.

4.2.4 PLAP - a potential biomarker for syncytial microvesicles

As mentioned, the syncytial layer of the chorionic villi sheds placental debris into the maternal blood including subcellular fragments, syncytial knots, apoptotic bodies, microvesicles, nanovesicles and exosomes (127). The placental debris carries placenta-specific molecules, proteins, immune molecules, organelles, DNA fragments and RNA fragments that may contribute to the regulation of normal placenta physiology (117, 127, 130). Hence studies of their functional properties are still not clear. It seems evident that syncytiotrophoblast microvesicles (STBM) contribute to maternal-fetal intercellular communication and inflammatory responses including activation of monocytes, granulocytes, and endothelium (127).

Other studies found an increased amount of circulating microvesicles in the plasma of PE pregnant women compared to normal pregnant women (52, 74). Redman and Sargent determined that oxidative stress might alter the placental physiology to cause the shedding of microvesicles into the maternal circulation (131). STBM carries a wide variety of pro-

inflammatory molecules, including cytokines and chemokines and others (127). Hence their function in pathophysiology and the release of STBM related to complications of pregnancy is still in a formative stage. The immunofluorescence analysis in this study showed expression of the PLAP at the apical surface of the syncytial plasma membrane in healthy placenta (**Figure 25**). However, with the super-resolution image, we were able to observe signal detection from the PLAP marker at the brushborder (apical surface) of hSTB. Thus, we could predict that the PLAP marker did work and was highly expressed at the apical surface of the healthy syncytium. Nevertheless, it was difficult to visualize the morphology of the microvesicles due to the size and structural diminution of the microscopy result. To observe the structures of microvesicles, further optimization is needed in addition to a thorough quantitative and morphological comparison of microvesicles in healthy placentas and placentas from women with preeclampsia,

A study reported quantitative analysis on placental-derived exosomes by determining the ratio of PLAP exosomes (132). The findings revealed that quantification of the number of placental-derived microvesicles in maternal circulation were higher in early-onset and late-onset PE compared with normal pregnancy (132). This discovery indicated that PLAP microvesicles could be a promising biomarker for quantitative research of the PE predictor. Due to time restrictions, we were not able to investigate PLAP markers in PE placentas. Thus, we can explore the PLAP marker on PE placentas for future research of understanding PLAP expression and the localization in relation to PE pathophysiology mechanisms. Since the studies have addressed that placental microvesicles are secreted by hSTB and deported into the circulation, it could be hypothesized that the microvesicles containing cargos that might have important diagnostic information about PE (132). Thus for the future aspect, it would be interesting to isolate and perform molecular profiling of PLAP STBM for diagnostics purposes which might have great importance in the PE prediction in the early stage of pregnancy. The procedure can be studied non-invasively.

4.2.5 Subcellular localization of laeverin in PE placenta

Laeverin is a member of the aminopeptidase family. This family is involved in the maintenance of homeostasis including maintenance of normal pregnancy hypertension regulation and antigen presentation (47, 133-135). In a study by Sitras *et al*. laeverin mRNA, among other genes, were significantly upregulated (increased tenfold) which led to several molecular studies of the involvement of laeverin in the pathophysiology of preeclampsia (95). Nystad *et al.* found

laeverin expression in the cell membrane of hCTB of term placentas from healthy women (48). In comparison placentas from women with preeclampsia demonstrated laeverin expression in the cytoplasm of trophoblast cells. It is evident from the microscope observation that plasma membrane expression of laeverin was shown in hSTB and hCTB, in addition to the cytoplasmic expression of laeverin in healthy placentas (17). Due to the expression and localization in normal placenta observed in the study, they were able to observe upregulation of laeverin protein in PE placentas thus further investigated the role of laeverin in the PE pathophysiology (17, 47, 48).

Furthermore, the immunoelectron microscopy analysis demonstrated that the protein was expressed in the microvesicles within the cytoplasm, including in extracellular space, syncytial knots and the fetal capillaries in the PE placenta, and that there was a large amount of protein expressed in the PE placenta compared to a healthy placenta (48). However, the study was only based on detection of the size in the electron microscopy studies, whereas in our study with PLAP biomarker showed specific expression in the syncytiotrophoblast-derived microvesicles.

In this current study, we used commercially available antibodies against laeverin and CK-7 to observe the expression using advanced immunofluorescence microscopy (Olympus VS120) in normal (n=5) and PE (n=5) placentas. It could be assumed from the microscope observation that co-localization of laeverin and CK-7 was detected in the healthy placentas. In PE placentas, we can assume that the laeverin expression was observed in the syncytial plasma membrane and cytoplasm of the trophoblast. Although the assumed observations support previous findings, it was difficult to observe the expression on the low-resolution images (**Figure 26**), therefore difficult to predict and pinpoint our observation. Further optimization of the multiple labeling with laeverin and CK-7 for the super-resolution method is needed. Additionally, a preliminary study with the application of life-cell imaging of placental villous explant could be more informative for observing the localization distribution of laeverin.

However, the assumed observation of accumulation of laeverin in preeclamptic placentas might have resulted from that the protein was not fully processed during folding which might have led to misfolding, protein damage or changes in post-translational modification in PE (133, 136). Changes in epigenetic regulation (DNA methylation, histone modification, non-coding RNA expression) may also play a key role in the cause of overexpression of the protein in PE (137, 138). Due to the protein's involvement in cellular homeostasis, it can be hypothesized that dysregulation of laeverin protein might disrupt homeostasis in cells (133).

Furthermore, a preliminary study using only laeverin antibody, CMO and DAPI allowed for super-resolution and enabled the observation of overexpressed laeverin in PE fetal capillary (**Figure 27B**). Although this is a preliminary study on a single tissue, it could be hypothesized that laeverin may function as a scavenger in the elimination of dangerous particles and clearance of toxins from circulation. This could also be the reason for laeverin expression in the normal fetal capillary walls. On another note, overexpression of laeverin in fetal capillaries might have to do with placental ischemia in PE. Hence, not enough reports are associated with the exact molecular mechanism behind this. Thus, it would be interesting to include a preliminary study with a severe preeclamptic (eclamptic) placenta sample to compare the distribution of the protein in the different stages of the diseases and thereby might have a better understanding of laeverin expression and subcellular location.

4.3 Strengths and limitations of the study

In this master project, the optimal preparation-steps including concentrations and incubation times of the biomarkers and labeling techniques for FFPE- and cryo-sections of the human placenta was found. Thus for future research, this methodology will be time-efficient. Due to the high-resolution and super-resolution microscopy method were sample-dependent, we were able to optimize the sample preparation for imaging as well. Additionally, the optimization of the methodology has minimized the use of equipment which contributes to more eco-friendly preliminary tests. Another advantage of the project was that the optimized technique for cryo-section allowed for studying the subcellular localization of compartments in placentas with an OMX microscope. The study revealed that ultra-thin cryo-sections improved the super-resolution ability to resolve and visualize the detailed morphology of the chorionic villi. Thus super-resolution images contained more detailed information compared to low-resolution images. Preliminary studies of biomarkers in this master project allowed for targeting interesting placenta-specific proteins which opened the perspective that biomarkers may have a potential role in the prediction and diagnosis of PE. However, a further thorough study is required to understand the role of the biomarkers in normal and PE placentas.

Nevertheless, there were several limitations in this study, primarily related to the lack of a sufficient number of PE cases to address the common PE placental lesions and morphology features. Additionally, the analysis of different placenta tissues from patients was also limited due to the anatomy and morphology differences of the patients. This might limit the possibility of predicting abnormal feature visualization of the tissues and thus difficult to predict if it is PE characteristics or not. However, investigating more samples from different PE women and comparing the finding to the controls gave us a better understanding of what might be placental attributes.

Secondly, the organ is dynamic, therefore it is difficult to identify the pathophysiological changes within a tissue section by only analyzing the section in a snapshot in time. As a consequence, the major limitation with histological investigations is that the placenta has an extremely convoluted nature and thus possible to be confused and difficult to pinpoint the abnormal structures using a microscope. This is because artifacts may occur from tangential sectioning of the microscope as mentioned earlier. For future recommendations, z-stack serial sectioning would provide more accurate and greater information about the tissue.

Furthermore, quantitative analysis of abnormal structures and placental lesions was observed in the microscope images. Due to a complex tissue and the fact that FFPE sections are large, it was difficult to perform a quantitative assay of the characterized features (actin spots and syncytial knots) on the whole tissue section. Large FOV images allowed us to identify the features on one region of the tissue. Consequently, the quantitative analysis was performed using naked eyes on a single large FOV for each sample. This resulted in uncertain predictions. Hence, adequate analysis is necessary to undoubtedly quantify the observations. A future aspect for enhancing quantitative studies in clinical histopathology research could be using artificial intelligence (AI) technology. A preliminary study could be performed on designing/training an AI-algorithm to characterize and quantify abnormal placenta features objectively. This aspect might have a significant improvement in clinical research and a diagnostic setting.

Another limitation of this study was the use of ultrathin cryosection which might be a disadvantage for pathological investigations. The ultra-thin section may limit the regions of the sample to examine due to the sections being extremely fragile and easily damageable as mentioned earlier. Thus, when we imaged the sections, we were able to observe some folded or damaged regions of the tissue which limited the imaging area for high-resolution and super-resolution. Consequently, this might lead to overlooking areas that may be abnormal, thus giving us false-positive or false-negative results.

5 Conclusions

In conclusion, the optimized methodology for FFPE- and cryo-sections of placenta tissues were well suited for histological investigation using the advanced fluorescence microscopy method. The FFPE sections were more preferable for acquiring large FOV low-resolution images. Whereas, ultra-thin cryo-sections were better for generating super-resolution images, which allowed to observe detailed morphology at a subcellular level of the chorionic tissue. In this study, we used immunofluorescence microscopy to compare the expression of placental biomarkers (laeverin, PLAP and CK-7) in combination with non-specific commercially available fluorescent dyes (phalloidin-Atto 647 N, CMO and DAPI). By using phalloidin-Atto 647 N marker for actin staining, we found abundant actin spots independently attached to the chorionic villi, and that there were no significant differences between healthy and preeclamptic placentas. Nevertheless, the actin spots seem to be associated with fibrosis deposition and thus attached to fibrin in the chorionic villi. The quantitative analysis revealed an increased amount of syncytial knots in PE compared to healthy tissues. Moreover, the biomarker investigation revealed expression localization of the placenta-specific proteins. The comparison study seems to show disorganized microvilli at the apical surface in PE placentas. The study also revealed that PLAP is STBM-specific and was expressed in the apical surface of the syncytiotrophoblast in healthy placentas. Additionally, laeverin seems to be expressed in the syncytial plasma membrane in the healthy placentas. The mixed multiple labeling technique using laeverin and CK-7 marker revealed co-localization in healthy placentas, whereas in PE placentas laeverin seems to be abundantly expressed in the syncytial plasma membrane and hTB cytoplasm. Lastly, the super-resolution microscope image showed laeverin expression in fetal capillary walls in healthy tissue, and overexpression of the protein was found in the PE fetal capillaries.

6 Future perspectives

The master project has been a great groundwork for immunofluorescence studies using advanced microscopy methods. However, further investigation must be performed to fill the gaps in our understanding of the placental biomarkers (laeverin, CK-7 and PLAP) related to preeclampsia. Given that the production of placental-specific factors may contribute to the development of preeclampsia, it was an interesting approach to study these placental-specific biomarkers. Thus in this present study, the immunofluorescence mixed technique on the expression of CK-7 (identified human trophoblasts), laeverin (discriminates in PE/healthy placentas), and PLAP (STBM-specific), was successfully performed and allowed for intriguing observations.

To date, the pathologists routinely use immunohistochemistry and sFlt/PIGF ratio along with other biomarkers as a predictor for PE. Therefore, this immunofluorescence pilot study of biomarkers may contribute to understanding the pathophysiology of preeclampsia and might be potential predictors for PE. However, these potential biomarkers as mentioned needs to be further studied in a bigger clinical material. Our ultimate goal is to find an early pregnancy test for the prediction of PE, thus it would be of great interest for future research to use these biomarkers for investigation of their potential to predict pregnancy-related diseases, as preeclampsia in maternal blood. Additionally, it can be achievable to perform a non-invasive test of PLAP or trophoblast fragments/cells in the maternal circulation in week 20 of gestation or first-trimester, thus predict the disorder at an early stage, closely monitor the pregnancy and give prophylactic medication.

References

1. Gude NM, Roberts CT, Kalionis B, King RG. Growth and function of the normal human placenta. Thrombosis Research. 2004;114(5-6):397-407.
2. Khan KS, Wojdyla D, Say L, Gülmezoglu AM, Van Look PFA. WHO analysis of causes of maternal death: a systematic review. Lancet. 2006;367(9516):1066-74.
3. Naimy Z, Grytten J, Monkerud L, Eskild A. The prevalence of pre‐eclampsia in migrant relative to native Norwegian women: a population‐based study. BJOG. 2015;122(6):859-65.
4. Chaiworapongsa T, Chaemsaithong P, Yeo L, Romero R. Pre-eclampsia part 1: current understanding of its pathophysiology. Nature reviews Nephrology. 2014;10(8):466-80.
5. Redman CW. Latest Advances in Understanding Preeclampsia. Science. 2005;308(5728):1592-4.
6. The Arctic University of Norway. Women's Health and Perinatology Research Group. 2021 [cited 2021 June 17]. Available from: https://en.uit.no/forskning/forskningsgrupper/gruppe?p_document_id=342567.
7. Rossant J. Human embryology: Implantation barrier overcome. Nature. 2016;533(7602):182-3.
8. Carlson BM. Transport of Gametes and Fertilization Human Embryology and Developmental Biology 6th ed. St. Louis, Missouri: Elsevier Health Sciences; 2019. p. 23-32.
9. Schoenwolf GC, Bleyl SB, Brauer PR, Francis-West PH. Larsen's human embryology. Gametogenesis, Fertilization and First week. 5th ed. Philadelphia, PA: Elsevier Health 2015. p. 14-37.
10. Silini AR, Di Pietro R, Lang-Olip I, Alviano F, Banerjee A, Basile M, et al. Perinatal Derivatives: Where Do We Stand? A Roadmap of the Human Placenta and Consensus for Tissue and Cell Nomenclature. Front Bioeng Biotechnol. 2020;8:610544.
11. Winslow T. Development of the Human Preimplantation Blastocyst. Washington, D.C.: The National Institute of Health; 2001 [cited 2020 October 28]. Available from: https://www.teresewinslow.com/#/urogenital/.
12. Zeldovich VB, Robbins JR, Kapidzic M, Lauer P, Bakardjiev AI. Invasive Extravillous Trophoblasts Restrict Intracellular Growth and Spread of Listeria monocytogenes. PLoS Pathog. 2011;7(3):e1002005-e.
13. Huppertz B. The anatomy of the normal placenta. Journal of Clinical Pathology. 2008;61(12):1296.
14. Cross JC. Placental function in development and disease. Reproduction, Fertility and Development. 2005;18(2):71-6.
15. Nesheim BI. Morkaken. Oslo: Store Medisinske Leksikon; 2020 [cited 2020 October 15]. Available from: https://sml.snl.no/morkaken.
16. Griffiths SK, Campbell JP. Placental structure, function and drug transfer. Continuing Education in Anaesthesia Critical Care & Pain. 2014;15(2):84-9.
17. Nystad M. Role of Laeverin in the pathophysiology of preeclampsia [PhD]. Norway: UiT The Arctic University of Norway; 2018.
18. Wang Y, Zhao, S. Vascular Biology of the Placenta. 2010 [cited 2021, October 23]. In: Structure of the Placenta [Internet]. San Rafael (CA): Morgan & Claypool Life Sciences, [cited 2021, October 23]. Available from: https://www.ncbi.nlm.nih.gov/books/NBK53256/.
19. Castellucci M, Scheper M, Scheffen I, Celona A, Kaufmann P. The development of the human placental villous tree. Anat Embryol (Berl). 1990;181(2):117-28.
20. Baergen RN. Chorionic Villi: Histology and Villous Development. Manual of Pathology of the Human Placenta. 2nd ed. Boston, MA: Springer US; 2011. p. 69-83.

21. Kingdom J, Huppertz B, Seaward G, Kaufmann P. Development of the placental villous tree and its consequences for fetal growth. Eur J Obstet Gynecol Reprod Biol. 2000;92(1):35-43.
22. Penn AA. 13 - Endocrine and Paracrine Function of the Human Placenta. In: Polin RA, Abman SH, Rowitch DH, Benitz WE, Fox WW, editors. Fetal and Neonatal Physiology (Fifth Edition): Elsevier; 2017. p. 134-44.e4.
23. Schmiedl UP, Komarniski K, Winter TC, Luna JA, Cyr DR, Ruppenthal G, et al. Assessment of fetal and placental blood flow in primates using contrast enhanced ultrasonography. J Ultrasound Med. 1998;17(2):75-80.
24. Sengupta A, Biswas P, Jayaraman G, Guha SK. Understanding utero-placental blood flow in normal and hypertensive pregnancy through a mathematical model. Med Biol Eng Comput. 1997;35(3):223-30.
25. Costa MA. The endocrine function of human placenta: an overview. Reprod Biomed Online. 2016;32(1):14-43.
26. Unknown. Pregnancy: pregnancy complications. : U.S. Department of Health & Human Services; 2010 [cited 2020 November 10]. Available from: https://www.womenshealth.gov/pregnancy/youre-pregnant-now-what/pregnancy-complications.
27. NICHD Information Resource Center. What are some common complications of pregnancy. Rockville, MD: National Institute of Child Health and Human Development; 2021 [cited 2021 February 2]. Available from: https://www.nichd.nih.gov/health/topics/pregnancy/conditioninfo/complications
28. American College of O, Gynecologists CoO, Gynecologists, Task Force on Hypertension in Pregnancy FoHiP. Hypertension in pregnancy. Report of the American College of Obstetricians and Gynecologists' Task Force on Hypertension in Pregnancy. Obstet Gynecol. 2013;122(5):1122-31.
29. Unknown. BMJ Best Practice Pre-eclmapsia. Walker JJ, Morley, L., editor. London, UK.: BMJ Best Practice; 2020.
30. Erez O, Romero R, Maymon E, Chaemsaithong P, Done B, Pacora P, et al. The prediction of late-onset preeclampsia: Results from a longitudinal proteomics study. PloS one. 2017;12(7):e0181468-e.
31. Chaiworapongsa T, Chaemsaithong P, Yeo L, Romero R. Pre-eclampsia part 1: current understanding of its pathophysiology. Nat Rev Nephrol. 2014;10(8):466-80.
32. Askelund KJ, Chamley LW. Trophoblast deportation part I: Review of the evidence demonstrating trophoblast shedding and deportation during human pregnancy. Placenta. 2011;32(10):716-23.
33. Chaiworapongsa T, Chaemsaithong P, Korzeniewski SJ, Yeo L, Romero R. Pre-eclampsia part 2: prediction, prevention and management. Nat Rev Nephrol. 2014;10(9):531-40.
34. Rolnik DL, Wright D, Poon LCY, Syngelaki A, O'Gorman N, de Paco Matallana C, et al. ASPRE trial: performance of screening for preterm pre‐eclampsia. Ultrasound Obstet Gynecol. 2017;50(4):492-5.
35. Macon B. Eclampsia. San Francisco, California, US: Healthline; 2018 [cited 2020 October 19]. Available from: https://www.healthline.com/health/eclampsia.
36. Liu S, Joseph KS, Liston RM, Bartholomew S, Walker M, León JA, et al. Incidence, risk factors, and associated complications of eclampsia. Obstet Gynecol. 2011;118(5):987-94.
37. Goldenberg RL, Culhane JF, Iams JD, Romero R. Preterm birth 1 - Epidemiology and causes of preterm birth. The Lancet (British edition). 2008;371(9606):75-84.
38. Duley L. The Global Impact of Pre-eclampsia and Eclampsia. Seminars in Perinatology. 2009;33(3):130-7.

39. Aitio A, Anderson D, Blain P, Bond J, Buratti M, Calder I, et al. Biomarkers and risk assessment: Concepts and principles. Environmental health criteria. 1993(155):3-82.
40. Organization W-WH. Biomarkers In Risk Assessment: Validity And Validation. Genève, Switzerland: WHO; 2001 [cited 2020 November 15]. Available from: http://www.inchem.org/documents/ehc/ehc/ehc222.htm.
41. Manokhina I, Del Gobbo GF, Konwar C, Wilson SL, Robinson WP. Review: placental biomarkers for assessing fetal health. Human Molecular Genetics. 2017;26(R2):R237-R45.
42. Cuffe JSM, Holland O, Salomon C, Rice GE, Perkins AV. Review: Placental derived biomarkers of pregnancy disorders. Placenta. 2017;54:104-10.
43. Maynard SE, Min JY, Merchan J, Lim KH, Li J, Mondal S, et al. Excess placental soluble fms-like tyrosine kinase 1 (sFlt1) may contribute to endothelial dysfunction, hypertension, and proteinuria in preeclampsia. J Clin Invest. 2003;111(5):649-58.
44. Stepan H, Herraiz I, Schlembach D, Verlohren S, Brennecke S, Chantraine F, et al. Implementation of the sFlt-1/PlGF ratio for prediction and diagnosis of pre-eclampsia in singleton pregnancy: implications for clinical practice. Ultrasound in obstetrics & gynecology : the official journal of the International Society of Ultrasound in Obstetrics and Gynecology. 2015;45(3):241-6.
45. Fujiwara H, Higuchi T, Yamada S, Hirano T, Sato Y, Nishioka Y, et al. Human extravillous trophoblasts express laeverin, a novel protein that belongs to membrane-bound gluzincin metallopeptidases. Biochem Biophys Res Commun. 2004;313(4):962-8.
46. Maruyama M, Hattori A, Goto Y, Ueda M, Maeda M, Fujiwara H, et al. Laeverin/Aminopeptidase Q, a Novel Bestatin-sensitive Leucine Aminopeptidase Belonging to the M1 Family of Aminopeptidases. Journal of Biological Chemistry. 2007;282(28):20088-96.
47. Nystad M, Sitras V, Nordbakken CV, Pedersen MI, Acharya G. Laeverin protein expression in normal and preeclamptic placentas using tissue microarray analysis. Acta Obstet Gynecol Scand. 2018;97(5):536-44.
48. Nystad M, Sitras V, Larsen M, Acharya G. Placental expression of aminopeptidase-Q (laeverin) and its role in the pathophysiology of preeclampsia. Am J Obstet Gynecol. 2014;211(6):686.e1-31.
49. Haigh T, Chen C-P, Jones C, Aplin J. Studies of mesenchymal cells from 1st trimester human placenta: expression of cytokeratin outside the trophoblast lineage. Placenta. 1999;20(8):615-25.
50. Maldonado-Estrada J, Menu E, Roques P, Barré-Sinoussi F, Chaouat G. Evaluation of Cytokeratin 7 as an accurate intracellular marker with which to assess the purity of human placental villous trophoblast cells by flow cytometry. J Immunol Methods. 2004;286(1-2):21-34.
51. Tannetta D, Collett G, Vatish M, Redman C, Sargent I. Syncytiotrophoblast extracellular vesicles - Circulating biopsies reflecting placental health. Placenta. 2017;52:134-8.
52. Germain SJ, Sacks GP, Sooranna SR, Sargent IL, Redman CW. Systemic inflammatory priming in normal pregnancy and preeclampsia: the role of circulating syncytiotrophoblast microparticles. J Immunol. 2007;178(9):5949-56.
53. Goswami D, Tannetta DS, Magee LA, Fuchisawa A, Redman CW, Sargent IL, et al. Excess syncytiotrophoblast microparticle shedding is a feature of early-onset pre-eclampsia, but not normotensive intrauterine growth restriction. Placenta. 2006;27(1):56-61.
54. Lichtman JW, Conchello J-A. Fluorescence microscopy. Nat Methods. 2005;2(12):910-9.
55. Leng Y. Light Microscopy. Materials Characterization: Introduction to Microscopic and Spectroscopic Methods. 2nd ed. Weinheim, Germany: Wiley; 2009. p. 1-44.

56. Sibarita J-B. Deconvolution Microscopy. Adv Biochem Eng Biotechnol. Berlin, Heidelberg: Berlin, Heidelberg: Springer Berlin Heidelberg; 2005. p. 201-43.
57. Combs CA, Shroff H. Fluorescence Microscopy: A Concise Guide to Current Imaging Methods. Curr Protoc Neurosci. 2017;79(1):2.1.-2.1.25.
58. Herman H., Centonze F.V.E., Lakowicz J.R., Murphy D.B., Spring K.R., Davidson M.W. Fluorescence Microscopy: Basic Concepts in Fluorescence. The Florida State University: Molecular Expressions; 2015 [cited 2021 February 18]. Available from: https://micro.magnet.fsu.edu/primer/techniques/fluorescence/fluorescenceintro.html.
59. Süel G. Use of Fluorescence Microscopy to Analyze Genetic Circuit Dynamics. In: Voigt C, editor. Methods in Enzymology. 497: Academic Press; 2011. p. 275-93.
60. Kobayashi Y, Lavenex P. Neuroanatomy Methods in Humans and Animals. Reference Module in Biomedical Sciences: Elsevier; 2015.
61. Coons AH, Creech HJ, Jones RN. Immunological Properties of an Antibody Containing a Fluorescent Group. Experimental Biology and Medicine. 1941;47(2):200-2.
62. Drew CP, Shieh W-J. Immunohistochemistry. In: Rupprecht C, Nagarajan T, editors. Current Laboratory Techniques in Rabies Diagnosis, Research and Prevention, Volume 2: Academic Press; 2015. p. 109-15.
63. Im K, Mareninov S, Diaz MFP, Yong WH. An Introduction to Performing Immunofluorescence Staining. Methods Mol Biol. 2019;1897:299-311.
64. Abcam. Immunohistochemistry (IHC): the complete guide. Cambridge, UK: Abcam 2019 [cited 2021 April 25]. Available from: https://www.abcam.com/content/immunohistochemistry-the-complete-guide.
65. Abbas AK, Lichtman AH, Pillai S. Antigen Capture and Presentation to Lymphocytes. Basic immunology : functions and disorders of the immune system. 6th ed. Philadelphia, PA, US: Elsevier; 2019. p. 51-72.
66. Wiley-Blackwell. Clinical immunology. In: Iles RK, Docherty SM, editors. Biomedical sciences - Essential laboratory medicine. Chichester, UK: Wiley-Blackwell; 2012. p. 311-26.
67. Unknown. Introduction to Immunohistochemistry. 2013 In: Dako's Guidebook to Immunohistochemical Staining Methods [Internet]. Dako. 6th. [12-8]. Available from: https://www.agilent.com/cs/library/technicaloverviews/public/08002_ihc_staining_methods.pdf
68. Abcam. Direct vs indirect immunofluorescence. Cambridge, UK: Abcam; 2021 [cited 2021 April 25]. Available from: https://www.abcam.com/secondary-antibodies/direct-vs-indirect-immunofluorescence.
69. Abcam. Choosing a primary antibody or secondary antibody. Cambridge, UK: Abcam 2021 [cited 2021 April 25]. Available from: https://www.abcam.com/protocols/choosing-an-antibody.
70. Davis AS, Richter A, Becker S, Moyer JE, Sandouk A, Skinner J, et al. Characterizing and Diminishing Autofluorescence in Formalin-fixed Paraffin-embedded Human Respiratory Tissue. The journal of histochemistry and cytochemistry : official journal of the Histochemistry Society. 2014;62(6):405-23.
71. Banerjee B, Miedema BE, Chandrasekhar HR. Role of basement membrane collagen and elastin in the autofluorescence spectra of the colon. Journal of investigative medicine: the official publication of the American Federation for Clinical Research. 1999;47(6):326-32.
72. Belichenko PV, Fedorov AA, Dahlström AB. Quantitative analysis of immunofluorescence and lipofuscin distribution in human cortical areas by dual-channel confocal laser scanning microscopy. Journal of neuroscience methods. 1996;69(2):155-61.
73. Baschong W, Suetterlin R, Laeng RH. Control of Autofluorescence of Archival Formaldehyde-fixed, Paraffin-embedded Tissue in Confocal Laser Scanning Microscopy (CLSM). J Histochem Cytochem. 2001;49(12):1565-71.

74. Billinton N, Knight AW. Seeing the wood through the trees: a review of techniques for distinguishing green fluorescent protein from endogenous autofluorescence. Analytical biochemistry. 2001;291(2):175-97.
75. Del Castillo P, Llorente AR, Stockert JC. Influence of fixation, exciting light and section thickness on the primary fluorescence of samples for microfluorometric analysis. Basic Appl Histochem. 1989;33(3):251-7.
76. Monici M. Cell and tissue autofluorescence research and diagnostic applications. Biotechnol Annu Rev. 2005;11:227-56.
77. Viegas MS, Martins TC, Seco F, do Carmo A. An improved and cost-effective methodology for the reduction of autofluorescence in direct immunofluorescence studies on formalin-fixed paraffin-embedded tissues. Eur J Histochem. 2007;51(1):59-66.
78. Beisker W, Dolbeare F, Gray JW. An improved immunocytochemical procedure for high-sensitivity detection of incorporated bromodeoxyuridine. Cytometry. 1987;8(2):235-9.
79. Beisker W, Dolbeare F, Gray JW. An improved immunocytochemical procedure for high‐sensitivity detection of incorporated bromodeoxyuridine. Cytometry. 1987;8(2):235-9.
80. Goodwin PC. Quantitative deconvolution microscopy. In: Waters JC, Wittman T, editors. Methods in Cell Biology. 123: Academic Press; 2014. p. 177-92.
81. Hard R, Hipp J, Tangrea MA, Tomaszewski JE. Applications of Image Science in Pathology and Cell Biology. In: McManus LM, Mitchell RN, editors. Pathobiology of Human Disease. San Diego: Academic Press; 2014. p. 3723-59.
82. Yamanaka M, Yamanaka M, Smith NI, Smith NI, Fujita K, Fujita K. Introduction to super-resolution microscopy. Microscopy (Oxf). 2014;63(3):177-92.
83. Gustafsson MGL, Shao L, Carlton PM, Wang CJR, Golubovskaya IN, Cande WZ, et al. Three-Dimensional Resolution Doubling in Wide-Field Fluorescence Microscopy by Structured Illumination. Biophysical Journal. 2008;94(12):4957-70.
84. Unknown. Structured Illumination Microscopy: 3D SIM Imaging: Oxford Instruments - Andor 2020 [cited 2020 November 5]. Available from: https://andor.oxinst.com/learning/view/article/super-resolution-imaging-structured-illumination-microscopy.
85. Swedlow JR. Quantitative fluorescence microscopy and image deconvolution. Methods Cell Biol. 2013;114:407-26.
86. Jensen EC. Types of Imaging, Part 2: An Overview of Fluorescence Microscopy. Anat Rec (Hoboken). 2012;295(10):1621-7.
87. Zanella R, Zanghirati G, Cavicchioli R, Zanni L, Boccacci P, Bertero M, et al. Towards real-time image deconvolution: application to confocal and STED microscopy. Scientific Reports. 2013;3(1):2523.
88. Robson A-L, Dastoor PC, Flynn J, Palmer W, Martin A, Smith DW, et al. Advantages and Limitations of Current Imaging Techniques for Characterizing Liposome Morphology. Front Pharmacol. 2018;9:80.
89. Staff AA, Andergaar AB, Heriksen T, Langesøter E, Magnussen E, Michelsen TM. Hypertensive pregnancy complications and eclampsia: Norwegian Gynecological Society; 2014 [cited 2021 April 18]. Available from: https://www.legeforeningen.no.
90. Grizzle WE. Special symposium: fixation and tissue processing models. Biotechnic & histochemistry : official publication of the Biological Stain Commission. 2009;84(5):185-93.
91. Thavarajah R, Mudimbaimannar VK, Elizabeth J, Rao UK, Ranganathan K. Chemical and physical basics of routine formaldehyde fixation. J Oral Maxillofac Pathol. 2012;16(3):400-5.
92. Atherton AJ, Clarke C. Multiple labeling techniques for fluorescence microscopy. Methods Mol Med. 2001;57:41-8.

93. Griffiths G, Slot J-W, Webster P. Cryosectioning and Immunolabeling: The Contributions of Kiyoteru Tokuyasu. Microscopy Today. 2018;26(4):44-9.
94. Villegas-Hernández LE, Nystad M, Ströhl F, Basnet P, Acharya G, Ahluwalia BS. Visualizing ultrastructural details of placental tissue with super-resolution structured illumination microscopy. Placenta (Eastbourne). 2020;97:42-5.
95. Sitras V, Paulssen RH, Grønaas H, Leirvik J, Hanssen TA, Vårtun Å, et al. Differential Placental Gene Expression in Severe Preeclampsia. Placenta. 2009;30(5):424-33.
96. Montanaro J, Gruber D, Leisch N. Improved ultrastructure of marine invertebrates using non-toxic buffers. PeerJ. 2016;4:e1860.
97. Unknown. VS120 Viritual Slide Microscope Olympus; 2021 [cited 2021 April 8]. Available from: https://www.olympus-lifescience.com/en/microscopes/virtual/vs120/.
98. Qin W, Luo M, Wang K, Yang M, Sheng H, He G. A combined treatment with erythrocyte lysis solution and Sudan Black B reduces tissue autofluorescence in double-labeling immunofluorescence. Microscopy. 2018;67(6):345-55.
99. Whittington NC, Wray S. Suppression of Red Blood Cell Autofluorescence for Immunocytochemistry on Fixed Embryonic Mouse Tissue. Curr Protoc Neurosci. 2017;81:2.28.1-12.
100. Kiernan J, Wessendorf, M. Autofluorescence: Causes and cures. 2001 [cited 2021 April 13]. Available from: https://hwpi.harvard.edu/files/iccb/files/autofluorescence.pdf?m=1465309329.
101. Bernhard W, Annie V. Improved Techniques for the Preparation of Ultrathin Frozen Sections. The Journal of cell biology. 1971;49(3):731-46.
102. King BF. The organization of actin filaments in human placental villi. J Ultrastruct Res. 1983;85(3):320-8.
103. Kaufmann P, Huppertz B, Frank H-G. The fibrinoids of the human placenta: origin, composition and functional relevance. Annals of Anatomy - Anatomischer Anzeiger. 1996;178(6):485-501.
104. Rockey DC, Bell PD, Hill JA. Fibrosis--a common pathway to organ injury and failure. N Engl J Med. 2015;372(12):1138-49.
105. Zeisberg M, Kalluri R. Cellular mechanisms of tissue fibrosis. 1. Common and organ-specific mechanisms associated with tissue fibrosis. Am J Physiol Cell Physiol. 2013;304(3):C216-25.
106. Ricard-Blum S, Baffet G, Théret N. Molecular and tissue alterations of collagens in fibrosis. Matrix Biol. 2018;68-69:122-49.
107. Ducray JF, Naicker T, Moodley J. Pilot study of comparative placental morphometry in pre-eclamptic and normotensive pregnancies suggests possible maladaptations of the fetal component of the placenta. Eur J Obstet Gynecol Reprod Biol. 2011;156(1):29-34.
108. Devisme L, Merlot B, Ego A, Houfflin-Debarge V, Deruelle P, Subtil D. A case-control study of placental lesions associated with pre-eclampsia. Int J Gynaecol Obstet. 2013;120(2):165-8.
109. Feng Y, Chen X, Wang H, Cao Y, Liu M, Lv J, et al. Collagen I Induces Preeclampsia-Like Symptoms by Suppressing Proliferation and Invasion of Trophoblasts 2021 [cited 2021 June 20]. Available from: https://www.frontiersin.org/article/10.3389/fendo.2021.664766.
110. Wahyudi H, Reynolds AA, Li Y, Owen SC, Yu SM. Targeting collagen for diagnostic imaging and therapeutic delivery. J Control Release. 2016;240:323-31.
111. Banerjee B, Miedema BE, Chandrasekhar HR. Role of basement membrane collagen and elastin in the autofluorescence spectra of the colon. J Investig Med. 1999;47(6):326-32.
112. Ohmaru-Nakanishi T, Asanoma K, Fujikawa M, Fujita Y, Yagi H, Onoyama I, et al. Fibrosis in Preeclamptic Placentas Is Associated with Stromal Fibroblasts Activated by the Transforming Growth Factor-β1 Signaling Pathway. Am J Pathol. 2018;188(3):683-95.

113. Xu X-H, Jia Y, Zhou X, Xie D, Huang X, Jia L, et al. Downregulation of lysyl oxidase and lysyl oxidase-like protein 2 suppressed the migration and invasion of trophoblasts by activating the TGF-β/collagen pathway in preeclampsia. Experimental & Molecular Medicine. 2019;51(2):1-12.
114. Janmey PA, Lamb JA, Ezzell RM, Hvidt S, Lind SE. Effects of actin filaments on fibrin clot structure and lysis. Blood. 1992;80(4):928-36.
115. Lee WM, Galbraith RM. The Extracellular Actin-Scavenger System and Actin Toxicity. N Engl J Med. 1992;326(20):1335-41.
116. Weisel JW, Litvinov RI. Fibrin Formation, Structure and Properties. Subcell Biochem. 2017;82:405-56.
117. Tong M, Chamley LW. Placental extracellular vesicles and feto-maternal communication. Cold Spring Harb Perspect Med. 2015;5(3):a023028-a.
118. Chua S., Wilkins T., Sargent I., Redman C. Trophoblast deportation in pre-eclamptic pregnancy. Placenta (Eastbourne). 1991;12(4):431-2.
119. Burton GJ, Jones CJP. Syncytial Knots, Sprouts, Apoptosis, and Trophoblast Deportation from the Human Placenta. Taiwanese journal of obstetrics & gynecology. 2009;48(1):28-37.
120. Huppertz B, Frank H-G, Reister F, Korr H, Kaufmann P. Apoptosis cascade progresses during turnover of human trophoblast: analysis of villous cytotrophoblast and syncytial fragments in vitro. Laboratory investigation; a journal of technical methods and pathology. 1999;79(12):1687-702.
121. Attwood HD, Park WW. Embolism to the lungs by trophoblast. J Obstet Gynaecol Br Commonw. 1961;68:611-7.
122. Johansen M, Redman CWG, Wilkins T, Sargent IL. Trophoblast Deportation in Human Pregnancy—its Relevance for Pre-eclampsia. Placenta. 1999;20(7):531-9.
123. Huppertz B, Frank H-G, Reister F, Kaufmann P. Villous cytotrophoblast regulation of the syncytial apoptotic cascade in the human placenta. Histochemistry and cell biology. 1998;110(5):495-508.
124. Benirschke K, Kaufmann P, Baergen R. Classification of villous maldevelopment. Pathology of the human placenta. 2006:491-518.
125. Heazell AEP, Moll SJ, Jones CJP, Baker PN, Crocker IP. Formation of Syncytial Knots is Increased by Hyperoxia, Hypoxia and Reactive Oxygen Species. Placenta. 2007;28:S33-S40.
126. Loukeris K, Sela R, Baergen R. Syncytial Knots as a Reflection of Placental Maturity: Reference Values for 20 to 40 Weeks' Gestational Age. Pediatric and developmental pathology : the official journal of the Society for Pediatric Pathology and the Paediatric Pathology Society. 2009;13:305-9.
127. Redman CWG, Tannetta DS, Dragovic RA, Gardiner C, Southcombe JH, Collett GP, et al. Review: Does size matter? Placental debris and the pathophysiology of pre-eclampsia. Placenta. 2012;33:S48-S54.
128. Smeets D, Neumann J, Schermelleh L. Application of Three-Dimensional Structured Illumination Microscopy in Cell Biology: Pitfalls and Practical Considerations. Totowa, NJ: Totowa, NJ: Humana Press; 2014. p. 167-88.
129. Atwa K, Farghaly L. Light and electron microscopic study of placental tissue in women suffering from severe preeclampsia. The Egyptian Journal of Histology. 2011;34:650-61.
130. Tannetta DS, Dragovic RA, Gardiner C, Redman CW, Sargent IL. Characterisation of Syncytiotrophoblast Vesicles in Normal Pregnancy and Pre-Eclampsia: Expression of Flt-1 and Endoglin. PLOS ONE. 2013;8(2):e56754.
131. Redman CW, Sargent IL. Pre-eclampsia, the placenta and the maternal systemic inflammatory response--a review. Placenta. 2003;24 Suppl A:S21-7.

132. Pillay P, Moodley K, Moodley J, Mackraj I. Placenta-derived exosomes: potential biomarkers of preeclampsia. Int J Nanomedicine. 2017;12:8009-23.
133. Kitamura A, Nagata K, Kinjo M. Conformational analysis of misfolded protein aggregation by FRET and live-cell imaging techniques. Int J Mol Sci. 2015;16(3):6076-92.
134. Yamahara N, Nomura S, Suzuki T, Itakura A, Ito M, Okamoto T, et al. Placental leucine aminopeptidase/oxytocinase in maternal serum and placenta during normal pregnancy. Life Sci. 2000;66(15):1401-10.
135. Mizutani S, Shibata K, Kikkawa F, Hattori A, Tsujimoto M, Ishii M, et al. Essential role of placental leucine aminopeptidase in gynecologic malignancy. Expert Opin Ther Targets. 2007;11(4):453-61.
136. Caramelo JJ, Parodi AJ. A sweet code for glycoprotein folding. FEBS Lett. 2015;589(22):3379-87.
137. Apicella C, Ruano CSM, Méhats C, Miralles F, Vaiman D. The Role of Epigenetics in Placental Development and the Etiology of Preeclampsia. Int J Mol Sci. 2019;20(11):2837.
138. Leavey K, Wilson SL, Bainbridge SA, Robinson WP, Cox BJ. Epigenetic regulation of placental gene expression in transcriptional subtypes of preeclampsia. Clinical epigenetics. 2018;10:28.

Supplementary information

Table S1: List of equipment, reagents and solutions

Name	Manufacturer	Cat. No.	Purpose
Sodium chloride (NaCl) 9 mg/mL	Fresenius Kabi AG	896968	Rinse the collected fresh tissue
EGTA[1]	Sigma-Aldrich	E4378-1006	Used to make 1X PHEM[4] buffer
HEPES[2]	VWR Chemicals	441476L	Used to make 1X PHEM[4] buffer
PIPES[3]	Sigma-Aldrich	P6757-500G	Used to make 1X PHEM[4] buffer
Magnesium sulfate	Sigma- Aldrich	M7506-500G	Used to make 1X PHEM[4] buffer
5M sodium hydroxide	Sigma-Aldrich	30620-1KG-R	Used to make 1X PHEM[4] buffer
FA[5]	Sigma-Aldrich	158127-500G	Prepare 16% PFA[6]
FA (16%) - **16 g FA[5] in 100 mL MilliQ water**	-	-	To further dilute to 8% FA[5]
FA[5] (8%) - **7 mL 16% FA[5] in 7 mL 1X PHEM[4]**	-	-	Used in 4% PFA[6] solution
PFA[6] solution (4%) - **15 mL 0.2 M PBS[7], 7.5 mL 8% FA[5] diluted in 4X PHEM[4], 7.5 mL MilliQ water**	-	-	Fixate tissue and preserve tissue morphology
Gelatine (12%) - **12 g gelatine diluted in 100 mL MilliQ water**	Fluka Analytical	48723-599G-5	Preserving tissue morphology
Sucrose (2.3 M) - **342 g sucrose diluted in 100 mL MilliQ water**	Sigma-Aldrich	16104-1KG	Preventing crystallization during freezing
Methylcellulose (2 %) - **2 g methyl cellulose in 100 mL MilliQ water**	Sigma-Aldrich	M6385-100G	To further dilute to 1% methylcellulose
Methyl cellulose (1%) - **250 µL 2% methyl cellulose in 250 mL 2.3 M sucrose**	-	-	Prevent the tissue section from drying
PBS[7] (0.2 M) - **10 Ml 1M PBS in 40 Ml MilliQ water**	VWR Chemicals	E404-200TABS	Used in fixative
PBS[7] (1 M) - **1 g PBS in 1L ddH_2O**	VWR Chemicals	E404-200TABS	Washing (Maintains intracellular Ph, which prevents cells rupturing or shriveling up due to osmosis)
BSA[8] (1 %) - **0.5 g BSA in 50 Ml 1 M PBS[7]**	Sigma-Aldrich	A8022	Used in blocking buffer
Xylene (mixture of isomers) 1L	VWR Chemicals	28975.291	Removed paraffin penetrated the tissue
Ethanol absolute 100 Vol. % 1L	VWR Chemicals	20821.296	The rehydration step reintroduces the water molecules into the tissue
Ethanol 96 Vol. % 5L	VWR Chemicals	20823.362	The rehydration step reintroduces the water molecules into the tissue
Ethanol 70 Vol. % - **diluted from 96 Vol. %**	-	-	Rehydration of FFPE samples
Citric acid monohydrate	Sigma-Aldrich	C-7129	Used in Citrate buffer

Name	Manufacturer	Cat. No.	Purpose
- Solution A: 10.5 g citric acid monohydrate in 500 Ml MilliQ water			
Sodium citrate - Solution B: 29.4 g sodium citrate in 1 L MilliQ water	Sigma-Aldrich	C-7254	Used in Citrate buffer
Citrate buffer - 18 ml solution A and 82 ml solution B	-	-	Enables rehydration and antigen retrieval by breaking cross-links between antigens and any substances in its fixation medium
Glycine (bleaching solution) - 150 mM → 11.6 g glycine + MilliQ water up to 1000 mL	Sigma-Aldrich	G7126-100G	Reducing the unspecific cross-binding of the fluorescent markers and antibodies to the sample.
TBST[9] (washing solution) - 2.5 ml 20% Tween 20 + in 1L 1X TBS	-	-	Decrease background staining and reagent spreading in procedures
10 X TBS[10] - 61 g Trizma base + 90 g NaCl + MilliQ water up to 1000 mL	-	-	To further dilute to 1X TBS for TBST (washing solution)
0.5M Tris base	-	-	Used in 10X TBS[10] solution
9% 1.54M Sodium chloride (NaCl)	-	-	Used in 10X TBS[10] solution
Tween 20	VWR Chemicals	663684B	Used in TBST (washing solution)
Wah-N-Dry coverslip rack	Sigma-Aldrich	WSDR-100	A rack for Cryo-section samples
Cryogenic storage vials	Thermo Fisher	5000-0020	the placenta samples on pins were placed in the vials and store in the nitrogen tank
Tube Rotator B7925	Agar Scientific Ltd.	-	-
22 x 22 mm #1.5 coverslip	VWR	48393-151	Tissue sample placed on the coverslip
British Standard Microscope slide	Thermo Fisher	-	Assemble coverglass
Poly-L-lysine (0.2 mg/Ml) - 0.2 mg poly-L-lysine in 1 mL Milli-Q water	Sigma-Aldrich	P1274	Provide adherence between tissue section and cover glass
Prolong Gold Antifade Mountant	Thermo Fisher	P36934	Mounting medium
Dental glue Picodent twinsil 22 - 1:1 Solution A and Solution B	-	-	Seal the edge of the mounted cover glass

[1]EGTA: Ethylene glycol tetraacetic acid (ethylene glycol-bis (β-aminoethyl ether)-N, N, N', N'-tetraacetic acid)
[2]HEPES: 4-(2-hydroxyethyl)-1-piperazineethanesulfonic acid
[3]PIPES: 1,4 piperazine bis (2-ethane sulfonic acid)
[4]PHEM: PIPES-HEPES-EGTA-Magnesium sulfate
[5]FA: Formaldehyde
[6]PFA: Paraformaldehyde
[7]PBS: Phosphate buffered saline
[8]BSA: Bovine serum albumin
[9]TBST: Tris buffered saline with Tween 20
[10]TBS – Tris buffered saline

Table S2: Labeling combination using Biomarkers and fluorescence markers

Reference No.	Human placenta	Preservation	Target	Antibody	Name	Manufacturer	Cat. No	Working concentration
1	Normal	Cryo-section	Syncytial microvesicles	1'Ab[3]	PLAP[4] (8B6) Mouse Monoclonal Antibody	Santa Cruz Biotechnology	Sc-47691	1:50
		FFPE[2] section		2'Ab[3]	Goat Anti-Mouse IgG (H+L) Cross-Adsorbed Secondary Antibody, Alexa Fluor Plus 488	Thermo Fischer	A11001	1:250
			Membrane	-	CellMask Orange	Thermo Fischer	C10045	1:2000
			Nuclei	-	DAPI[5]	Thermo Fischer	62247	1:1000
2	Normal	FFPE[2] section	Laeverin	1'Ab[3]	Anti-Laeverin Rabbit Polyclonal Antibody	Abcam	Ab185345	1:100
	PE[1]			2'Ab[3]	Donkey Anti-Rabbit IgG (H+L) Highly Cross-Adsorbed Secondary Antibody, Alexa Fluor 647	Thermo Fischer	A31573	1:500
		Cryo-section	Trophoblast cytoplasm	1'Ab[3]	Cytokeratin 7 Mouse Monoclonal Antibody	Santa Cruz Biotechnology	Sc-23876	1:100
				2'Ab[3]	Goat Anti-Mouse IgG (H+L) Cross-Adsorbed Secondary Antibody, Alexa Fluor Plus 488	Thermo Fischer	A11001	1:250
			Nuclei	-	DAPI[5]	Thermo Fischer	62247	1:1000
3	Normal	FFPE[2] section	Trophoblast cytoplasm	1'Ab[3]	Cytokeratin 7 Mouse Monoclonal Antibody	Santa Cruz Biotechnology	Sc-23876	1:100
	PE[1]			2'Ab[3]	Goat Anti-Mouse IgG (H+L) Cross-Adsorbed Secondary Antibody, Alexa Fluor Plus 488	Thermo Fischer	A11001	1:250
			Membrane	-	CellMask Orange	Thermo Fischer	C10045	1:2000
			Nuclei	-	DAPI[5]	Thermo Fischer	62247	1:1000
4	Normal	FFPE[2] section	Actin	-	Phalloidin-Atto 647 N	Sigma-Aldrich	65906	1:100
	PE[1]		Membrane	-	CellMask Orange	Thermo Fischer	C10045	1:2000
			Nuclei	-	DAPI[5]	Thermo Fischer	62247	1:1000
5	Normal	Cryo-section	Trophoblast cytoplasm	1'Ab[3]	Cytokeratin 7 Mouse Monoclonal Antibody	Santa Cruz Biotechnology	Sc-23876	1:100
				2'Ab[3]	Goat Anti-Mouse IgG (H+L) Cross-Adsorbed Secondary Antibody, Alexa Fluor Plus 488	Thermo Fischer	A11001	1:250
			Actin	-	Phalloidin-Atto 647 N	Sigma-Aldrich	65906	1:100
			Nuclei	-	DAPI[5]	Thermo Fischer	62247	1:1000

Reference No.	Human placenta	Preservation	Target	Antibody	Name	Manufacturer	Cat. No	Working concentration
6	Normal	Cryo-section	Membrane	-	CellMask Orange	Thermo Fischer	C10045	1:2000
	PE[1]		Nuclei	-	DAPI[5]	Thermo Fischer	62247	1:1000
7	Normal	Cryo-section	Laeverin	1'Ab[3]	Anti-Laeverin Rabbit Polyclonal Antibody	Abcam	ab185345	1:100
	PE[1]			2'Ab[3]	Donkey Anti-Rabbit IgG (H+L) Highly Cross-Adsorbed Secondary Antibody, Alexa Fluor 647	Thermo Fischer	A31573	1:500
			Membrane	-	CellMask Orange	Thermo Fischer	C10045	1:2000
			Nuclei	-	DAPI[5]	Thermo Fischer	62247	1:1000

[1]PE: Preeclampsia
[2]FFPE: Formalin-fixed paraffin-embedded
[3]Ab: Antibody
[4]PLAP: Placental alkaline phosphatase
[5]DAPI: 4',6-diamidino-2-phenylidole, dihydrochloride

S3: Microscope image representation of poor deparaffinization and rehydration technique

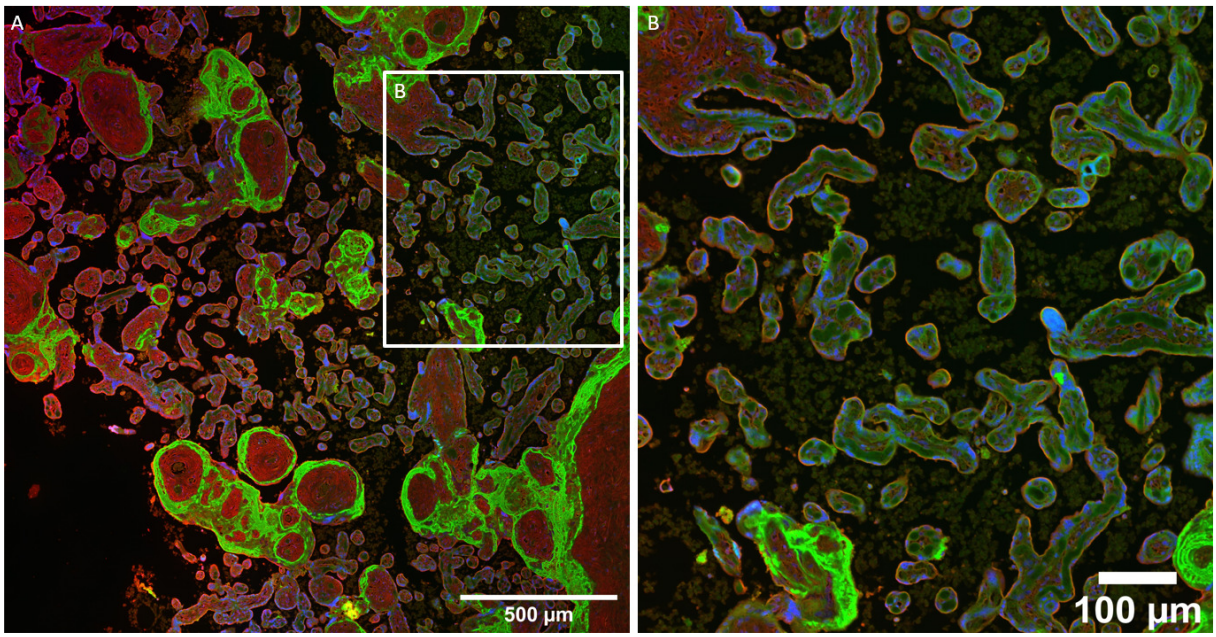

S3: Microscope image representation of poor deparaffinization and rehydration technique. *4µm thick FFPE healthy placenta section labeled with phalloidin-Atto 647 N for F-actin staining (displayed in green), membrane stained with CellMask Orange (displayed in red), nuclei counterstained with DAPI (displayed in blue). (A) Large FOV generated using DV microscope with 20X magnification. (B) Enlarged image from (A). Reduced signal, blurry and unclear regions are observed due to poor deparaffinization and rehydration technique of some regions in the slide.*

S4: Orthogonal view of the point spread function

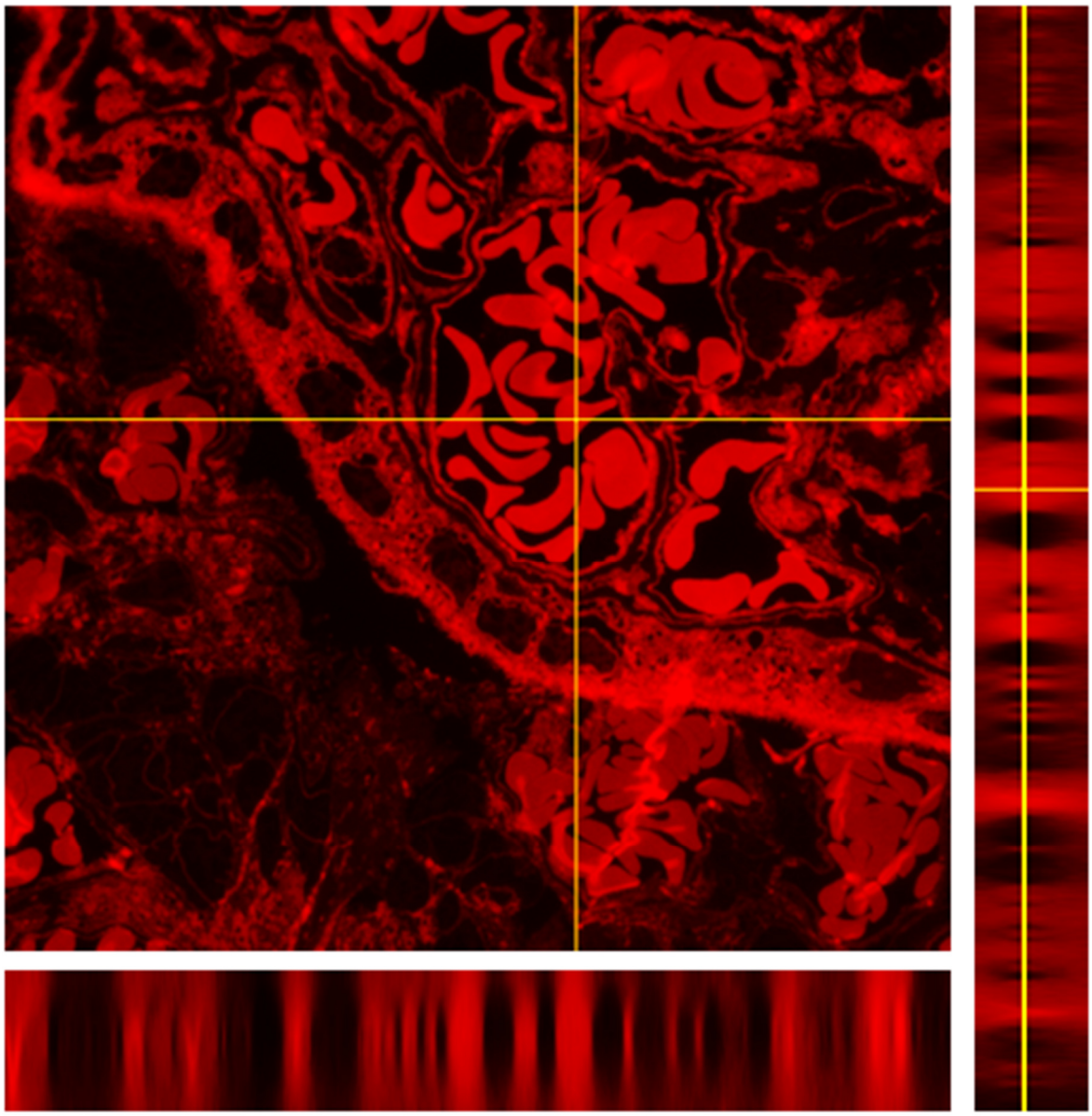

S4: Orthogonal view of point spread function. *The point spread function is viewed on an orthogonal view. In this case, the PSF is symmetrical which indicated an optimal refractive index match between the immersion medium and the microscope objective.*

S5: A general protocol for fluorescent immunolabeling on FFPE tissue sections

Samples:
Semithin sections (4µm-5µm) of Formalin-Fixed Paraffin-Embedded (FFPE) tissue.
Mounting substrate #1.5 coverslips (VWR cat# 48393-151 or equivalent) coated with Poly-L-Lysine (Sigma, cat# P1274)

Handling tips:
When working on samples laying directly on coverslips, it is convenient to place them in a coverslip rack, staining jar or similar, during the deparaffinization steps, and manipulate them with wide tip tweezers.

Reagents (fill in the information according to the experiment plan)

Available excitation wavelengths for fluorescence imaging on the DV/OMX:
642nm / 568nm / 488nm / 405nm

Washing buffer TBST: 1X TBS + 0.05% Tween 20 (pH 8.4)

- 2.5 ml 20% Tween 20 + in 1L 1X TBS

Preparation of **10X TBS** (0.5M Tris base, 9% 1.54M NaCl-pH8.4)

- 61 g Trizma base + 90 g NaCl + Milli-Q water up to 1000 mL
- Adjust pH to 8.4 using concentrated HCl

Blocking / Dilution buffer: **1% BSA in TBST** (1 g BSA in 100 ml TBST).

Citrate buffer (pH 5.98):

- Solution A: 10.5 g citric acid monohydrate in 500 ml Milli-Q water
- Solution B: 29.4 sodium citrate in 1L Milli-Q water
- 18 ml solution A and 82 ml solution B, make up to 1L with Milli-Q water

Bleaching solution:

- 150 mM Glycine solution (SIGMA-ALDRICH cat# G7126-100G)

Procedure:
Do not let the samples dry out at any point in the protocol.

1. **Deparaffinization and rehydration** (change all the solutions every 2 weeks, fill up in between). After sectioning, leave the sections in 60°C overnight, then proceed with the following steps:

- 3 x 5 min: Xylene
- 2 x 10 min: 100 % Ethanol
- 2 x 10 min: 96% Ethanol
- 1 x 10 min: 70% Ethanol
- 1 x 30 min Bleaching solution
- 1 x 5 min: MilliQ water

2. **Antigen retrieval**, 10 min microwaving in citrate buffer (pH 5.98)

- Pre-warm buffer to around 95°C, and place sections in a beaker filled with hot buffer.
- Microwave 2 x 5 min @50% power. Fill up with a hot buffer in between if the level gets low.
- Let cool down sections in the buffer for 20 min at RT.

3. **Washing and blocking steps**

- wash sections 3 x 2 min with Milli-Q water and aspirate excess liquid from slides.
- wash in TBST for 2 min
- incubate in blocking buffer for 30 min at RT.

4. **Labeling with primary antibodies**

- Spin down all antibodies and dilute them in blocking buffer according to the recommended concentration. Makeup to 100 - 150 µl / coverslip, depending on the size of the tissue section.
- Place the slides in a wet chamber (e.g., petri dish with a moisturized paper or equivalent) and incubate the antibodies on slides according to the recommended incubation time. Best results obtained with an overnight incubation at 4°C.

5. **Labeling with secondary antibodies**

- All steps from now on will be done under the aluminum foil, to prevent photobleaching.
- Dilute secondary antibodies in blocking buffer according to the recommended concentration and incubate on slides for 1h at RT.
- Wash 3 x 5 min in TBST
- Wash 2 x 5 min in PBS

6. **Actin membrane staining (direct labeling)**

- Dilute CellMask Orange in PBS (1:2000) and incubate on slides for 15min.
- Wash 2 x 5 min in PBS

7. **Cell membrane staining (direct labeling)**

- Dilute Cell Mask Orange in PBS (1:2000) and incubate on slides for 15min.
- Wash 2 x 5 min in PBS

8. **Nuclear staining (direct labeling) and mounting.**

- Add DAPI in PBS (1:1000) and incubate at RT for 15 min.
- Wash 2 x 5min in Milli-Q water
- Aspirate excess liquid from sections, but not let them dry.
- Apply mounting medium Prolong Gold in the center of the glass slide (see image below), and place the sample facing the mounting medium. Remove excess mounting medium by tapping gently on top of the slide with absorbent paper. Remove visible air bubbles from the sample by tapping gently with a plastic tweezer.
- Seal with nail polish

- Store the sample at 4°C and protect it from the light.

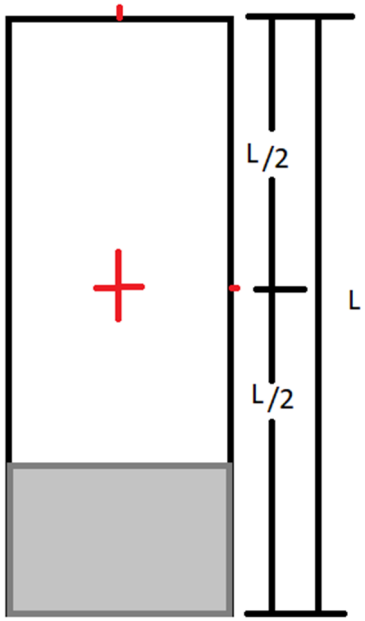

S6: A general protocol for labeling of Placenta Cryosections

1. Place the coverslips with the sections on a parafilm-covered metal plate on a heating plate.

2. Warm wash 3 x 20 minutes with PBS on the heating plate (40°C).

3. Indirect immunofluorescence staining:
   - Incubate 30 min with blocking buffer
   - Wash 2 x 5 min with PBS
   - Incubate 1 hour with primary antibody at RT
   - Wash 2 x 5 min with PBS
   - Incubate 1 hour with secondary antibody at RT
   - Wash 2 x 5 min with PBS

4. Actin staining (direct labeling):
   - Incubate 10 min with Phalloidin-Atto 647N
   - Wash 2 x 5 min with PBS

5. Membrane staining (direct labeling):
   - Incubate 10 min with CMO
   - Wash 2 x 5 min with PBS

6. Nucleic staining (direct labeling):
   - Incubate 10 min DAPI
   - Wash 3 x 5 min with MilliQ-water
   - Mount with Prolong Gold, seal with dental glue and cold storage (4°C)

S7: Coating of coverslips with Poly-L-lysine

1. Sterile #1.5 coverslips are washed with 70% ethanol, rinsed with ddH_2O, and air-dried on a coverslip rack.
2. The dry coverslips are coated with 50 µL 0.2 mg/mL Poly-L-Lysine to improve the adherence of the cell sample to the coverslip and preventing it from detaching during labeling and washing.
3. The Poly-L-lysine coated coverslips are transferred to dust-free dishes and stored at room temperature until use.